Geological Survey of Israel
Ministry of Energy

Saline Groundwater in Mt. Scopus Group in the Southern Golan Heights: Sources and Geochemistry

Hadas Ben-nun Levanon

Report GSI 13 2023

December 2023

32 Yeshayahu Leibowitz St. Jerusalem 9692100, Israel

Picture: The Yarmouk River in the southern Golan Heights
Picture was taken by Hadas Ben-nun Levanon.

Design: Tirza Tzuberi

Geological Survey of Israel
Ministry of Energy

Saline Groundwater in Mt. Scopus Group in the Southern Golan Heights: Sources and Geochemistry

Hadas Ben-nun Levanon

Thesis submitted in partial fulfillment of the requirement for the degree of MSc. at the Department of Earth and Environmental Sciences, Faculty of Science, the Hebrew University of Jerusalem.

This work was carried out under the supervision of:

Dr. Itay Reznik – Geological Survey of Israel

Prof. Avraham Starinsky – the Hebrew University of Jerusalem

And in Collaboration with:

Dr. Avi Burg – Geological Survey of Israel

Dr. Ittai Gavrieli – Geological Survey of Israel

Dr. Yoav Rosenberg – Geological Survey of Israel

Dr. Ronen Gersman – Genie Oil and Gas Ltd.

Dr. Yuval Bartov – Genie Oil and Gas Ltd.

Dr. Yakov Livshitz – the Hydrological Service, Water Authority of Israel

Report GSI/13/2023 December 2023

תודות

עבודה זו התאפשרה בזכות הגיאולוגים של חברת אפק, שבמסגרת חיפושי הנפט שנערכו בדרום רמת הגולן, עסקו במקביל באיסוף מידע יקר ערך על הגיאולוגיה המקומית.

ברצוני להודות במיוחד לרונן גרסמן, על שהעביר את הנתונים והמידע שאסף בשקידה ועל בסיסם נעשתה עבודה זו.

תודה רבה ליובל ברטוב, על עזרתו באיסוף דוגמאות המים מקידוחי נס ובהבנת הגיאולוגיה המקומית, עזרה שניתנה תמיד ברוחב לב ועם חיוך.

תודה לשותפי המחקר מהמכון הגיאולוגי. לאבי בורג על עזרה עצומה בהבנה של המערכת ההידרוגיאולוגית ברמת הגולן ובהבנת הידרוגיאולוגיה בכלל. תודה רבה לאיתי גבריאלי על שאלותיו החדות, שהעמיקו את הבנתי על התהליכים הגיאוכימיים. אני מודה לכם על כך שלא נתתם לי לדבר שטויות ובכך גרמתם לי לבדוק כל פרט קטן ביסודיות.

ברצוני להודות מקרב ליבי לשני המנחים:

לאיתי רזניק, על עזרה שלא ניתן למדוד אותה. תודה על הדיונים הפילוסופיים מרחיבי האופקים שלימדו אותי מהי המשמעות של חשיבה מדעית ועל יסודיות וקפדנות שדחפה אותי לנסות ולחשוב על כל פרט קטן שאולי פספסתי. אין ספק שהסטנדרטים הגבוהים שהצבת העמיקו בהרבה את ההבנה שלי.

תודה לאברהם סטרינסקי, על עזרה אין סופית בכל נושא שהוא, על פגישות מעניינות ומרוממות נפש שבמהלכן למדתי גיאוכימיה מהשורש. תמיד ידעת להגיד את המשפט שיהפוך את הדבר המסובך ביותר לפשוט וזו הייתה זכות גדולה לעבוד איתך.

תודה לרשות המים על מימון המחקר. אני מודה לרפרנט העבודה, יעקב ליבשיץ מהשירות ההידרולוגי על עזרתו הרבה.

בנוסף ארצה להודות לעובדי המכון הגיאולוגי: לידידיי איאד סואעד ואלון משה על עזרה רבה בדיגומים ותמיכה נפשית. אני מודה לדינה שטיבר, גילת שרעבי, קרן וייס, אולגה ברלין, תמי זילברמן, נבות מורג ורענן בודז'ין על עזרה באנליזות ועל הסבלנות להסביר הכל מאפס.

ארצה להודות לסגל המכון למדעי כדור הארץ באוניברסיטה העברית: תודה לאמתי כץ על עזרה בהבנת ההרכב הכימי של התמלחות. תודה לאריאל היימן, עודד נבון, ארי מטמון, עמוס פרומקין, חיים גבירצמן ולנדב לנסקי על קורסים מעניינים שבמהלכם למדתי דברים שהשתלבו בעבודה זו. אני רוצה להודות לראש החוג רונית קסל ולרכזות סנדרה קפלן ומגי פרקין על עזרתן האדיבה.

אחרונים חביבים ארצה להודות לכל משפחתי וחבריי על כל התמיכה והעידוד, אני רוצה להודות במיוחד לאמא ואבא שלי, לרחלי וליוני על העידוד שהיה מאוד נחוץ בשלבי הסיום.

עבודה זו מוקדשת לבני היקר לי מכל, ארז שלום, שהוא האור המאיר את דרכי.

Abstract

Water samples collected from deep research boreholes drilled into the aquitards- aquicludes of Mt. Scopus Group (Taqiye, Ghareb and Mishsah Formations) in the Southern Golan Heights were chemically analyzed for major elements, water isotopic compositions and strontium isotopes. The water samples were found to exhibit relatively high salinities (2,000-10,000 mg Cl/L), low Na/Cl (<0.75) and Mg/Ca (<0.4) equivalent ratios, and a Ca-Chloride composition ($Ca>(HCO_3+SO_4)$). $\delta^{18}O_{V\text{-}SMOW}$ and $\delta D_{V\text{-}SMOW}$ values were relatively depleted (~-7‰ and ~-42‰, respectively).

This composition is suggested to be derived from at least two endmembers: (a) Hypersaline Dead Sea Rift brines, which have originally evolved from seawater that transgressed into the Dead Sea Rift and underwent evaporation, mineral precipitation, and water-rock interactions. These brines intruded into the subsurface host rocks of the Mt. Scopus group in the Southern Golan Heights, surrounding the Dead Sea Rift and the Kinnarot basin; (b) Freshwater originating from recharge at higher altitudes, most likely from the Hermon Mountain in the north.

Due to the large salinity differences between the two endmembers, the ionic ratios are dictated mostly by the saline component, while the isotopic composition of the water is dictated by the freshwater component. The low Mg/Ca ratios further imply that the brines that intruded the Mt. Scopus Group, were formed during the early evolutionary stage of the Dead Sea Rift (lagoonary stage), coeval to the precipitation of the halite body (Bira Formation) within the Kinnarot Basin (9.5-7 ma). Over the geological time the brines were gradually washed and diluted at the subsurface by freshwater that was sourced in high altitudes. These findings exemplify the long-term hydrological memory of impermeable-semipermeable deep hydrogeological systems, and the way it is reflected in the water composition.

Table of Contents

1. Background 12
1.1 Geological background 12
1.2 Stratigraphy 14
1.3 Hydrogeological background 15
1.4 The chemical composition of water bodies in the region 18
The basaltic aquifer 18
The Jurassic aquifer 18
Hammat Gader springs 18
Meizar 3 well 18
Meizar 2 well 19
The Kinneret brines 19
1.5 Research purpose 20
2. Methods 21
2.1 Sampling 21
Drill Stem Tests 21
Drilling 21
2.2 Analysis 22
Major cations and sulfate (Na^{+}, K^{+}, Ca^{2+}, Mg^{2+}, Sr^{2+}, SO_4^{2-}) 22
Chlorides and alkalinity 22
Bromine 22
Stable oxygen and hydrogen isotopes ($\delta^{18}O$, δD) 22
Strontium isotopes ($^{87}Sr/^{86}Sr$) 23
Reaction Error 23
3. Results 24
3.1 Mt. Scopus Group in the Ness boreholes 24
3.2 Drill Stem Tests – hydrostatic pressures and apparent hydraulic conductivities 33
3.3 Information collected during drilling 38
Field observations 38
Water level measurements 39
3.4 Representative sample selection 40
Drill Stem Tests samples 41
Samples collected while drilling 47

3.5 Salinity, chemical and isotopic composition of the water samples 48
Major ion concentrations 48
Averaging the Major ion concentrations of DST samples 48
Corrections to the major ionic concentrations 51
Ionic ratios 52
Stable oxygen and hydrogen isotopes ($\delta^{18}O$ and δD) 54
Stable strontium isotopes ($^{87}Sr/^{86}Sr$) 55
4. Discussion 56
4.1 Hydrology 56
Hydrostatic pressures, water levels and apparent hydraulic gradients 56
Hydraulic conductivities and possible dual permeability behavior 58
Sources of salinity 59
Evolution of Ca-Chloride brines and intrusion mechanism into host rocks 61
Major ions composition 66
Stable water isotopes 70
Strontium isotopes ($^{87}Sr/^{86}Sr$) 74
Relationship to the Yarmouk Gorge outlets 77
4.3 Conceptual palaeohydrological model 80
Conclusions 85
References 87
Appendices 91
Appendix 1 – Bottom Hole Pressure measurements 92
Appendix 2 – The major ion composition of the water samples 96
Appendix 3 – pH, oxidation-reduction potential and isotopic composition of the water samples 97
Appendix 4 – Major ions composition of water sources in the GH 98
Appendix 5 – Isotopic composition of water sources in the GH 100
Appendix 6 – Major ions composition of the Kinneret brines 101
Appendix 7 – Isotopic composition of the Kinneret brines 103

Figures

Fig. 1.1 – Cross section through the GH……..……11

Fig. 1.2 – Geological map of the study area……12

Fig. 3.1 – Location map of Ness boreholes along with the main faults……...24

Fig. 3.2 – General lithological section of Ness 02 borehole……25

Fig. 3.3 – General lithological section of Ness 03 borehole……26

Fig. 3.4- General lithological section of Ness 05 borehole……27

Fig. 3.5- General lithological section of Ness 06 borehole……28

Fig. 3.6 - General lithological section of Ness 12 borehole……29

Fig. 3.7 - General lithological section of Ness 10 borehole……30

Fig. 3.8 – Generalized lithological cross section from Ness 02 to Ness 10……31

Fig. 3.9 - BHP of the Upper Mishash Formation in Ness 02 zone 2……...32

Fig 3.10 – BHP recordings of the build-up tests…….…….33

Fig. 3.11 –Hydrostatic pressures as a function of depths……34

Fig 3.12 - Calculated water levels as a function of depths……...35

Fig. 3.13 – Apparent hydraulic conductivities……..…36

Fig. 3.14 - Chemical composition during production in Ness 03 zone 2……...40

Fig. 3.15 - Chemical composition during production in Ness 03 zone 3……...41

Fig. 3.16 - Chemical composition during production in Ness 03 zone 2……...42

Fig. 3.17 - Chemical composition during production in Ness 02 zone 3……...43

Fig. 3.18 - Chemical composition during production in Ness 02 zone 4……...44

Fig. 3.19 - Chemical composition during production in Ness 02 zone 5……...45

Fig 3.20 - TDS of the studied water……47

Fig 3.21 (a-h) – Ion concentrations in the studied water……....49

Fig. 3.22 (a-f) – Ionic ratios (equivalent) of the studied water……52

Fig 3.23 (a-b) –$\delta^{18}O$ and δD values of the studied water……...54

Fig. 3.24 –$^{87}Sr/^{86}Sr$ values of the studied water……...54

Fig. 4.1 –Hydrostatic pressures in the Mt. Scopus Group……...56

Fig. 4.2 – Water levels of the open section and the tested intervals……57

Fig. 4.3 (a-b) – (a) Location map and TDS of water sources in the GH region……...59

Fig. 4.4 – Salinity and hydraulic conductivity as a function of depth…….59

Fig. 4.5 – Mineral precipitation during seawater evaporation…….61

Fig. 4.6 – Na/Cl and Mg/Ca equivalent ratios during seawater evaporation……...61

Fig 4.7 – TDS and density during seawater evaporation…….62

Fig. 4.8 – The extent of evaporitic deposits and brines along the DSR……...63

Fig. 4.9 – Na/Cl vs. Mg/Ca of the DSR brines and the studied water…….64

Fig. 4.10 – The Na/Cl ratio during the theoretical dilution brines……...65

Fig. 4.11 (a-g) – Ion concentrations of the studied water and the Kinneret brines…….…….68

Fig. 4.12 – Mg^{2+} vs. Ca^{2+} concentrations of the studied water and the Kinneret brines……..…69

Fig. 4.13 (a-e) – Stable water isotopes in the studied water and the Kinneret brines……..71

Fig. 4.14 – $\delta^{18}O$ values of the rainwater and groundwater in the GH……..73

Fig. 4.15 – Generalized columnar section of Zemah-1 borehole…….74

Fig. 4.16 - $^{87}Sr/^{86}Sr$ vs. Na/Cl ratios……75

Fig. 4.17 – The isotopic composition of Sr^{2+} in sources from the region……76

Fig. 4.18 – Temperature-salinity-$\delta^{18}O$ relationship of Hammat Gader springs……...77

Fig. 4.19 – Schematic illustration of brines intrusions……81

Fig. 4.20 – Schematic illustration of E-W cross section through the Kinnarot Basin…….82

Fig. 4.21 – NE-SW cross section through the southern Kinneret basin……...83

Figures in Appendix 1

1.1 – BHP of the Lower Mishash Formation in Ness 03 zone 1……..91

1.2 - BHP of the Lower Mishash Formation in Ness 03 zone 2…….…….91

1.3 - BHP of the Ghareb Formation in Ness 03 zone 3……...92

1.4 - BHP of the Lower Mishash Formation in Ness 02 zone 1……..92

1.5 - BHP of the Upper Mishash Formation in Ness 02 zone 2……...93

1.6 - BHP of the Upper Mishash-Ghareb boundary in Ness 02 zone 3……...93

1.7 – BHP of the Ghareb Formation in Ness 02 zone 4……...94

1.8 - BHP of the Taqiye Formation in Ness 02 zone 5……94

Tables

Table 1.1 – The hydrogeological units in the GH-Ajloun region……..16

Table. 3.1- Summary of results from DSTs…….36

Table 3.2 - Summary of field observations……...37

Table 3.3- Produced water and injected fluid volume per zone……...39

Table 3.4 – Major ion concentrations of studied water……48

Table 3.5 – Measured and corrected Cl^- concentrations……..50

Table 3.6 – Average of the ionic ratios of the studied water……...51

Table 3.7 – The isotopic composition of the studied water……53

Tables in the Appendices

1) The major ion composition of the water samples……95

2) pH, oxidation-reduction potential and isotopic composition of the water samples……96

3) Major ions composition of water sources in the GH……...97

4) Ionic ratios of water sources in the GH……...98

5) Isotopic composition of water sources in the GH……99

6) Major ions composition of the Kinneret brines……100

7) Ionic ratios of the Kinneret brines……101

8) Isotopic composition of the Kinneret brines……..102

1. Background

1.1 Geological background

The Golan Heights (GH), located in the northeastern part of Israel, is an elevated plateau covered mostly by young basalts. The basalts overlie in disconformity with a sedimentary syncline which extends from the Hermon anticlinal structure in the north to the Ajloun anticline in the south (Fig. 1.1). The syncline is bordered by the Dead Sea Transform faults in the west, while extending eastwards into Syria. The GH is situated between two tectonic systems (Meiler et al., 2011; Shulman et al., 2004): (I) The Palmyride fold Belt, a 400 km long transpressive belt, which has been subjected to compression and episodic uplift since the Cretaceous and formed the synclinal structure of the Golan. (II) The Dead Sea Transform (DST), a plate boundary between the Arabian (east) and African (west) plates, which have been active since the Miocene. The Palmyride fold belt strikes obliquely to the DST resulting in a sinistral movement at its northern part, which formed the uplifted structure of Mt. Hermon (Heimann et al., 1990). The DST also branches into two major faults in the Golan Heights, the Shamir and Sheikh-Ali faults (Fig. 1.2), while another divergent fault is assumed to be located beneath the Yarmouk Gorge (Roded et al., 2013).

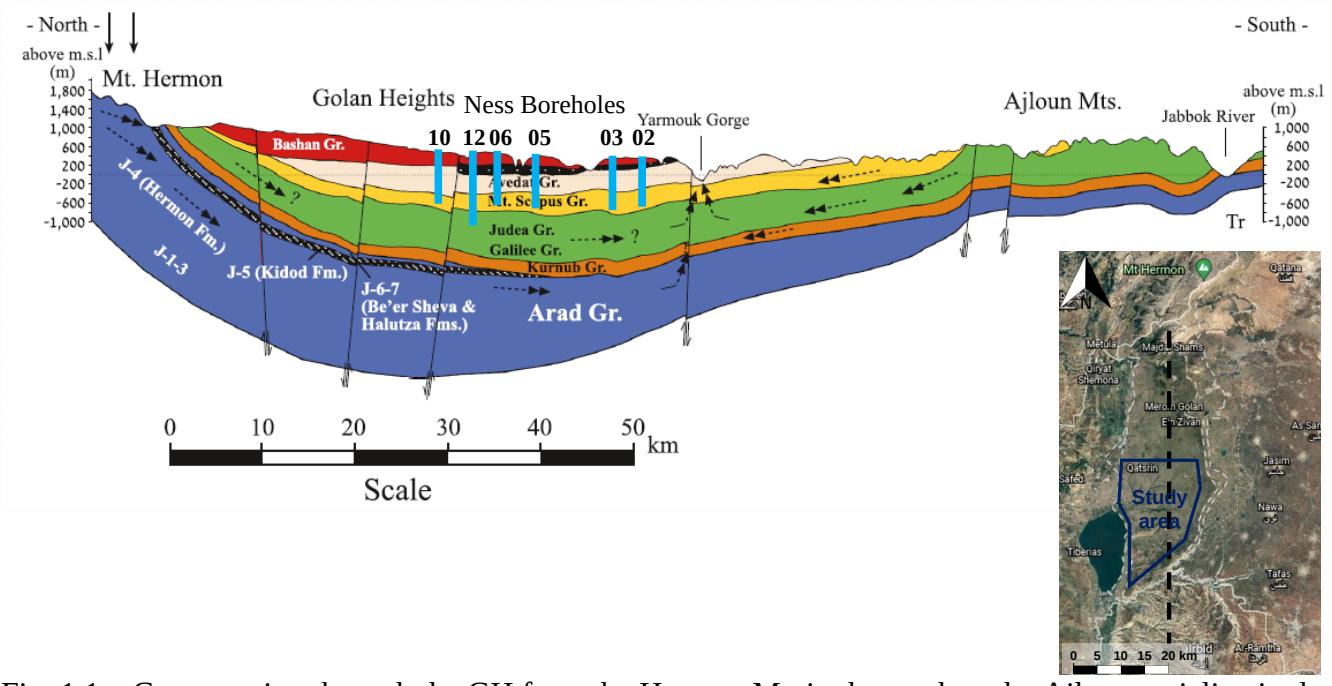

Fig. 1.1 – Cross section through the GH from the Hermon Mt. in the north to the Ajloun anticline in the south and the location of Ness boreholes. Modified after Burg and Gev (2019).

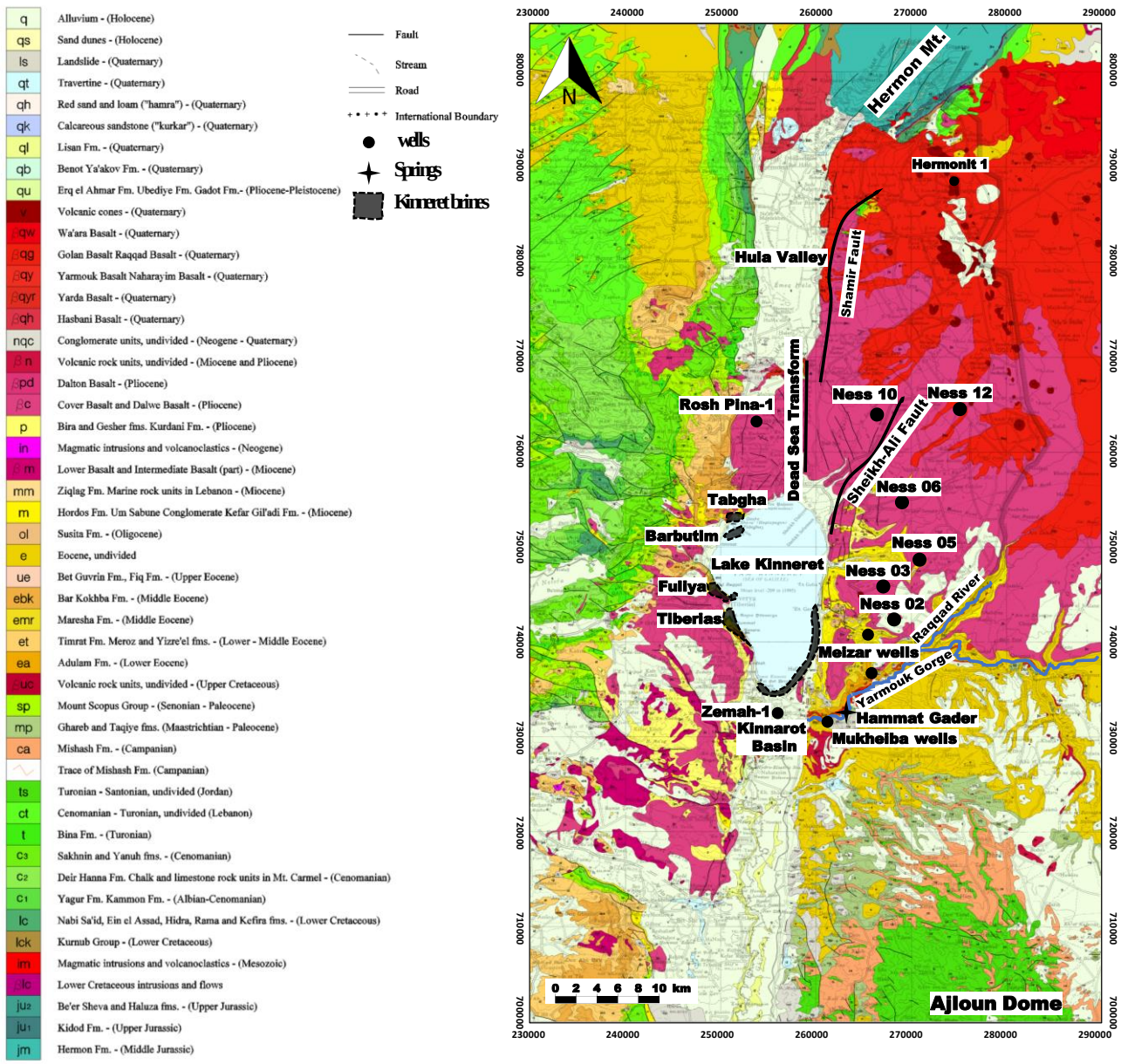

Fig. 1.2 – Geological map of the study area and locations of wells and saline water bodies. Modified after Sneh et al. (1998). The Mt. Scopus Group outcrops on the eastern side of the Dead Sea rift is limited to the remote Palmyra mountain range in Syria (> 1,000 km^2), to the slopes of the Hermon Mt. (<10 km^2) (Michelson, 1979) and to the slopes of the Ajloun dome, which is considered to be a separated hydrological unit from the Golan Heights (>300 km^2) (Margane et al., 2002).

During most of the Phanerozoic, the GH region was a sedimentary depocenter, which accumulated over 6 km of sediments, mostly carbonates. The synclinal structure of the GH was formed during the Late Cretaceous-Cenozoic while major deformation of the region resulted from the activity of the DST since

the Miocene. The recent volcanic activity in the region also began during the Miocene and enabled to measure the displacement on the DST, as basalts of the same age (15.5 ma) were displaced by 20 km (Shaliv, 1991). The GH was then covered by numerous basaltic flows during the Pliocene-Pleistocene, that erupted during two additional volcanic phases (Mor, 1993; Sneh and Weinberger, 2003). The basalts cover most of the surface of the GH and the sedimentary section underlying them is only exposed at the slopes of the Hermon and Ajloun anticlines.

On top of the Hermon anticline, a thick section of Triassic and Jurassic rocks constitutes most of the surface, while younger sedimentary units are exposed at long narrow strip along the southern flanks of the anticline (Fig. 1.2). The exposed section in the Hermon anticline includes the Kurnub, Judea, Mt. Scopus and Avedat Groups from Lower-Cretaceous to Eocene (Michelson, 1979; Sneh et al., 1998) The exposed section on the top of the Ajloun anticline includes the Judea and Mt. Scopus Groups, while at the slopes of the Ajloun anticline and towards the Yarmouk Gorge, rocks from Avedat Group (Eocene) are exposed (Fig. 1.2).

1.2 Stratigraphy

The Lower Mesozoic section includes the Arad Group from the Jurassic period, which is composed mostly of limestone and dolomite and contains developed karst, the formation thickens from the Ajloun region towards the North (Meiler et al., 2011; Sneh et al., 1998).

The Judea Group from Lower Cretaceous is composed mostly of karstic dolomite and limestone and appears to be relatively constant in thickness and lithology at the GH region.

The Mt. Scopus Group from Senonian-Early Eocene include the Menuha, Mishash, Ghareb and Taqiya formations (base to top, respectively) which are composed of chalk, chert and phosphate which are partly highly rich in organic material (kerogen and bitumen). The Mt. Scopus Group was deposited in a geological structure strongly affected by the Palmyride fold belt, resulting in sharp facial changes and thickness variations (Mimran et al., 1985). The thickness of Mt. Scopus Group at the southern flanks of the Hermon anticline is only 60 m while 10 km south, at the Hermonit 1 well (Fig. 1.2), the Mt. Scopus Group section is 215 m thick (Guttman, 2018). The group thickens dramatically at the center of the syncline and reaches a maximum thickness of over 500 m at the Yarmouk Gorge area (in the Meizar wells). Southwards from the Yarmouk Gorge, the thickness decreases gradually towards the outcrops of the group at the northern slopes of the Ajloun, where it reaches a minimal thickness of around 200 m (Margane et al., 1999).

Overlying the Mt. Scopus Group is the Avedat Group from Eocene. The Avedat Group appears in two different facies; at the northern GH, the Avedat Group includes the Adulam and Bar-Kokhba Formations, which are composed of limestone, and south of Shamir, the Avedat Group includes the Adulam and Maresha Formations, which are composed mostly of soft chalk (Sneh and Weinberger, 2003).

The top of the geological section includes the Saqiya Group from the Late Miocene (Fiq and Hordos Formations), which are composed of conglomerates and marls, the Saqiya Group was deposited after the DST formed a tectonic depression at the western margins of the GH and therefore, it exhibits significant thickness variations, and in some parts of the GH the group is missing from the section (Michelson et al., 1986). The Hordos Formation is also related to the early volcanism along the DST, which filled the local basins as they began to form (Shaliv, 1991).

The top of the sedimentary section of the GH is marked by thick basaltic flows from the Pliocene-Pleistocene. The Cover Basalt covers most of the surface of the southern GH (Fig. 1.2). The volcanic flows of the Cover Basalts are 5.5 in the southern GH and have younger ages towards north, the northernmost and youngest age is 3 ma (Heimann et al., 1996). In the northern GH, younger basaltic flows from the Pliocene (the Golan Group) overly the Cover Basalt.

1.3 Hydrogeological background

The stratigraphic column outcropped at the Hermon-Golan-Ajloun was divided into several hydrogeological units according to the lithological variations (Bein and Burg, 2003; Margane et al., 2002; Michelson, 1979; TAHAL, 1989). Several hydrogeological units in the region were identified as producible aquifers, separated by aquiclude and aquitard units (Table 1.1).

The main aquifer in the GH region is the Basaltic aquifer, which is divided into sub-aquifers, recharged directly by local precipitation. The Basaltic aquifer is considered to be relatively isolated from other hydrogeological units, as no major leakage was traced from the aquifer to others or oppositely (Dafny et al., 2006).

Another aquifer known from the northern GH is the Jurassic aquifer, which is recharged by direct precipitation on top of the Arad Group outcrops of Mt. Hermon (Fig. 1.1). At the GH, the aquifer is exploited by several wells along the Shamir fault, but beneath the GH the flow in the aquifer is only estimated (Burg and Gev, 2019). In fact, due to the lack of representative samples and other information about the systems, the deep hydrogeological units of the GH are not well understood.

The deep hydrogeological units in the GH are hydraulically bounded from west by the clayey filling of the DST. From south, the Yarmouk Gorge is thought to be located at an area of higher vertical permeability zone, possibly from a tectonic origin, through which water are rising from the deep hydrogeological units of Jurassic-Eocene. The water flowing from the GH mix with water precipitated at the northern Ajloun and discharges into several springs along the Lower Yarmouk Gorge (Fig. 1.1), some of which are geothermal, as the Hammat Gader hot springs (Fig. 1.2). The Yarmouk Gorge therefore serves as a water divide between the Golan and Ajloun, and the most probable discharge area of the deep aquifers in the southern GH (Bein and Burg, , 2003; Roded et al., 2013). Several studies have attempted to assess the relative contribution of each hydrogeological unit to the water outflow of the springs along the Yarmouk Gorge (Arad and Bein, 1986; Siebert et al., 2014; Starinsky et al., 1979) but conclusions remained indecisive.

Previous studies have classified the Mt. Scopus group in the GH as hydrogeologically undeveloped (aquicludic) systems (Bein and Burg, 2003; Dafny et al., 2003; Roded et al., 2013; TAHAL, 1989). This classification was based on lithological and hydrologic information from outcrops and analogues units in other areas. Another reason to assume that the hydrological system of the Mt. Scopus group is undeveloped is the limited area of outcrops available for direct recharge (Fig. 1.2).

The Mt. Scopus Group hydrogeological unit is exploited by only one Israeli well, Meizar 3 which is located at the juncture between Meizar Creek and Yarmouk River (Fig. 1.2). In northern Jordan, the Mt. Scopus Group provides the main source aquifer for civil water supply and is exploited by several boreholes at the Lower Yarmouk Gorge as a joint aquifer along the Bina Formation of the Judea Group (Bajjali et al., 1997; Margane et al., 1999).

Age	Group	Formation (hydrogeological unit)	Hydrological classification
Pleistocene	Golan	Young basalts	Aquifer
Pliocene		Cover basalt	Aquifer
Late Miocene-Pliocene	Upper Saqiya	Bira/Gesher	Aquitard
Miocene	Lower Saqiya	Hordos (WC)	Aquitard
Eocene		Susita/Fiq	Aquitard
	Avedat	Maresha/Adulam (B5)	Aquitard
Paleocene	Mt. Scopus	Taqia (B4)	Aquiclude
Maastrichtian		Ghareb (B2-b)	Aquitard
Campanian		Mishash (B2-a)	Aquitard
Santonian		Menuha (B1)	Aquiclude
Turonian	Judea	Bina (A5-A7)	Aquifer
Cenomanian		Sakhnin (A4)	Aquifer
		Dir Hanna (A2-A3)	Aquitard
Albian		Yagur (A1)	Aquifer
Jurassic	Arad	Haluza/ Be’er Sheva (J6/J7)	Aquitard
Jurassic	Arad	Kidod (J5)	Aquiclude
		Hermon (J4)	Aquifer

Table 1.1 – The hydrogeological units in the GH-Ajloun region.

1.4 The chemical composition of water bodies in the region

The compilation of all the compositional data is presented in Appendix 4-5.

The basaltic aquifer

The regional basaltic aquifer in the GH is divided into numerous sub aquifers, all characterized by low salinity (TDS < 550 mg/L) and a composition that reflect the dissolution of basaltic minerals (Dafny et al., 2006) . Major cations in the water are Mg^{2+}, Ca^{2+} and Sr^{2+} which are balanced mostly by HCO_3^- while containing low concentrations of Na^+, Cl^- and SO_4^{2-}. The Na/Cl and Mg/Ca ratios are close or higher than 1, reflecting on the basaltic origin. The $\delta^{18}O$ of the water ranges between -6.2‰ to -7.3‰ where these variations between sub-aquifers were associated to the elevation of the outcrops in the recharge areas (Dafny et al., 2006).The $^{87}Sr/^{86}Sr$ values of the water is mostly dictated by the value of the cover basalt, which is between 0.703-0.704 (Siebert et al., 2014).

The Jurassic aquifer

In the northern Golan Heights, water from the Jurassic aquifer is produced at the foothills of Mt. Hermon. The salinity of the water is relatively high (1,400 mg/L) and the dissolved solids in the water are derived from dissolution of Triassic-Jurassic carbonates and gypsum deposits, resulting in high Ca^{2+}, SO_4^{2-} and HCO_3^- concentrations. The $\delta^{18}O$ of the Jurassic aquifer is -7.5‰ and the δD is -38.5‰, indicating on the high recharge elevations. The $^{87}Sr/^{86}Sr$ value of the water is 0.70754 was associated with the Triassic gypsum (Babad et al., 2020; Burg and Gev, 2019).

Hammat Gader springs

The thermal spring system in Hammat Gader constitutes of five springs discharging at temperatures of 25-50 °C with a salinity that ranges between 700-1400 mg/L. The Cl^- concentrations of the water in the springs increases with temperature (Starinsky et al., 1979) and the $\delta^{18}O$ decreases slightly with temperature, from a value of -5.8‰ in the least saline spring to a value of -6.4‰ in the warmest and most saline spring (Gavrieli and Burg, 2002). The three warmest and most saline springs have low Na/Cl ratios (<0.8) and low Mg/Ca ratios (<0.5). The $^{87}Sr/^{86}Sr$ in all the springs is similar and varies between 0.70772-0.70782 (Farber et al., 2007).

Meizar 3 well

The water produced from the Mt. Scopus Group in Meizar 3 well are characterized by relatively low salinities (TDS < 700 mg/L). The water composition shows similarity to the basaltic aquifer with high

concentrations of HCO_3^-, Mg^{2+} and Ca^{2+} and Na/Cl ratio higher than 1. The $\delta^{18}O$ of the water is -6‰±0.2‰ and the δD is -33‰±2‰ which are similar to water discharging from Hammat Gader springs. The $^{87}Sr/^{86}Sr$ of the water in Meizar 3 is 0.70765, which is significantly higher than the basaltic ratio (Gavrieli and Burg, 2002)

Meizar 2 well

The Meizar 2 well produces water from the Judea Group aquifer at an exceptionally warm temperature of 64°C and at a TDS of 1,400 mg/L, which is significantly more saline than the water produced from Meizar 3 well. The water from Meizar 2 well contain high concentrations of Na^+, Ca^{2+} and Cl^- with a Na/Cl ratio of ~0.85 and Mg/Ca ratio of ~0.4 (Gavrieli and Burg, 2002). Therefore, the composition is distinctly different from the Meizar 3 well and the basaltic aquifer. The water from Meizar 2 well also exhibits a $\delta^{18}O$ of -7.2‰ and therefore it is considered depleted in comparison to other sources in the Yarmouk gorge. $^{87}Sr/^{86}Sr$ are 0.70782, which is higher than the value of the host rocks (0.70737). The composition of the water shows variations over the years as a result of local subtractions or a malfunction in the well which causes the inflow of water from overlying aquifers (Siebert et al., 2014).

The Kinneret brines

Saline water bodies surrounding the Kinneret were characterized by previous work as the derivatives of Dead Sea Rift brines (Starinsky, 1974). The DSR brines surrounding the Kinneret are found in a wide salinity range, between ~2,000 mg/L to ~40,000 mg/L which reflects different degrees of dilution by freshwater. North of the Kinneret lake, a hypersaline brine with a salinity of 172,000 mg/L was found in the deep Rosh Pina-1 borehole (RP brine), at a depth of 3,850 m BGL. The Kinneret brines are characterized by a Ca-chloride composition, where the equivalent concentration of Ca^{2+} is larger than the sum (SO_4^{2-}+HCO_3^-), the brines are also characterized Na/Cl ratios of 0.5-0.75, lower than the marine value (0.86). The brines found west of the Kinneret lake and at Rosh Pina-1 differ from the brines found east of the Kinneret lake by the Mg/Ca and Sr/Ca ratios, the brines from the west have low Mg/Ca (<0.6) and Sr/Ca ratios (<0.01) while brines from the east have high Mg/Ca (2.7-3) and Sr/Ca (0.02-0.05) ratios.

The high initial salinity of the original brines was at least 200,000 mg/L, which is the threshold required for the precipitation of halite (Katz and Starinsky, 2009).Therefore, the brines have been diluted by freshwater while retaining the ion ratios of the original hypersaline end-member. Previous work related the low Na/Cl and Mg/Ca ratios found in the warmest springs of Hammat Gader to the traces of highly diluted brines. The initially low SO_4^{2-} and HCO_3^- in the brines relative to the freshwater diluting it masked

the Ca-chloride composition (Ca^{2+} > (HCO_3^-+SO_4^{2-})), but the original Na/Cl and Mg/Ca ratios are still controlled by minor traces of the brines in the water (Siebert et al., 2014; Starinsky et al., 1979).

1.5 Research purpose

One of the main challenges in studying deep hydrogeological systems, such as the Mt. Scopus Group in the GH, is attaining representative samples and information from inaccessible depths. The information acquired from Ness boreholes included water samples and hydrological information abstracted from different layers and different boreholes, and other valuable information from one of the least studied hydrogeological systems of the GH. The information on which this work was based, enabled to understand some of the processes in deep aquitards-aquicluds systems, and to demonstrate the strong relationship between the hydraulic properties and the composition of the water they contain, to the regional geological history.

2. Methods

2.1 Sampling

Water samples from Ness 02, Ness 03 and Ness 12 boreholes were collected by Afek between November 2014 to August 2016. The water samples were collected both during drilling operations and during Drill Stem Tests (DSTs) which were performed after the well has been completed (cased and cemented).

Drill Stem Tests

Between March-May 2016, eight DSTs were conducted in Ness 02 and Ness 03 boreholes. The DSTs were performed in eight different zones, each zone targeted a 15 m interval within the Mishash, Ghareb and Taqiye Formations. The DSTs included pressure measurements which allowed to derive the hydraulic head as well as the apparent of a given 15 m interval. The main makeup fluid used between tests for circulating purposes as well as pressure testing operations was a 3% KCl solution therefore resulting in some unwanted fluids in the wellbore which initially contaminated the produced formation fluids. Moreover, various reservoir stimulation techniques were carried out where acid, solvent, and surfactant were injected into the formation, to enhance fluid production rates. These operations led to the contamination of the majority of collected samples. However, since the water produced throughout the tests were monitored every 15 minutes for EC and Temperature, it was possible to carefully select the least contaminated samples, as detailed below. Fluid production during the DSTs was performed by either one of the following methods: (a) N_2 lift, which allowed continuous production at a relatively high rate in comparison with (b) Mechanical swabbing, which allowed fluid samples to be collected without diluting the associated gas. Regardless of the implemented production method, water was collected and rapidly sealed in glass bottles to minimize degassing and interaction with atmospheric gases.

Drilling

Water samples were collected from different intervals of the open section during the drilling operations of Ness 02 and Ness 12, both of which were drilled underbalanced (Under Balanced Drilling- UBD), to allow inflow of water to the borehole (opposite with overbalanced drilling where drilling fluids are normally lost to the formation, which usually contaminate the formation fluids when they are back produced). Even though drilling was performed underbalanced, some drilling fluids, predominantly a 3% KCl solution, still contaminated to a certain degree the near wellbore environment as well as the formation fluids in part. Therefore, prior to each sampling, few unloading attempts were carried out (by airlift), in order to minimize the presence of drilling fluids in the well. The unloading was performed by

straight circulation injection of compressed air through the drill pipe and production of water via the annular space between the casing and drill pipe. This was performed as a stepwise procedure where water was initially removed from a depth slightly deeper than the equilibrated hydrostatic level. Following each unloading cycle, the depth of the drill pipe was incrementally increased by gradually tripping in and producing an additional water volume. Samples were collected during the final stages of the airlift.

2.2 Analysis

Onsite measurements of the produced liquids included EC, temperature and pH every 15 minutes. Following the measurement of the field parameters, water samples were collected in sealed glass bottles at 15 minutes intervals. Samples were analyzed at the Geological Survey of Israel for major ions, trace elements, $\delta^{18}O$, δD and $^{87}Sr/^{86}Sr$ both during exploration but also during the course of the current research, after the samples have been stored for 3 years.

Major cations and sulfate (Na^+, K^+, Ca^{2+}, Mg^{2+}, Sr^{2+}, SO_4^{2-})

Major cations and sulfate were measured by Inductively Coupled Plasma Optical Emission Spectrometry (ICP-OES, Optima 3300, Perkin Elmer). Samples were acidized using HNO_3 and 5 ppm Scandium was used as an internal standard. The measurement precision (1σ) is ±2% for all cations and ±5% for SO_4^{2-}.

Chlorides and alkalinity

The sum of Cl^- and Br^- was measured using automated potentiometric titration with $AgNO_3$ (702 SM Titrino, Methorn). Alkalinity was measured using titration with 0.05 N HCl up to a pH of ~4.5. This was done either by automatic titration (785 DMP Titrino, Methorn) or manually, using a pH meter. Calibration for all the devices was performed before and after the analysis and verified every 10 samples using standards. The precision (1σ) for both chloride and alkalinity measurements was ±2%.

Bromine

The concentration of Br^- was determined using Ion Chromatograph (IC, ICS-200, Dionex). The Cl^- concentrations was determined by subtracting the Br^- concentration from the sum of Cl^- and Br^- which was measured using potentiometric titration. The Br^- measurement precision (1σ) is ±5%.

Stable oxygen and hydrogen isotopes ($\delta^{18}O$, δD)

Stable oxygen (^{18}O) and hydrogen (Deuterium) isotopes ($\delta^{18}O$, δD) were analyzed using Isotope Ratio Mass Spectrometer (IRMS, Delta plus XP, Thermo Finnigan). Prior to the measurement, a 200 µl water sample was kept in contact for 48 hours with helium (99.5%) and 0.5% CO_2 gas mixture during which

the water isotopic composition was exchanged with CO_2 according to the following reaction: $CO_2 + H_2O \rightleftharpoons H_2CO_3$. The oxygen isotopic composition was than measured and corrected to Vienna Standard Mean Ocean Water (V-SMOW). Hydrogen was converted into H_2 gas by pyrolysis at 1400°C, gas and then subsequently measured for its isotopic composition using both IRMS and GC. Values were corrected to V-SMOW standard as well. Precision (1σ) for $\delta^{18}O$ and δD are ±0.1% and ±1%, respectively.

Strontium isotopes ($^{87}Sr/^{86}Sr$)

Isotopic composition of Sr was measured using Multi-collector Inductively Coupled Plasma Mass Spectrometer (MC-ICPMS, Nu Plasma-I, Wrexham, UK). Following the ICP-OES Sr^{2+} concentration measurement, the Sr^{2+} was separated from solution using columns that contained Eichrom-Sr-Resin (50-100 mesh). The $^{87}Sr/^{86}Sr$ ratio of the extracted Sr^{2+} was subsequently measured and corrected using a standard (SRM-987 55 ppb), that was measured before and after the analysis and every 3 samples. Each result was corrected using the standard that was measured within the closest time proximity. Precision (1σ) for $^{87}Sr/^{86}Sr$ is ±0.0025‰.

Reaction Error

Reaction Error (RE) was calculated in % as the difference between the sum of cations to anions, divided by the sum of all ions, all in $meq \cdot L^{-1}$. A threshold RE value of ±3% was used, above which the measurements were either repeated or eliminated.

3. Results

3.1 Mt. Scopus Group in the Ness boreholes

The geological sequence of the southern Golan exhibits both complex stratigraphic and structural features. The sedimentary units of the Late Cretaceous to Eocene characterize deep marine depositional environment, which has shifted during the Oligocene to a terrestrial depositional environment. Overlying the sedimentary sequence are numerous basaltic flows from two major volcanic events that occurred during the Late Pliocene- Pleistocene (Mor, 1993). The southern Golan Heights basin is divided by a differential branching fault (Sheikh Ali Fault, Fig. 3.1) extending from the Dead Sea rift to the North-East where it decays (Meiler et al., 2011; Reznik and Bartov, 2021). In the southern up-thrown block, 5 wells were drilled (Ness 02, 03, 05, 06, 12, Figs. 3.2-3.6, respectively), while in the northern down-thrown block, only one well was drilled (Ness 10, Fig. 3.7). The resulting offset due to the vertical displacement caused by the Sheikh Ali Fault between the southern and northern blocks, as well as the southern Golan Heights synclinal structure of the Mt. Scopus group is presented in Fig. 3.8. The syncline depo-center is situated nearby Ness 03. The syncline folds upwards both northward and southward from Ness 03, with a steeper flexure southward. Despite the syncline structure in the southern block which leads to elevation variations of the Mt. Scopus group base and top, the most significant elevation change occurs due to the throw across the Sheik Ali Fault (in the order of 900 m). The thickness and facies change variations in the Mt. Scopus group are not significant throughout the basin. The variations in the thickness of the Taqiye Formation is between 110 m (in Ness 12) and 150 in Ness 02 and Ness 03 (Figs. 3.2-3.3), the Ghareb Formation is the thickest in Ness 10 (150 m, Fig. 3.7), while thinning southward to 100 m in Ness 02. The base of the Lower Mishash Formation was not reaches by all boreholes, but there seem to be a slight thickening southward, from 180 m in Ness 12 (Figs. 3.6) to 215-230 in Ness 02, Ness 03 and Ness 05 (Figs. 3.2-3.4).

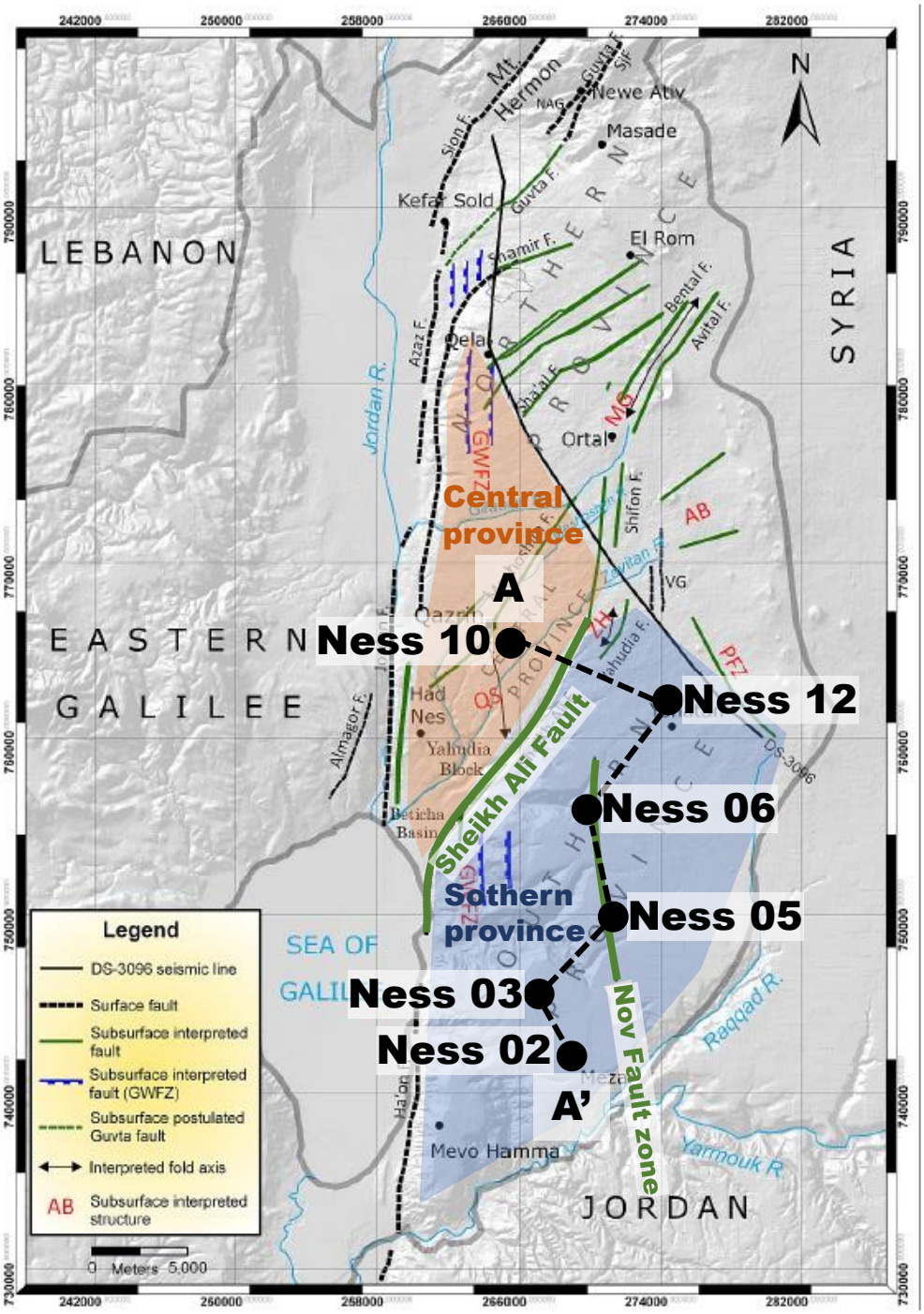

Fig. 3.1 – Location map of Ness boreholes along with the main faults as outlined by Meiler, 2011. A-A' denotes the cross section between the Ness wells (Fig. 3.8).

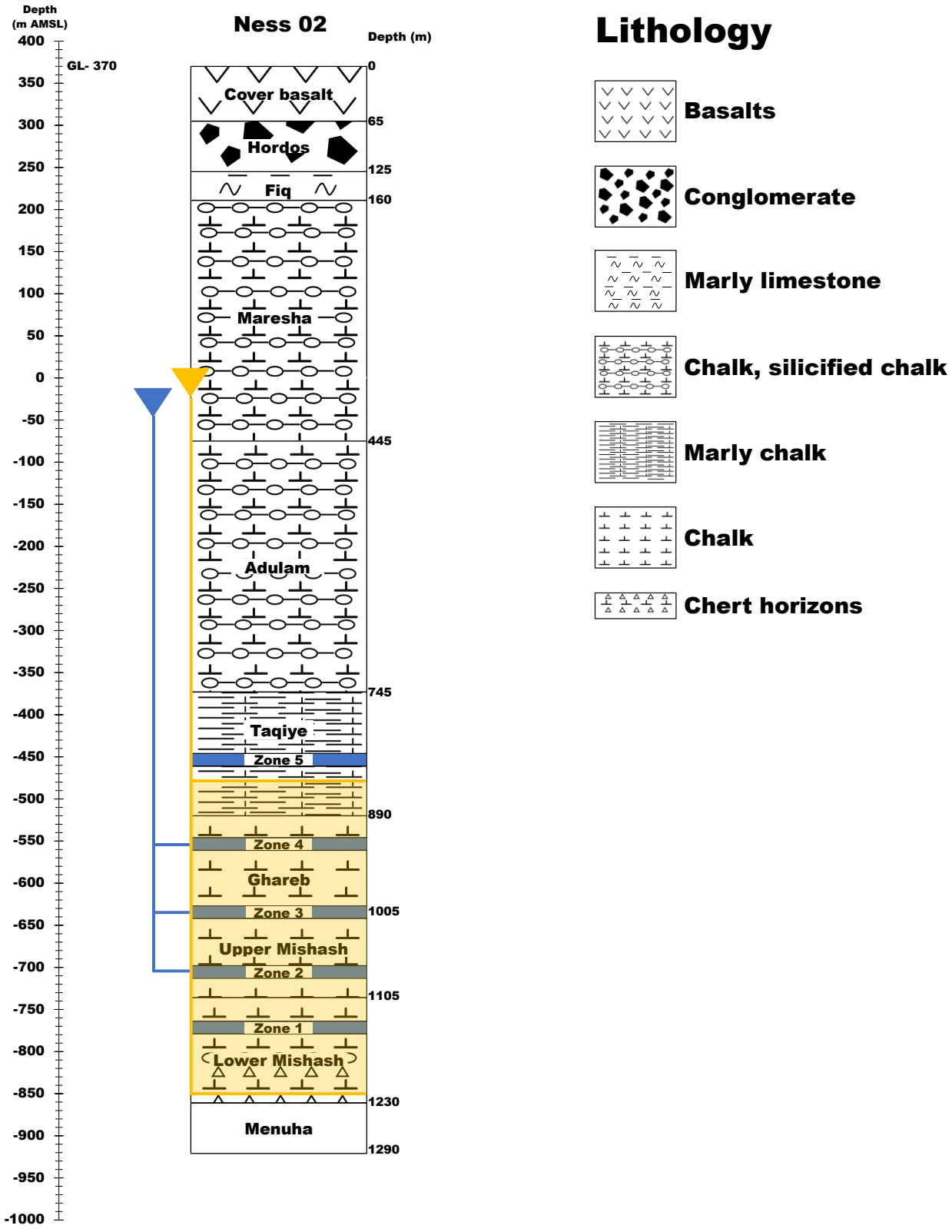

Fig. 3.2 – General lithological section of Ness 02 borehole. The tested targeted Drill Stem Test (DST) intervals are labeled as Zones 1-3. The DST derived hydrostatic water levels are shown in blue triangles. The open section (850-1223 m BGL) during water level measurement (yellow triangle) and sample collection is highlighted in yellow.

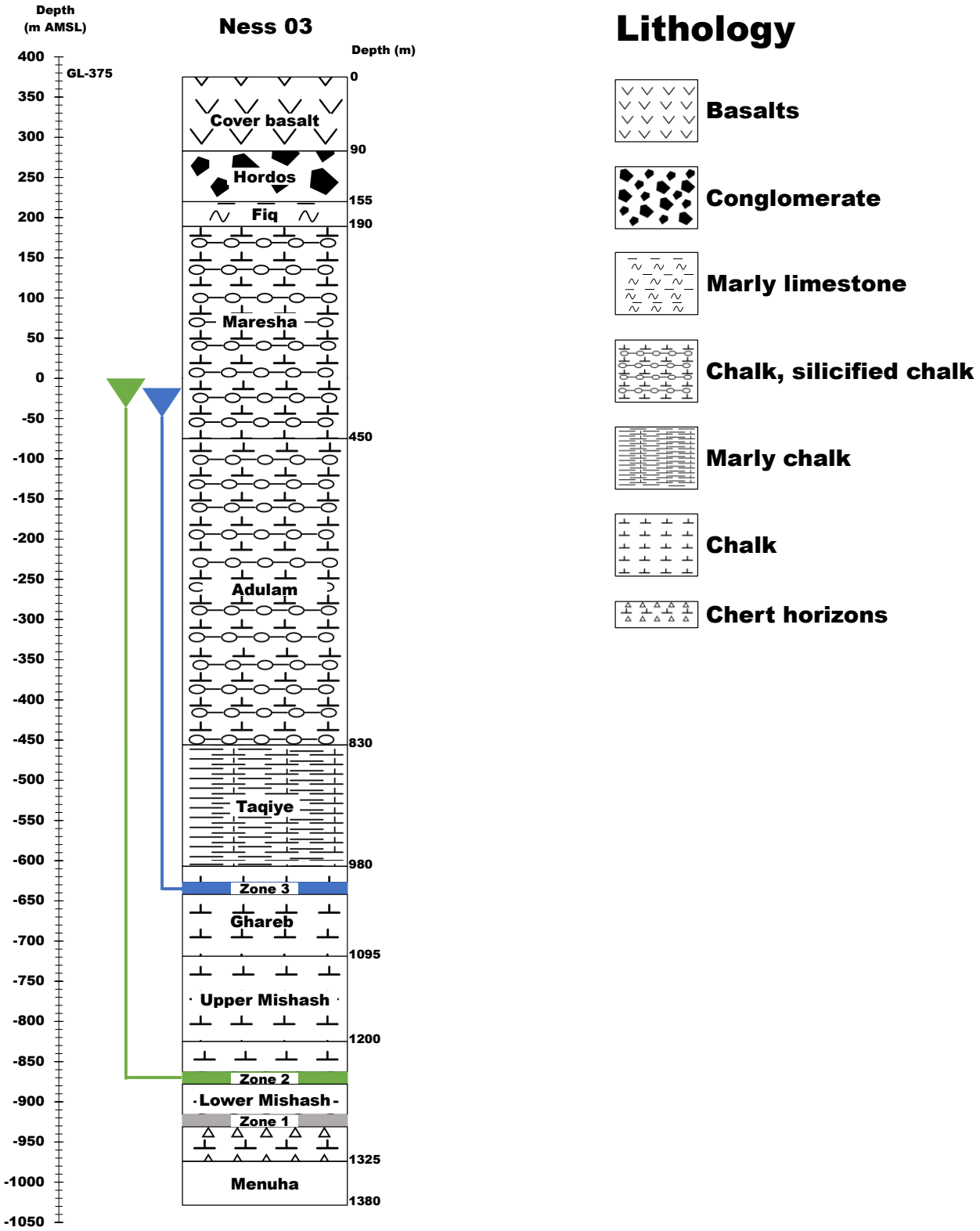

Fig. 3.3 – General lithological section of Ness 03 borehole. The tested targeted Drill Stem Test (DST) intervals are labeled as Zones 1-3. The DST derived hydrostatic water levels are shown in blue triangles.

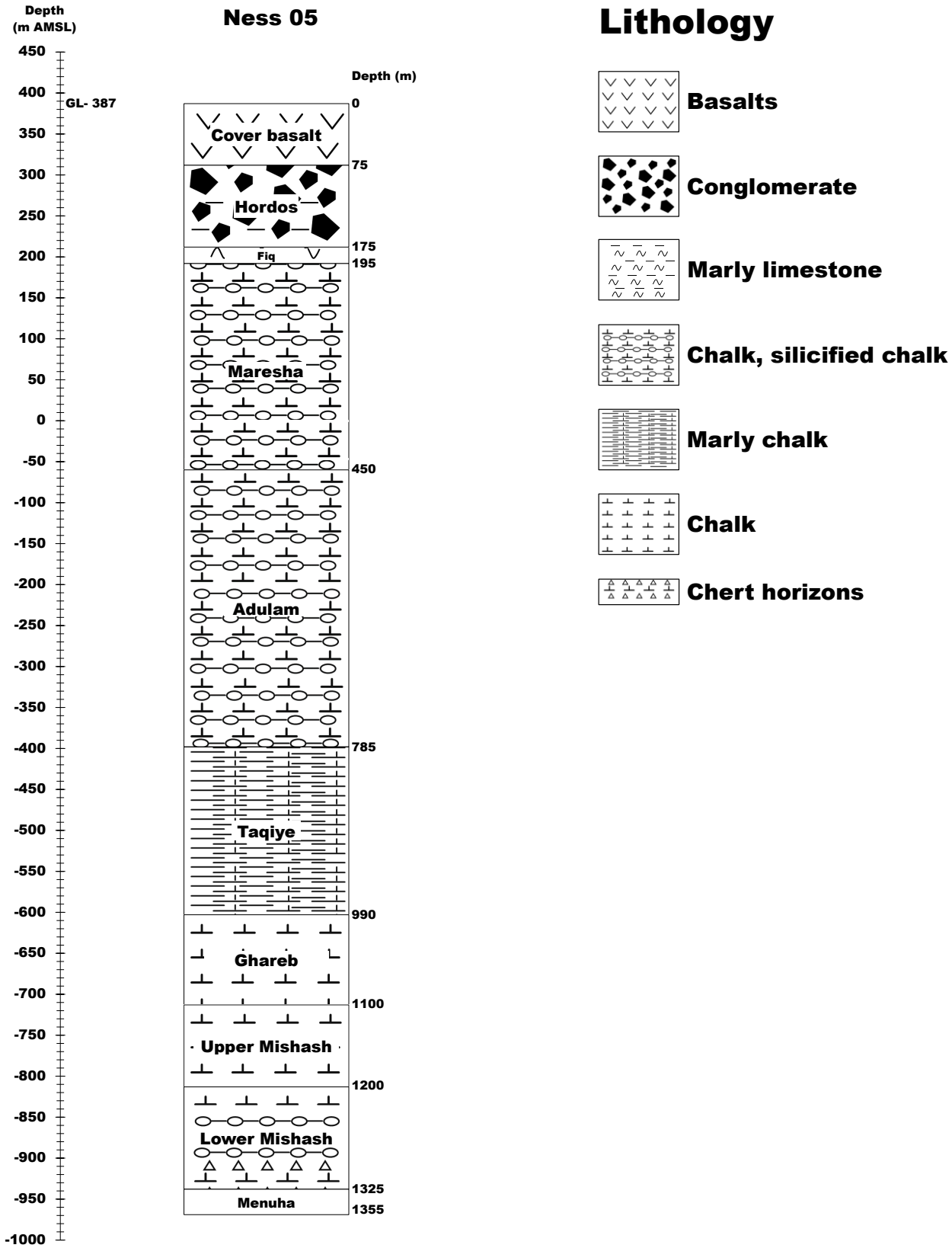

Fig. 3.4- General lithological section of Ness 05 borehole.

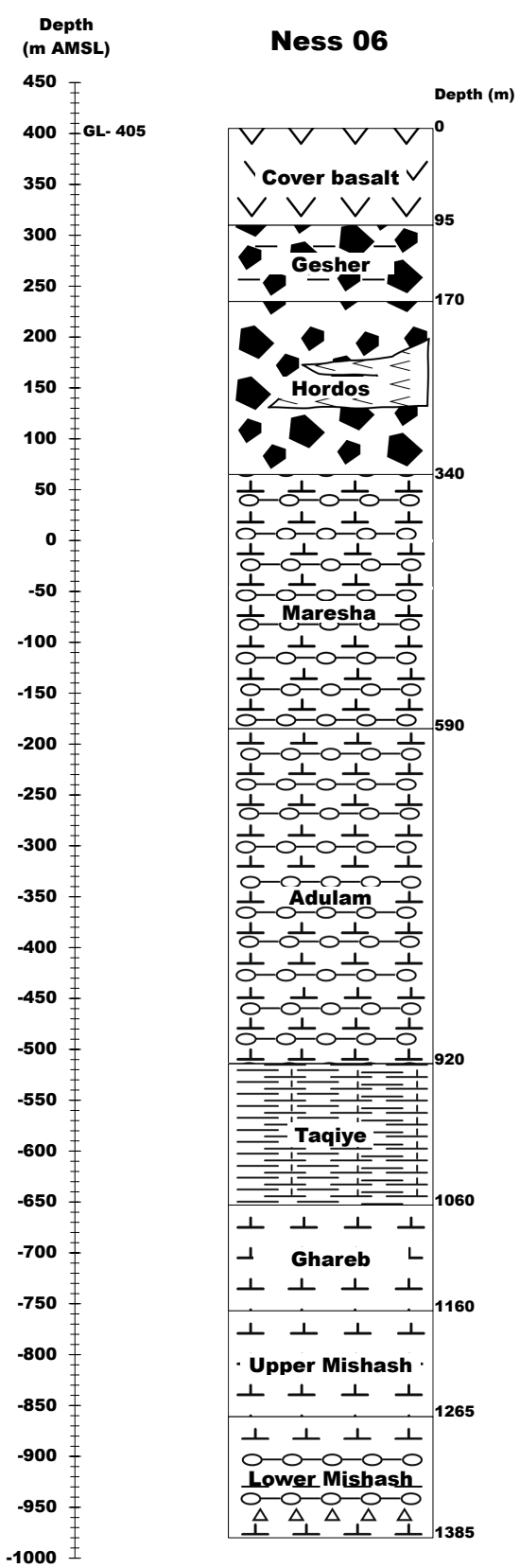

Fig. 3.5- General lithological section of Ness 06 borehole.

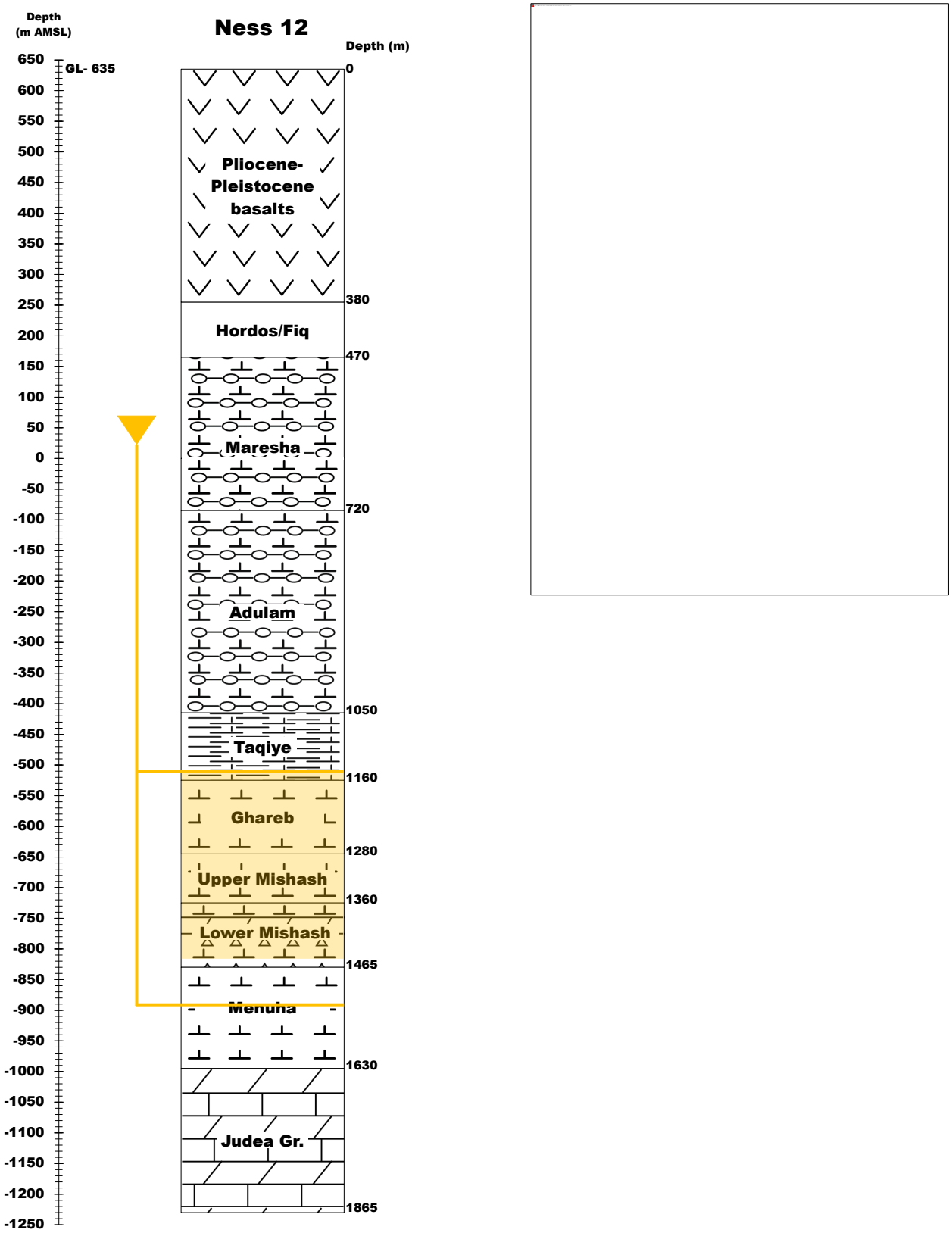

Fig. 3.6 - General lithological section of Ness 12 borehole. Open section during collection of unloading sample (1146.5-1400 m BGL) is highlighted in yellow. The water level (yellow triangle) was measured after an additional drilling of 130 m (yellow line).

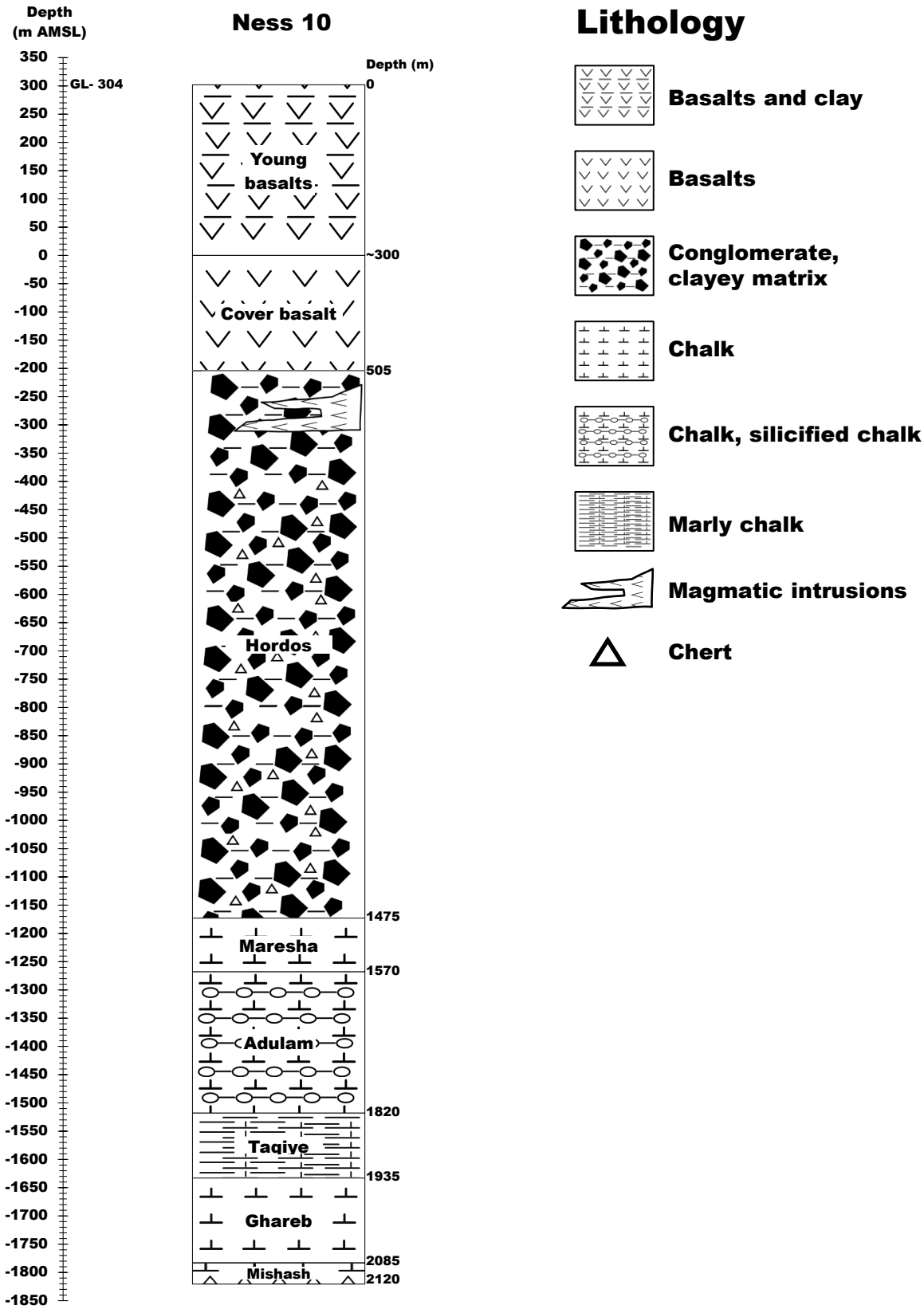

Fig. 3.7 - General lithological section of Ness 10 borehole.

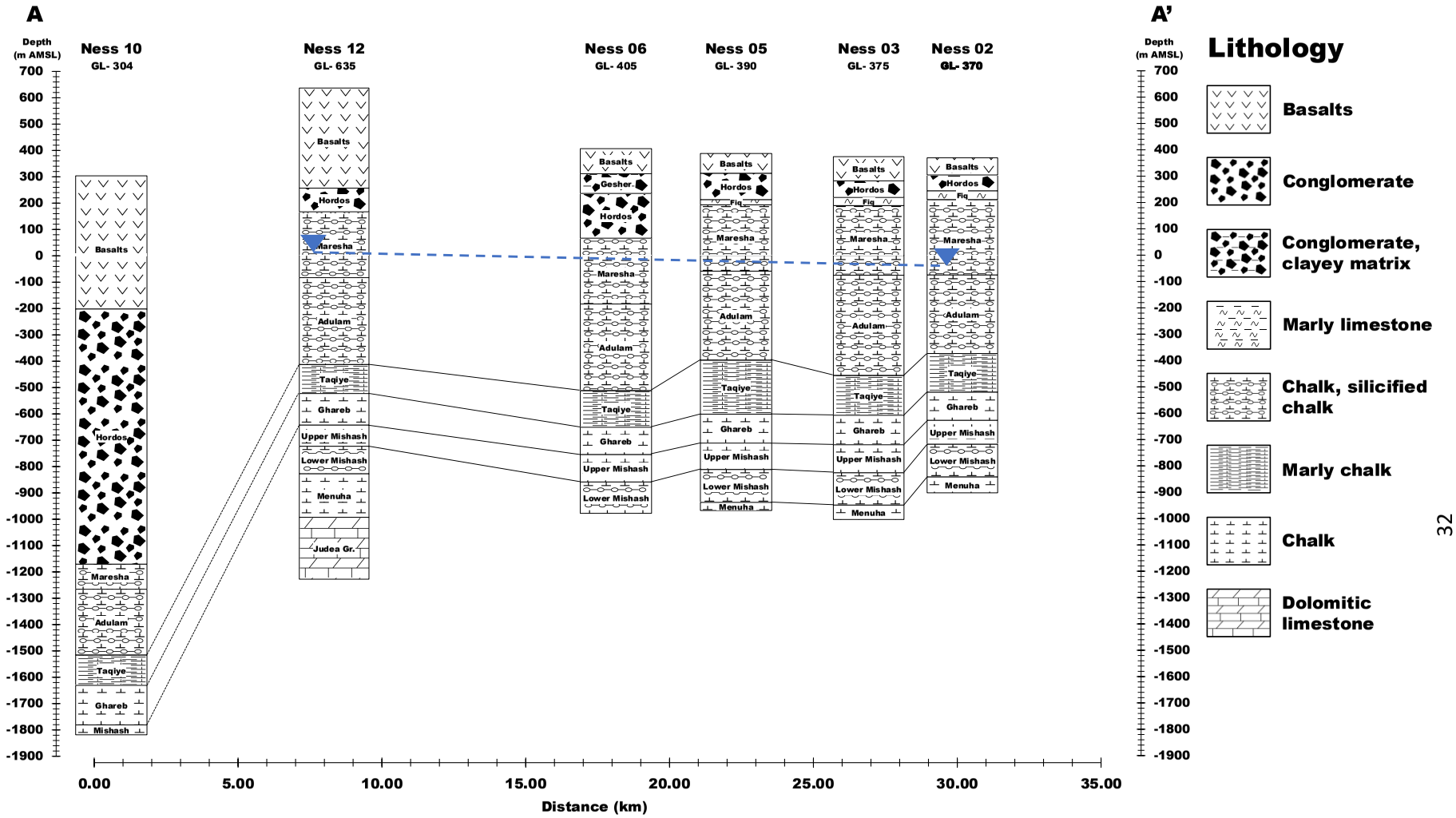

Fig. 3.8 – Generalized lithological cross section from Ness 02 to Ness 10 (A-A'in Fig 3.1). Blue triangles represent measured water levels of the Mt. Scopus Group open section. The measured water levels (explained below) account for an apparent hydraulic gradient of ~2 m/km.

3.2 Drill Stem Tests – hydrostatic pressures and apparent hydraulic conductivities

Eight DSTs were performed in Ness 02 and Ness 03 boreholes. Each DST targeted a separate and isolated 15 m interval along the Mt. Scopus Group (Figs. 3.2 and 3.3). Hydrostatic pressures and hydraulic conductivities (Table 3.1) were determined based on the continuous Bottom Hole Pressure (BHP) measurements recorded throughout the DSTs by a downhole pressure gauge located at a known depth above the perforated interval. The hydrostatic pressures were determined based on a pressure stabilization periods which followed buildup tests (shut-down periods), during which the readings were constant (i.e., below a pressure change rate (dP/dT) of 0.004 barg/h).

An example of BHP measurements is given in Fig. 3.9 for the Upper Mishash Formation in Ness 02 zone 2 (BHP recordings for all zones are presented in Appendix 1). For this zone, a hydrostatic pressure of 62.6 bars was reached twice, once before acidization (20 h duration below a change rate of 0.004 barg/h) and following acidization, (more than 30 h below a change rate of 0.004 barg/h).

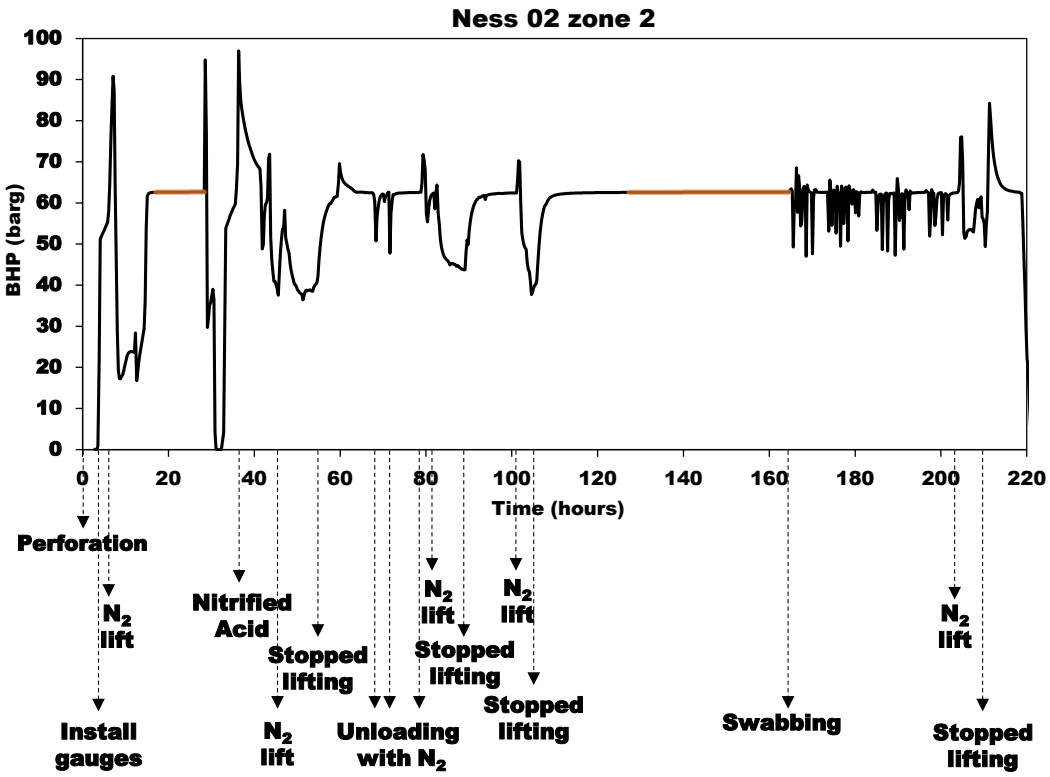

Fig. 3.9 - Bottom Hole Pressure (BHP) of the Upper Mishash Formation in Ness 02 zone 2. Stabilization periods are highlighted by solid orange lines.

Out of the eight DSTs (Fig. 3.2 and 3.3), three stabilize in terms of pressure due to a combination of low permeability and/or short buildup tests (Fig. 3.10). Therefore, hydrostatic pressures were defined for only five out of the eight zones tested.

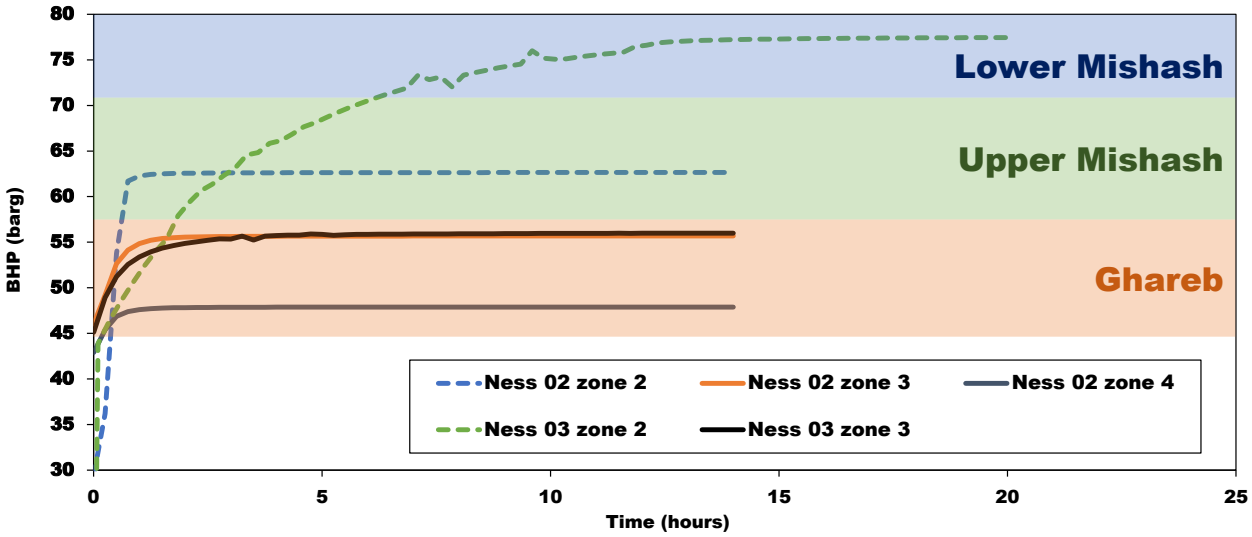

Fig 3.10 – BHP recordings of the build-up tests and pressure stabilization periods conducted for the different DSTs.

The hydrostatic pressures as a function of depth, across both the Lower Mishash and the Ghareb Formations in Ness 02 and Ness 03 are presented in Fig. 3.11. All the measured pressures are sub-hydrostatic (compare the recorded values to the hydrostatic line as well as the negative intercept of the linear regression (-63.7 m AMSL) which is significantly lower than the ground level (370-375 meters AMSL). The derived pressure gradient (9.9 bar/m) indicates that the fluid within the formation is relatively freshwater with a specific gravity of close to 1 g/cc and not brine. Furthermore, it is unlikely that the fluid contains significant amounts of oil and free gas, otherwise the density would have been significantly lower than 1.

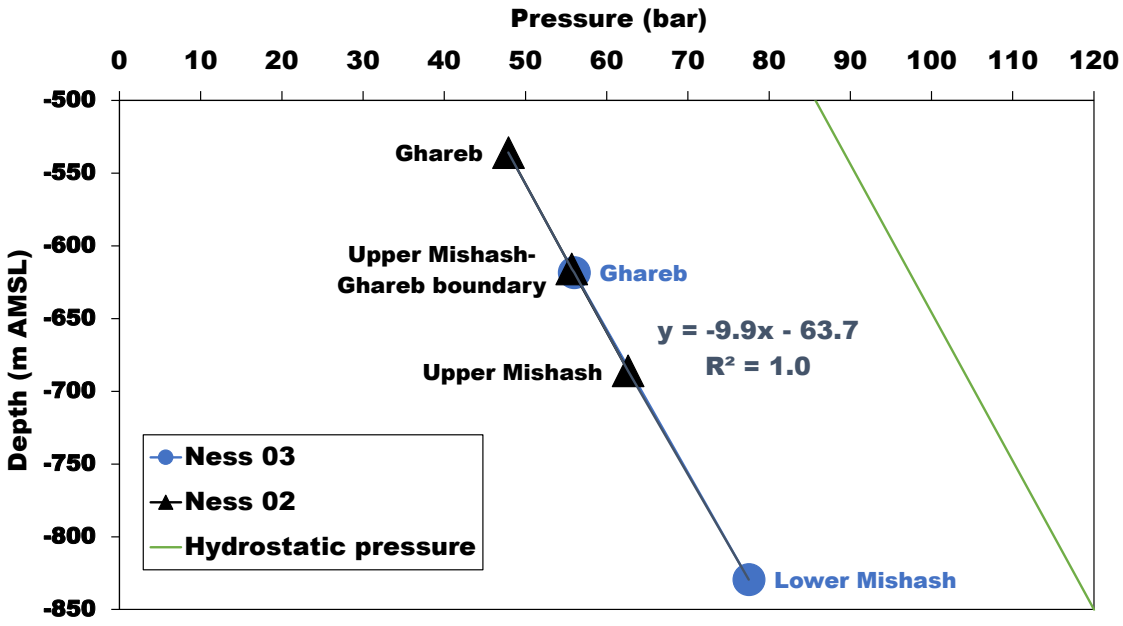

Fig. 3.11 –Hydrostatic pressures in Ness 02 (black) and Ness 03 (blue) as a function of depth (m AMSL). The linear regression is based all tested zones across 2 wells. For reference, a synthetic hydrostatic pressure curve (green) was added from the surface.

Using the hydrostatic pressure measurements, the water table elevation was calculated using the following equation: $(h\,(m) = \frac{P}{\rho g})$, where P is the hydrostatic pressure (Pa), ρ is the water density measured on the collected fluids during production periods (g/m^3), and g is the gravitational constant (9.8 m/s^2). Since the water density measurement of the collected fluids was performed at the surface following some heat loss, the density was corrected to account for Bottom Hole Temperature (BHT) using the following the equation: $\rho_T = \frac{\rho_t}{1+\beta(BHT-ST)}$ where ρ_t is the measured specific gravity, β is the thermal expansion coefficient of water which is equal to $210 \cdot 10^{-6}$ 1/°C (Urone et al., 2012). and $(BHT - ST)$ is the difference between the measured BHT and the temperature measured at the surface (ST) by a hydrometer in conjunction with the density measurement (Table 3.1). While the calculated water levels (Fig. 3.12) in the four zones performed on the Ghareb and Upper Mishash Formations were virtually the same, with an average of 47.3±0.4 m AMSL, the water level in the zone performed on the Lower Mishash Formation was significantly higher (by 9 m). Note that a slight increase in the hydrostatic water table elevation is observed as a function of depth.

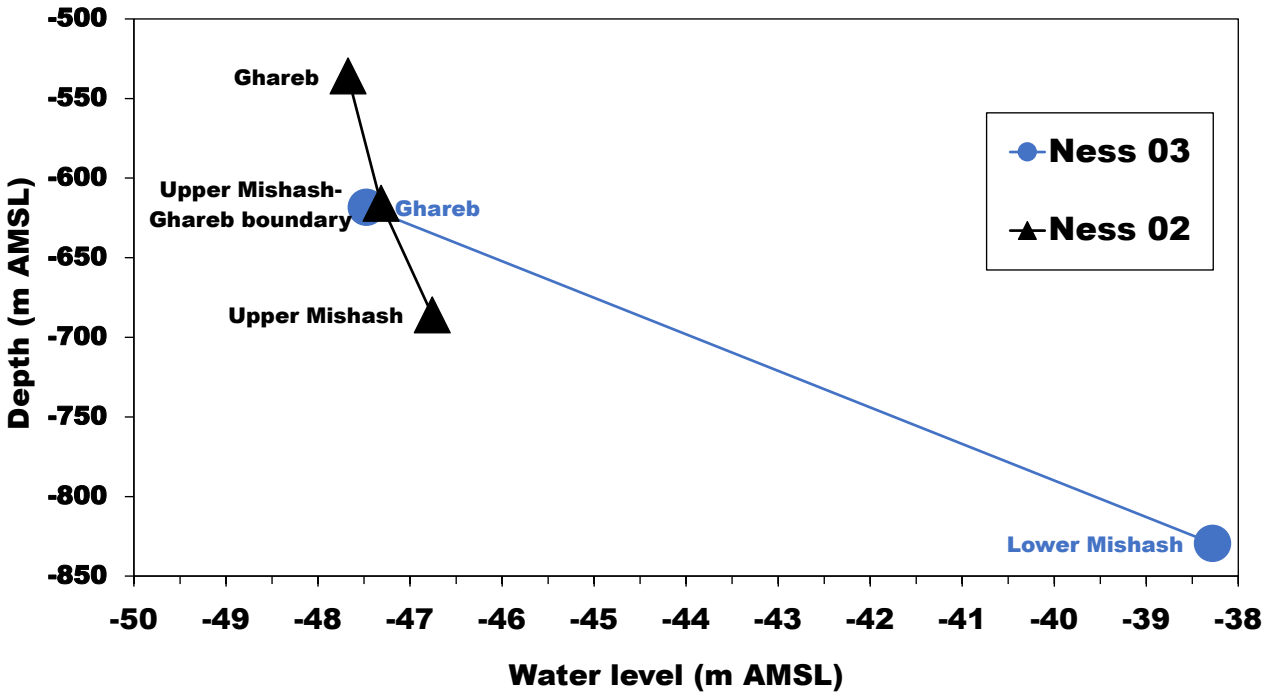

Fig 3.12 - Calculated water levels as a function of depth in the DSTs performed in Ness 02 (black) and Ness 03 (blue).

The change of pressure as a function of time presented in Fig. 3.10 highlights the permeability differences between zones. For instance, the slow recovery rates in the Lower Mishash Formation indicates low permeability of in comparison with faster recoveries in the Ghareb formation (higher permeability). Despite not reaching pressure stabilization in all the zones, the permeabilities were derived for all zones using Pressure Transient Analysis (PTA). The apparent permeability of each zone was then converted to apparent hydraulic conductivities (Table 3.1) according to the following equation: $K = \frac{k\rho g}{\mu}$ where K is the apparent hydraulic conductivity (m/s), k is the apparent permeability (Darcy), ρ is the temperature corrected water density and μ is the water viscosity (poise), fitted to the BHT of the zone (Table 3.1). The results (Fig. 3.13) indicate that the Lower Mishash and Taqiye Formation are impervious. The Upper Mishash Formation is ranges from semi-impervious to impervious while the Ghareb Formation are semi-impervious (Bear, 1972).The faster recovery rates in the Upper Mishash and Ghareb Formations (Fig. 3.10) resulted in a conductivity higher by 1-5 orders than the Lower Mishash.

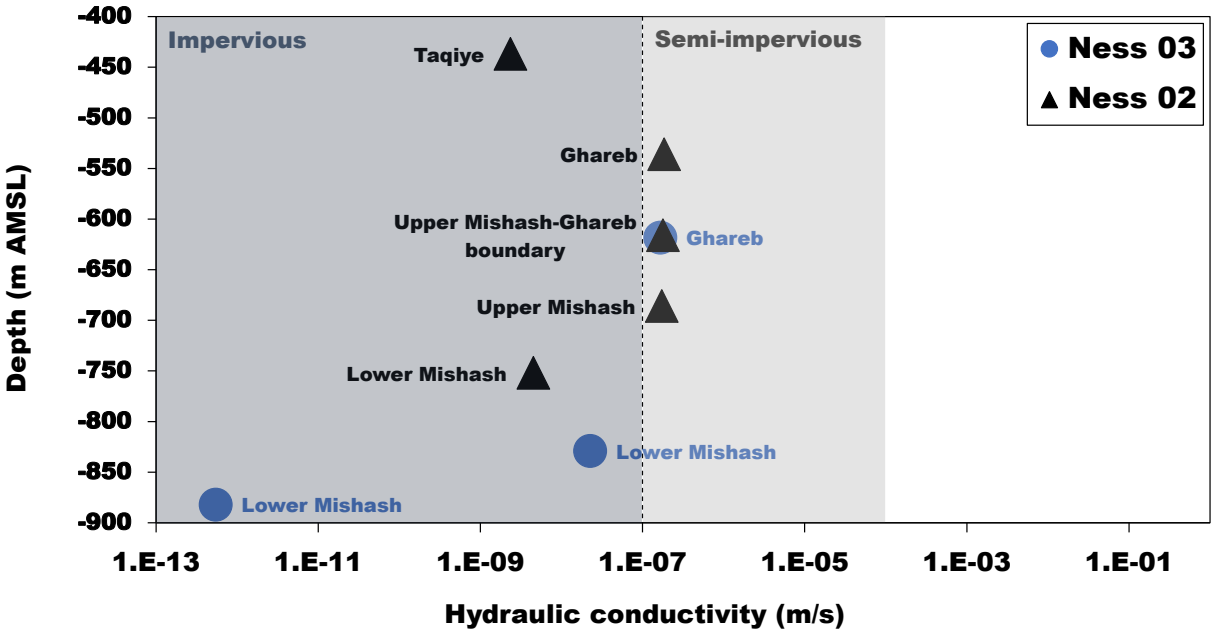

Fig. 3.13 – Apparent hydraulic conductivities of all tested zones. Hydraulic conductivity classification is based on Baer, 1972.

Borehole	Zone	Formation	Gauge depth (m BMSL)	BHT (°C)	Hydrostatic pressure (bar)	Temperature corrected density (g/cm^3)	Temperature corrected water table elevation (m)	Apparent hydraulic conductivity (m/s)
Ness 03	1	Lower Mishash	-876.6	65.2	Not determined	0.998	-	$5 \cdot 10^{-13}$
	2	Lower Mishash	-823.6	62.7	77.5	0.998	-38.3	$2 \cdot 10^{-8}$
	3	Ghareb	-612.9	53.8	56	1.000	-47.5	$2 \cdot 10^{-7}$
Ness 02	1	Lower Mishash	-752.0	64.0	Not determined	0.995	-	$4 \cdot 10^{-9}$
	2	Upper Mishash	-686.0	61.0	62.6	0.998	-46.8	$2 \cdot 10^{-7}$
	3	Mishash-Ghareb boundary	-616.0	57.5	55.7	0.998	-47.3	$2 \cdot 10^{-7}$
	4	Ghareb	-536.0	53.0	47.9	1.000	-47.7	$2 \cdot 10^{-7}$
	5	Taqiye	-437.0	50.0	Not determined	1.007	-	$2 \cdot 10^{-9}$

Table. 3.1- Summary of hydrostatic water table elevation, and apparent hydraulic conductivities based on the DST pressure measurements.

3.3 Information collected during drilling

Field observations

The Mt. Scopus Group was drilled using Under Balanced Drilling (UBD method in Ness 02, Ness 06, Ness 10 and Ness 12 During which water was produced from depths where a noticeable amount of water flowed into the well. In Ness 02, the open section started generating considerable amounts of water when the drill bit reached the Lower Mishash Formation, at a depth of ~1100 m BGL (Fig 3.2). The amount of water produced peaked at a depth of 1230 m BGL, where drilling operation stopped for sample collection. In Ness 06, the borehole generated considerable amounts of water from the Lower-Mishash Formation at a depth of 1294 m BGL (Fig. 3.3) and the drilling was converted to Over Balanced Drilling (OBD). In Ness 12 borehole, considerable amounts of water were generated from the borehole when the UBD reached a depth of 1390 m BGL, 35 m into the Lower Mishash Formation (Fig. 3.4). The drilling operation in Ness 12 stopped at a depth of 1400 m BGL for collection of unloading samples, and production continued for over 3 hours, during which a constant flow of 60 m^3/hr was reported (per ~250 m open section). The large amount of water generated from the Lower Mishash peaked at a depth of ~1450 m BGL. Due to technical and safety issues, similar operations were not conducted on the water-generating section (the Lower Mishash Formation) in Ness 06, but a rough estimation suggests that flow and recovery rates in Ness 06 are more similar to the ones recorded in Ness 12, which were significantly higher than the ones recorded in Ness 02. Significantly low recovery rates were recorded at Ness 10 when the section was open to the Mt. Scopus Group between the depths 1870-2122 m BGL (Fig. 3.5). The well was unloaded completely at the end of the drilling operation and then recovered for a duration of over 11 hours. The total volume of water produced after the recovery was only 13.2 m^3 accounting to an average recovery rate of 1.2 m^3/h per ~250 meters of open section, which is 50 times lower than the rates recorded in Ness 12, from an open section of the same thickness.

Well	Depths open (m BGL)	Formations	Estimated water flux
Ness 02	850-1230	Lower-Mishash	
Ness 06	1062-1294	Lower-Mishash	
Ness 12	1146.5-1400	Lower Mishash	60 m^3/hr per 253.5 meters

Table 3.2 - Summary of boreholes and depths upon which considerable inflows of water were encountered during UBD operations were observed.

Water level measurements

Two direct measurements of water levels were performed in Ness 02 and Ness 12 boreholes. The measurements were taken at the end of the drilling operation, at a single point in time, when a section that included the Mt. Scopus Group was open. In Ness 02 borehole, the water level was measured when the section was open between the depths 850-1223 m BGL (Upper Taqiye- Lower Mishash Formations). The measurement was taken after the initial unloading of the water column in the borehole followed by a 48-hour waiting period. The measured water level elevation was -22 m which should be regarded as a minimal elevation since it is not possible to determine whether this value represents hydrostatic conditions. The water level in Ness 12 was measured after the initial drilling operations ended, and the section was open between the depths 1146.5-1530 m BGL (Lower Taqiye- Lower Mishash Formations). The water level that was measured two days after the final unloading was at an elevation of 19 m. Similar to the water table elevation in Ness 12, this value should be regarded as a minimal elevation since it is not possible to determine whether this value represents hydrostatic conditions.

3.4 Representative sample selection

As described above, a wide range of operational fluids (Table 3.3) were used during the DST tests (KCl as the makeup water for drilling fluids, HCl used to acidize and decrease the skin factor of the well, solvents to reduce the viscosity of bituminous oils at the subsurface and surfactants to alter the surface tension between the bitumen and the carbonate rocks). These fluids are considered as contaminates in the water that was back-produced. Such contamination usually changes both the salinity of the sample and chemical composition and therefore, in conjunction with the exact timing of the injection, these contaminations and their gradual cleanout/dilution are easily identified while examining the measured EC and the chemical composition as a function of the produced fluid volume. The primary consideration in assessing whether the water produced could be considered as representative of the formation fluids was to examine whether the gradual cleaning of the contaminant fluids has resulted in a stable and constant EC and composition during production.

In two zones, Ness 03 zone 1 and Ness 02 zone 1, all the samples were considered as totally contaminated and were not analyzed. In Ness 03 zone 1, several production attempts were performed before and after acidizing procedure, but the slow recovery rates limited the amount of water produced by each injection, so the total amount of water produced during this test was smaller than the amount of acid injected (15 m^3). Slow recovery rates were also reported in Ness 02 zone 1, where 2.2 m^3 solvent was injected in the beginning of the test and production attempts were able to produce only 7.4 m^3 of water. Data recorded in the field indicated the last water sample produced during the test still contained solvent and therefore, samples from this test could not be considered as representative.

Borehole	Zone	Formation	Water Produced (m^3)	injected fluids	No. of selected samples
Ness 03	**Zone 1**	Lower Mishash	~5	HCl, KCl	0
	Zone 2	Lower Mishash	76.9	HCl, KCl	0
	Zone 3	Ghareb	98.2	KCl	5
Ness 02	**Zone 1**	Lower Mishash	7.4	Solvent, KCl	0
	Zone 2	Upper Mishash	88.7	HCl, KCl	0
	Zone 3	Mishash-Ghareb boundary	111.8	Surfactant, KCl	3
	Zone 4	Ghareb	68.7	Surfactant, KCl	4
	Zone 5	Taqiye	65.0	HCl, KCl	3

Table 3.3- Produced water and injected fluid volume per zone in Ness 02 and 03. No. of samples are samples that can were selected for detailed chemical analysis.

Drill Stem Tests samples

Ness 03 zone 2

In the test performed in Ness 03 zone 2 (Fig. 3.14), acid stimulation was performed almost immediately after the test started. Despite the fact the more than 70 m^3 of water was produced by the end of the test, a marked effect on the chemistry of the produced fluids still exists as a result of acidization and dissolution of the carbonate minerals, which is visible particularly in the instable values of the EC. Since Cl^- contamination cannot be estimated, neither the remaining effect of the acid on Ca^{2+} concentrations, no samples from this zone was selected for further analysis.

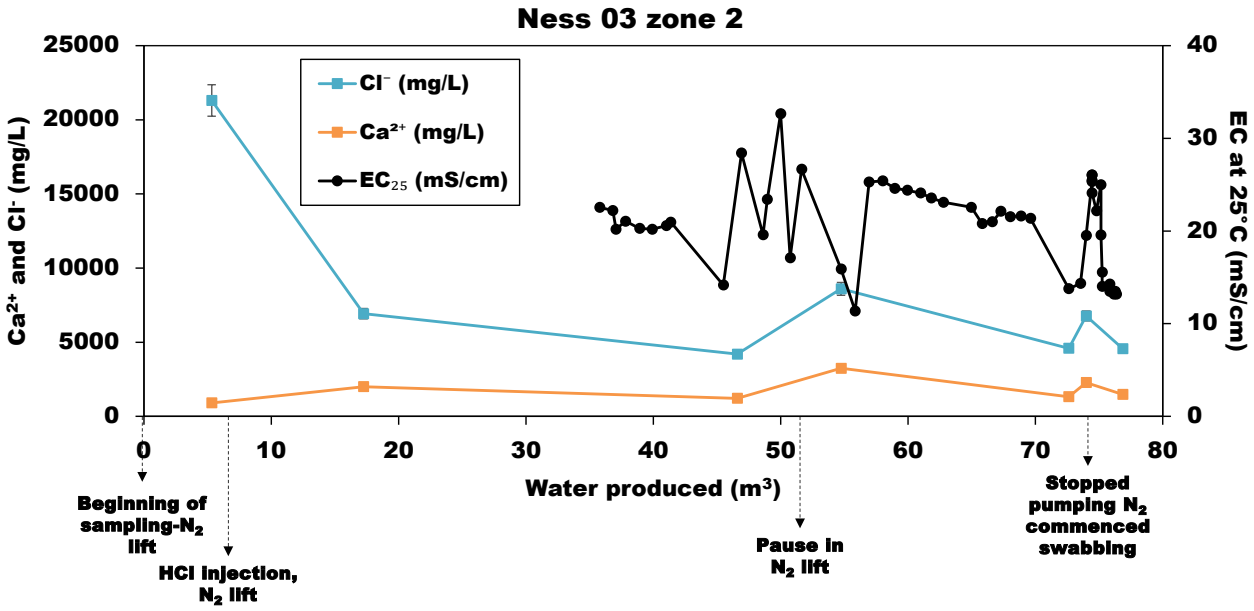

Fig. 3.14 - Change in $EC_{25°C}$ and Ca^{2+} and Cl^- concentrations as a function of the total volume produced Ness 03 zone 2.

Ness 03 zone 3

In the test performed in Ness 03 zone 3 (Fig. 3.15), the samples collected in the beginning of the test are clearly affected by the presence of 3% KCl solution. The effect of the KCl solution gradually decreased, so after the production of approximately 70 m^3, the composition seems to reach stable K^+ and Cl^- concentrations. While the EC in this zone is affected by the altering injections rates of N_2, as well as the mechanical mixing of the water column caused by the swabbing, samples collected during the final production stage using a stable N_2 lift, show table EC values. Therefore, the samples which were identified as the most representative for detailed chemical analysis were produced between production volumes of 80-90 m^3.

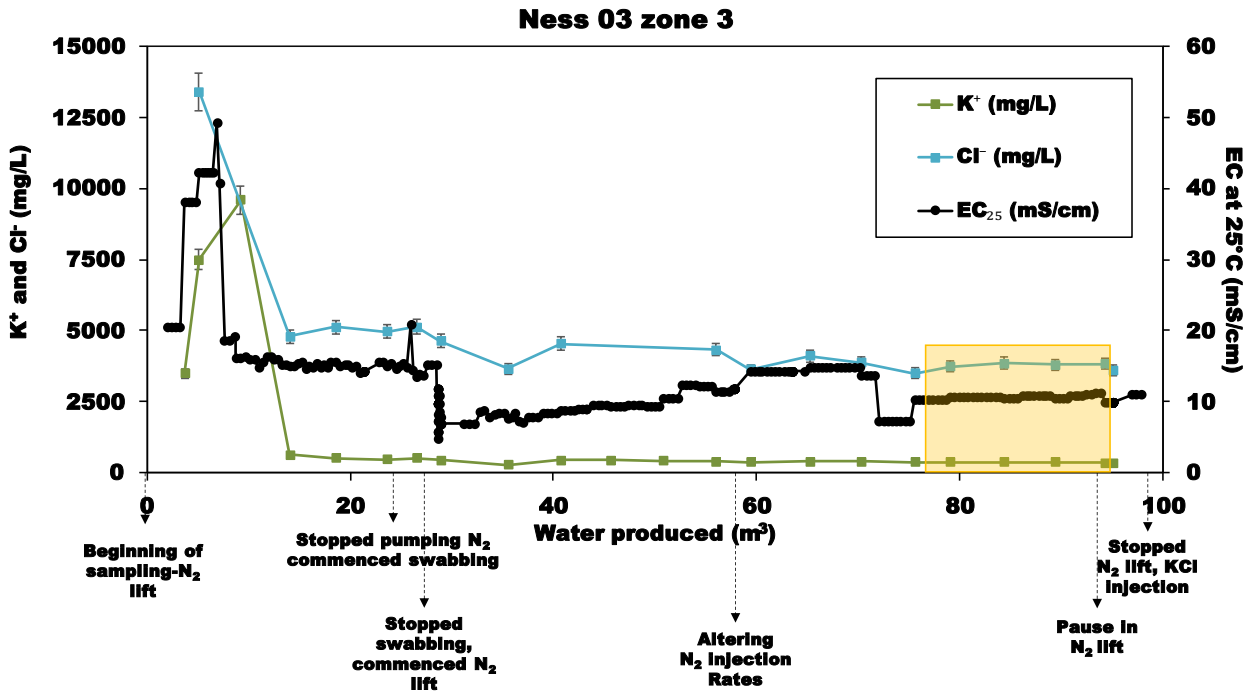

Fig. 3.15 - Change in $EC_{25°C}$ and K^+ and Cl^- concentrations as a function of the total volume produced Ness 03 zone 3, selected samples are highlighted in yellow.

Ness 02 zone 2

In the following test (Fig. 3.16), acid injection was performed after an initial production attempt. Though Ca^{2+} concentrations seem to reach stability, the Cl^- and EC still show a linear decrease. Since the remaining effect of the acid cannot be quantified, no samples from this test were chosen as representative.

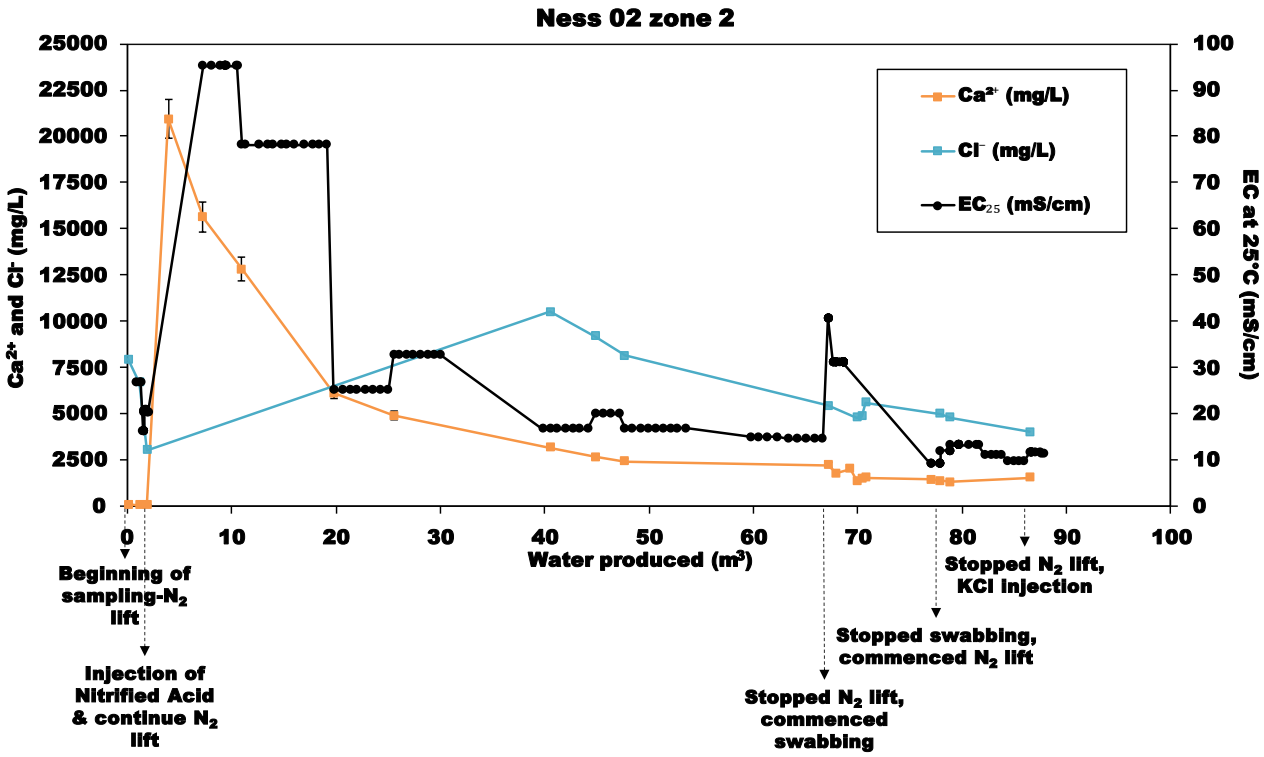

Fig. 3.16 - Change in $EC_{25°C}$ and Ca^{2+} and Cl^- concentrations as a function of the total volume produced Ness 03 zone 2.

Ness 02 zone 3

The operational liquid used in this zone (Fig. 3.17) was 3% KCl solution, which is present in the samples collected in the beginning of the test. The decrease in K^+ and Cl^- concentrations before the injection of surfactant seem to decrease and slightly stabilize, while the EC reaches a constant value. Since the samples collected during this stage of the test contain only one known contaminant, it's remaining effect can be corrected. Three samples from this zone were chosen for a detailed chemical analysis.

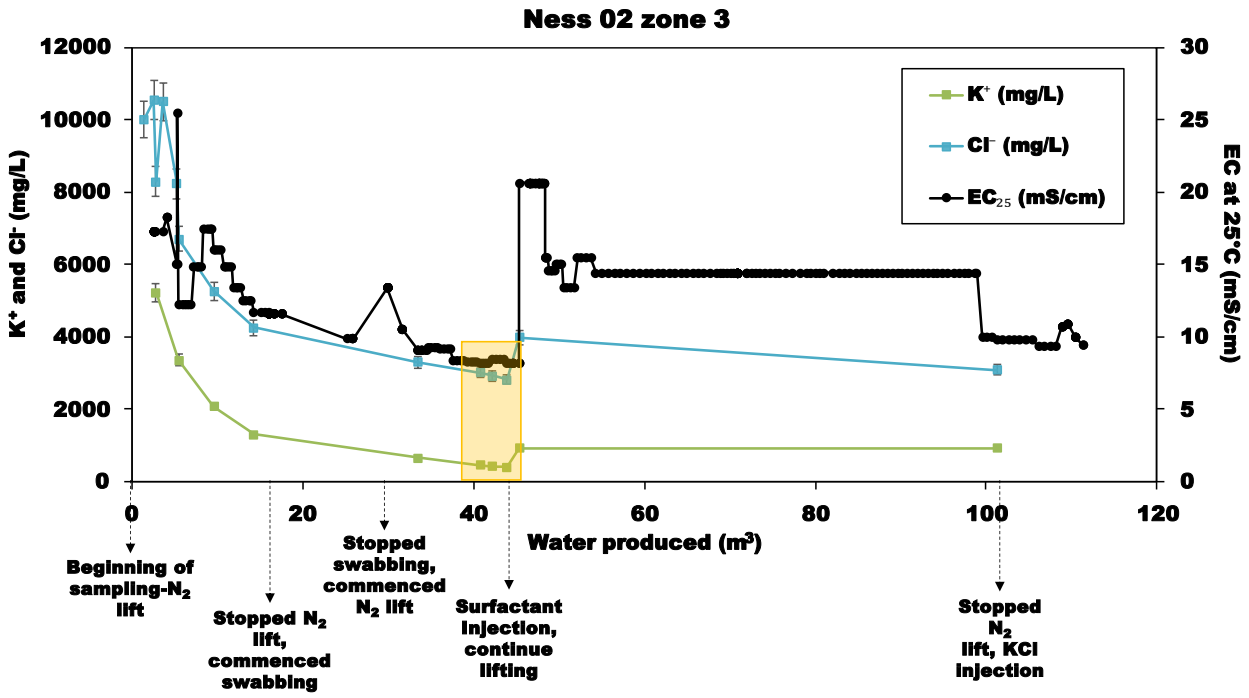

Fig. 3.17 - Change in $EC_{25°C}$ and K^+ and Cl^- concentrations as a function of the total volume produced Ness 02 zone 3, selected samples are highlighted in yellow.

Ness 02 zone 4

In the following zone (Fig. 3.18), the operational fluid used was a 3% KCl solution. While samples collected in the beginning of the test show high K^+ and Cl^- concentrations, as well as high EC, the samples collected following the production of 55 m^3 and prior to the injection of surfactant solution, reached constant values both in K^+ and Cl^- concentrations, as well as the EC. Therefore 4 samples from this test were selected for a detailed chemical analysis.

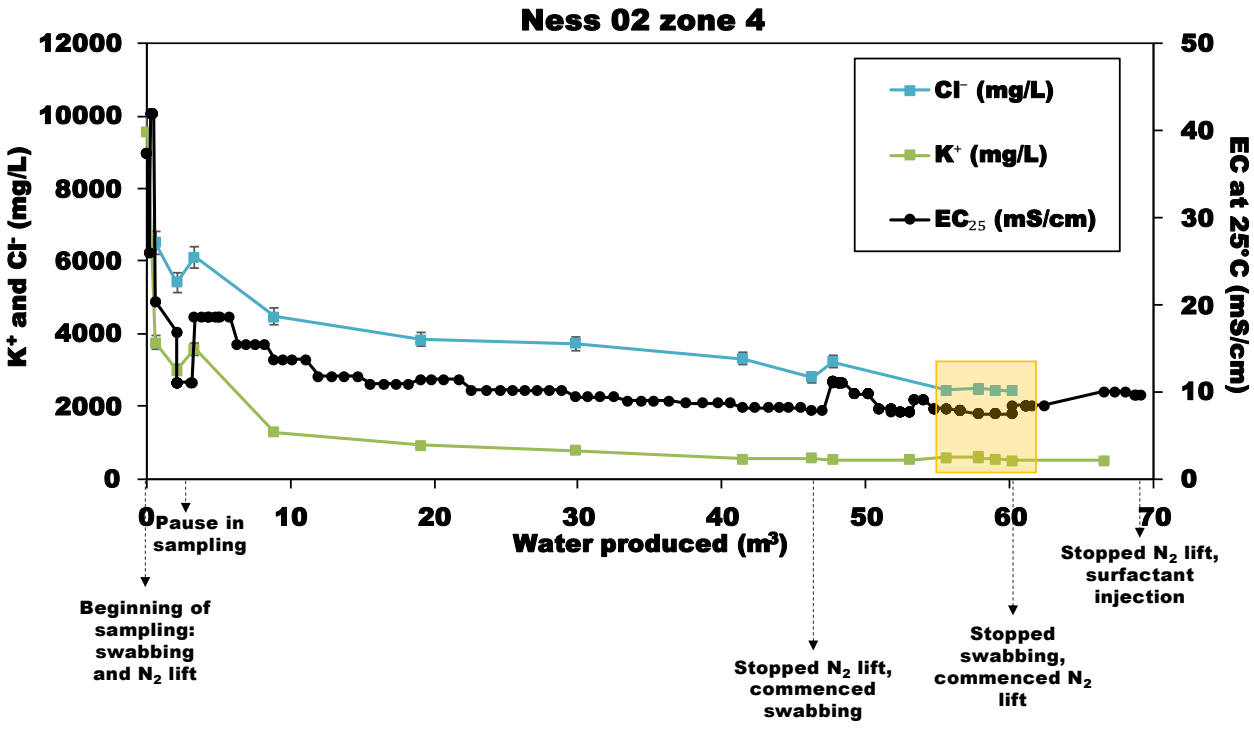

Fig. 3.18 - Change in $EC_{25°C}$ and K^+ and Cl^- concentrations as a function of the total volume produced Ness 02 zone 4, selected samples are highlighted in yellow.

Ness 02 zone 5

This zone was the only test performed on the Taqiye Formation (Fig. 3.19). However, it included the injection of nitrified acid at the beginning of the test. Therefore, only following the production of 50 m^3, Ca^{2+} and Cl^- concentrations reached constant values. Samples selected from this stage show high Cl^- concentrations (~10,000 mg/L) and therefore, the remaining effect of the acid on the ion concentrations and ionic ratios is minor. Three samples from this zone were selected for further chemical analysis.

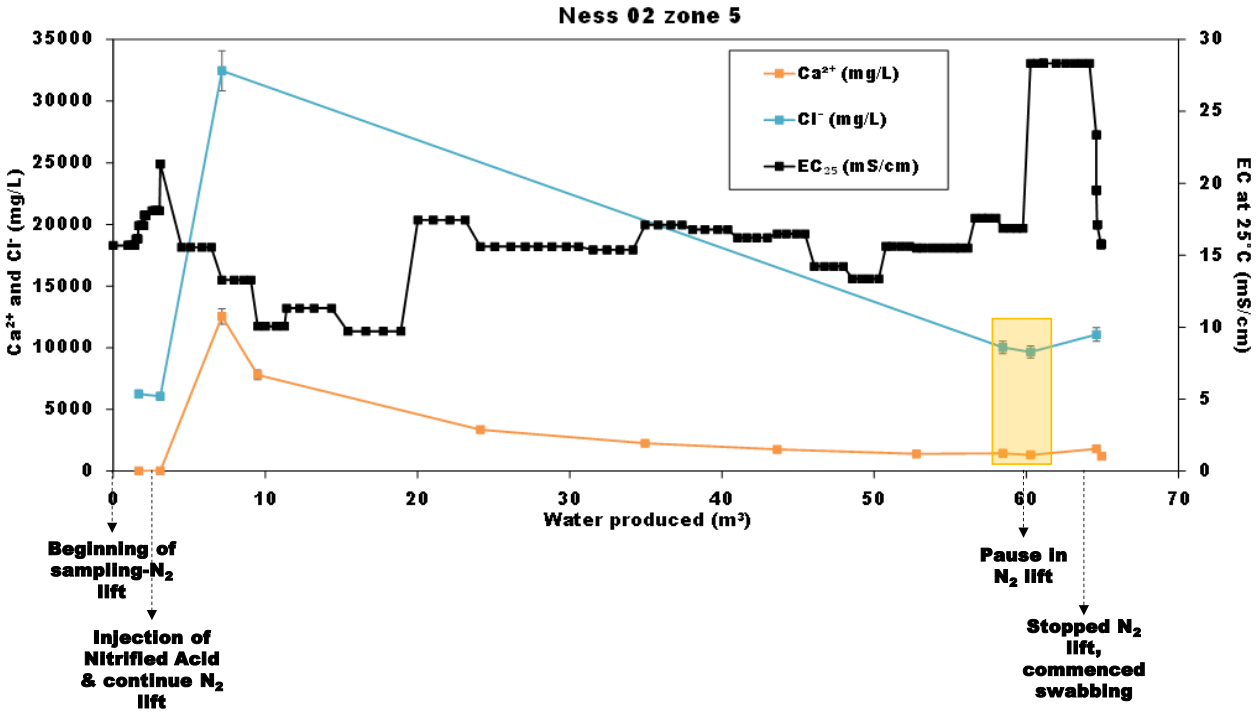

Fig. 3.19 - Change in $EC_{25°C}$ and Ca^{2+} and Cl^- concentrations as a function of the total volume produced Ness 02 zone 5, selected samples are highlighted in yellow.

Samples collected while drilling

Two samples collected while drilling were collected in Ness 02 and Ness 12 boreholes. Samples were taken after the water column in the borehole has been removed. Then, production stopped to allow recovery for 48 hours before additional production and sampling was performed. In Ness 02, One sample was collected at the final stage of production from a depth of 1126 m BGL (Lower Mishash Formation), while the section was open between the Lower-Taqiye to the Lower-Mishash Formations (Fig. 3.2). A similar procedure was performed in Ness 12, one sample collected for chemical analysis was taken from a depth of 1400 m BGL (Lower-Mishash Formation), when the section was also open between the Lower-Taqiye to the Lower-Mishash Formations (Fig 3.6). Note that the depths of the collected sample do not represent the formations at the sampled depth but an unknown composite of the formations that contributed water to the open hole section at the time of sampling.

3.5 Salinity, chemical and isotopic composition of the water samples

Major ion concentrations

The salinity (or Total Dissolved Solids - TDS) and major ion concentrations of the water samples selected for detailed chemical analysis are summarized in Table 3.4 and are presented in Figs. 3.20-3.21. The salinities of the analyzed samples span over three orders magnitude, each defined as a different composition. The samples collected from Ness 12 open section (Lower-Taqiye- Lower-Mishash) are defined as freshwater (TDS < 400 mg/L). The samples from the Upper-Mishash and the Ghareb Formations (MGF) in Ness 02 and Ness 03 are defined as brackish water (1000-10,000 mg/L TDS) and samples from the Taqiye Formation in Ness 02 are considered saline (~19,000 mg/L TDS).

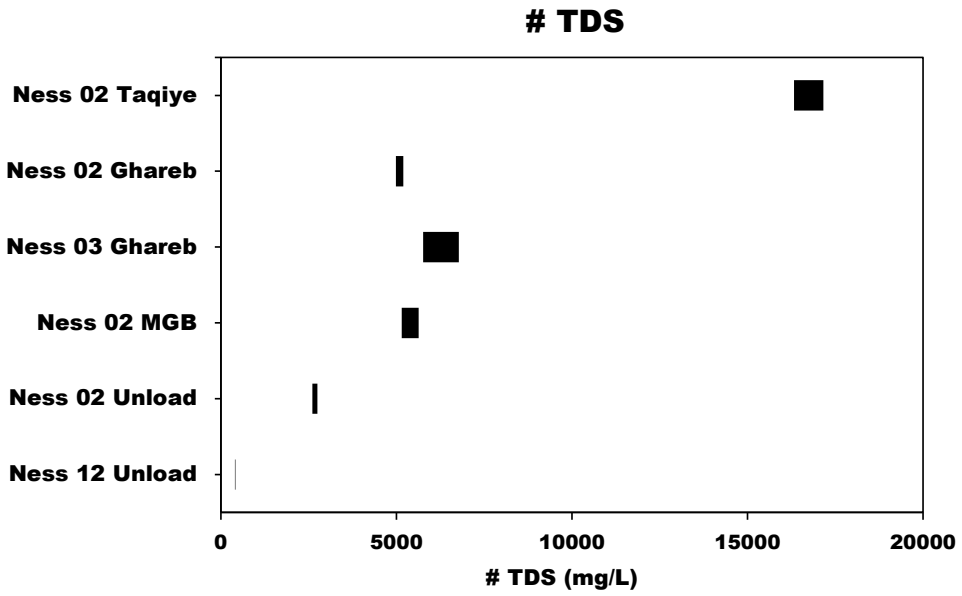

Fig 3.20 - Total Dissolved Solids (TDS) of the studied water. MGB – Mishash Ghareb Boundary.

Averaging the Major ion concentrations of DST samples

In order to determine the water composition of the DST samples in the different zones, the analysis of at least three samples from each zone was used to average the composition (Table 3.5, full analysis of all samples in given in Appendix 2). The standard deviation values calculated for most ions is less than 10%. The average for each zone will be used for further geochemical interpretation.

				Concentrations in mg/L											
Source	**Formation**	**Sampling date**		**pH**	**Na^+**	**K^+**	**Ca^{2+}**	**Mg^{2+}**	**Sr^{2+}**	**Cl^-**	**Corr. Cl-**	**Br^-**	**SO_4^{2-}**	**HCO_3^-**	**#TDS**
Ness 02 DST 5	Taqiye	19/05/2016	Average	7.3	4489	163	1271	169	43.4	9967		55.7	40.2	548	16746
			Stdev	0.3	78.1	4.2	110	6.6	1.0	282		4.6	5.8	22.3	421
			% stdev	4%	2%	3%	9%	4%	2%	3%		8%	14%	4%	3%
Ness 02 DST 4	Ghareb	10/05/2016	Average	6.3	903	553	433	68.6	12.9	2451	1950	23.7	51.9	607	5090
			Stdev	0.1	27.1	31.6	18.1	2.7	0.3	18.0	22.3	0.3	11.4	72.0	106.1
			% stdev	2%	3%	6%	4%	4%	2%	1%	1%	1%	22%	12%	2%
Ness 03 DST 3	Ghareb	18/03/2016	Average	6.7	1189	341	784	85.0	22.4	3433	3123	18.6	28.6	552	6270
			Stdev	0.3	16.9	5.2	16.7	2.6	0.7	172	169	6.2	18.8	104	507
			% stdev	5%	1%	2%	2%	3%	3%	5%	5%	34%	66%	19%	8%
Ness 02 DST 3	Mishash-Ghareb boundary	26/04/2016	Average	6.7	824	422	757	87.0	18.2	2921	2538	10.5	31.9	479.2	5391
			Stdev	0.1	41.3	23.0	20.6	1.9	0.4	77.7	56.8	0.8	2.4	124	241
			% stdev	1%	5%	5%	3%	2%	2%	3%	2%	7%	7%	26%	4%
Ness 02 Unload	Lower Taqiye-Lower Mishash	02/07/2016		8.3	717	46.0	101	53.0	8.8	1240		8.1	7.0	565	2746
Ness 12 Unload	Lower Taqiye-Lower Mishash	21/12/2015		8.1	76.0	8.0	27.0	14.0	1.3	90.0		0.5	13.0	187.0	417

Table 3.4 – Major ion concentrations of studied water. Samples from the same test were averaged.

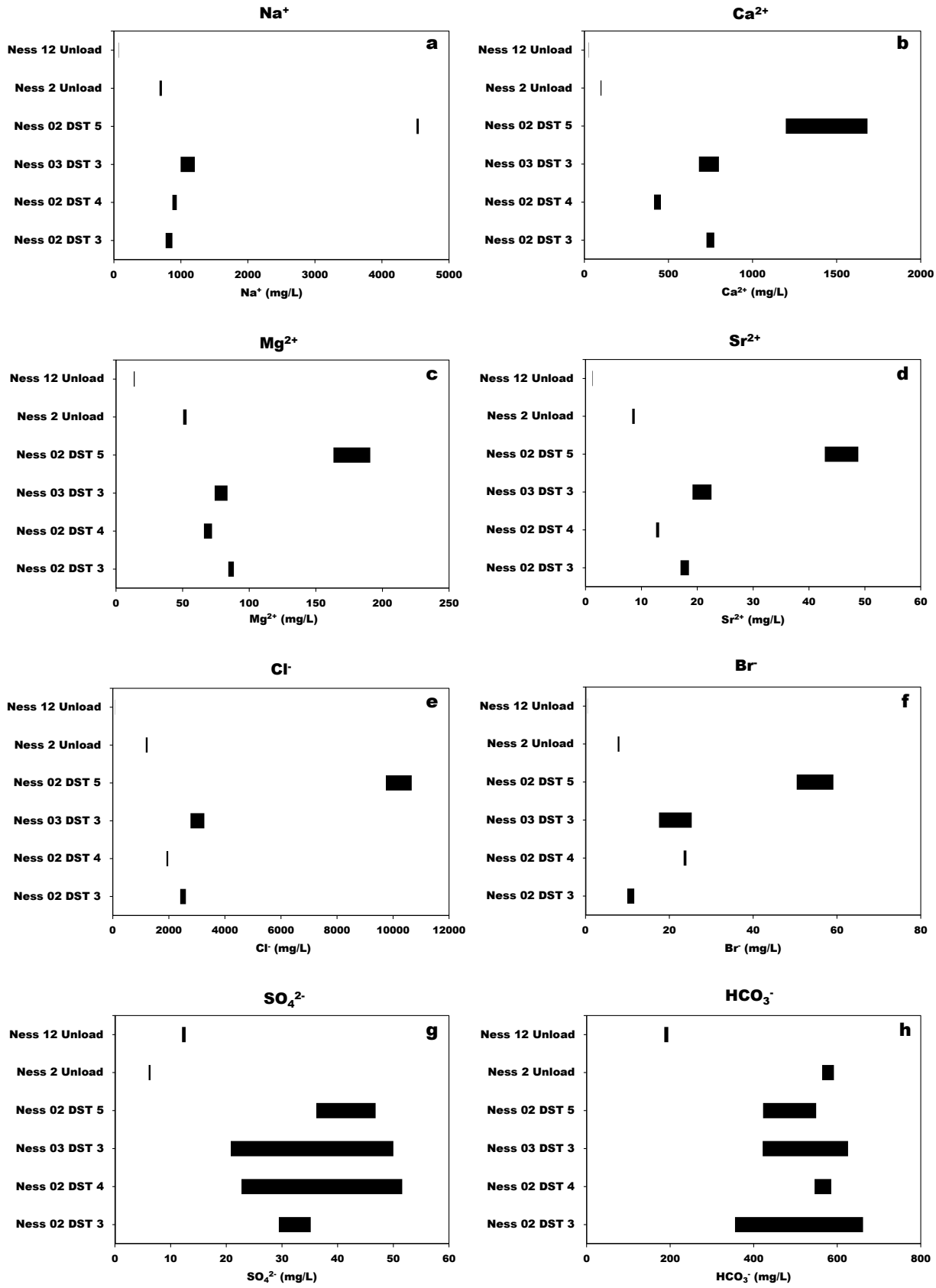

Fig 3.21 (a-h) – Ion concentrations in the studied water.

Corrections to the major ionic concentrations

Though heavily contaminated samples by drilling, completion and stimulation fluids were disregarded based on the observed gradual cleanout/dilution as a function of water produced, it is likely that the chemical composition of the water samples is still affected to a certain degree by remnants of these contaminants, particularly KCl which was most often used. The contamination is detected by the high K/Cl ratios which are higher than expected in natural groundwater, which usually exhibit K/Cl values lower than 0.1. In order to examine the maximal possible Cl^- contamination sourced from the KCl solution, an equivalent concentration K^+ was subtracted from the Cl^- concentration and K^+ concentrations will not be regarded in the interpretation. The maximum difference between corrected equivalent concentrations of Cl^- before and after the correction accounted to 20% of the measured Cl^- in the sample (Table 3.5). Note that with increasingly higher salinities of the different samples selected as representative, the relative percentage of the correction becomes smaller.

The samples from the DST performed on the Taqiye Formation have K/Cl values of 0.01 (Table 3.6) and the measured Cl^- concentrations are 10,000 mg/L (Table 3.4), therefore a correction of 100 mg/L would not create any difference in the chemical composition and these samples were not corrected. The samples collected during drilling have significantly lower K/Cl ratios (0.03-0.08) and low Cl- concentrations (Table 3.4). Since the salinities of these samples are low, a KCl contamination would have been reflected by extremely high K/Cl ratios, like the ones that were measured in samples from Ness 02 zone 4 (0.2), therefore the Cl^- concentrations in these samples were not corrected.

Source	Formation	Measured Cl^- (mg/L)	Corrected Cl^- (mg/L)	% Correction (K/Cl ratio)
Ness 02 DST 3	Mishash-Ghareb boundary	2921	2538	13%
Ness 02 DST 4	Ghareb	2451	1950	20%
Ness 03 DST 3	Ghareb	3433	3123	9%

Table 3.5 – Measured and corrected Cl^- concentrations, as well as the % correction or the precent of measured K^+ that was subtracted from the Cl^- concentrations (percentage K/Cl ratio).

Ionic ratios

Selected ionic equivalent ratios in the water samples are presented in Table 3.6 and in Fig. 3.23 (a-f). Despite the differences in salinity, all samples collected during the DSTs show similar equivalent ratios, including low Na/Cl ratios (<0.75), low Mg/Ca ratios (<0.3) and are all defined as having Ca-chloride composition where the Ca/(HCO_3+SO_4) equivalent ratio is greater than 1 (Starinsky, 1974).

The water that was produced while drilling Ness 12 exhibit different ionic ratios, as well as the samples collected from Ness 02 which do not completely coincide with the compositions measured in the DST tests. Na/Cl and Mg/Ca ratios are higher and none of the water produced while drilling are characterized by a Ca-chloride composition.

Source	Formation		Equivalent ratios						
			Na/Cl	Mg/Ca	Mg/Cl	Ca/Cl	Sr/Cl	Ca/ (HCO_3+SO_4)	K/Cl
Ness 02 DST 5	Taqiye	Average	0.69	0.22	0.05	0.23	0.004	6.48	0.01
		Stdev	0.01	0.01	0.00	0.01	0.00	0.69	0.00
		% Stdev	2%	4%	1%	5%	1%	11%	4%
Ness 02 DST 4	Ghareb	Average	0.71	0.26	0.10	0.40	0.005	2.24	
		Stdev	0.02	0.00	0.00	0.02	0.00	0.09	
		% Stdev	3%	2%	4%	4%	2%	4%	
Ness 03 DST 3	Ghareb	Average	0.59	0.18	0.08	0.44	0.006	4.04	
		Stdev	0.02	0.01	0.01	0.02	0.00	0.46	
		% Stdev	4%	3%	7%	4%	6%	11%	
Ness 02 DST 3	Mishash-Ghareb boundary	Average	0.50	0.19	0.10	0.53	0.006	4.70	
		Stdev	0.03	0.00	0.00	0.01	0.00	1.24	
		% Stdev	7%	1%	1%	1%	1%	26%	
Ness 02 Unload	Lower Taqiye-Lower Mishash		0.89	0.87	0.12	0.14	0.006	0.54	0.03
Ness 12 Unload	Lower Taqiye-Lower Mishash		1.30	0.86	0.45	0.53	0.012	0.40	0.08

Table 3.6 – Average and standard deviation of the ionic ratios of the studied water. Ratios were calculated using corrected Cl^- concentrations.

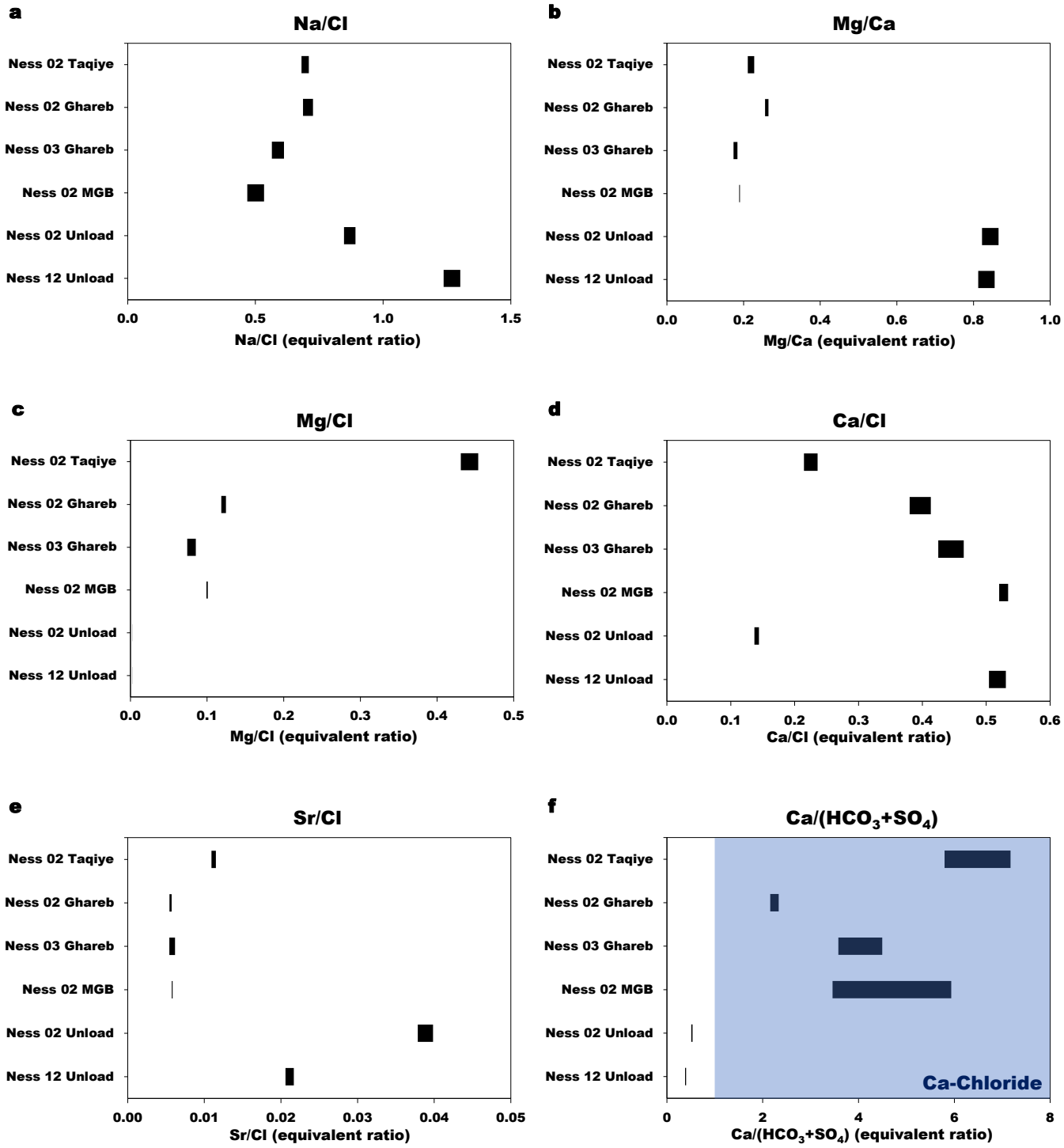

Fig. 3.22 (a-f) – Ionic ratios (equivalent) of the studied water.

Stable oxygen and hydrogen isotopes ($\delta^{18}O$ and δD)

The measured $\delta^{18}O$ and δD values of the water samples are presented in Table 3.7 and in Fig. 3.24 (a-b). The $\delta^{18}O$ values in all the water samples are ~-7‰, except for samples from the Taqiye formation, which are substantially higher (by 1‰). δD values are close or lower than -40‰ in all samples, excluding the samples from the Taqiye which exhibit δD values of around -36‰. The variation in $\delta^{18}O$ values between samples from the same zone is less than 3% and less than 5% for δD values. These minor variations cause a significant variation in d-excess values. The samples collected while drilling from Ness 12 and Ness 02 have the same $\delta^{18}O$ and δD values, which are similar to the values measured in samples from the DSTs (except for samples from the Taqiye).

Source	Formation		$\delta^{18}O$ (‰ V-SMOW)	δD (‰ V-SMOW)	D-excess (‰)	$^{86}Sr/^{87}Sr$
Ness 02 DST 5	Taqiye	Average	-6.01	-36.3	11.8	0.70782
		Stdev	0.14	0.4	1.4	
		% Stdev	2%	1%	12%	
Ness 02 DST 4	Ghareb	Average	-7.24	-41.0	17.0	0.70773
		Stdev	0.25	1.3	2.5	
		% Stdev	3%	3%	15%	
Ness 03 DST 3	Ghareb	Average	-6.99	-42.1	13.8	0.70766
		Stdev	0.13	1.9	1.9	
		% Stdev	2%	5%	14%	
Ness 02 DST 3	Mishash-Ghareb boundary	Average	-7.45	-40.7	18.9	0.70773
		Stdev	0.10	0.67	0.5	
		% Stdev	1%	2%	3%	
Ness 02 Unload	Lower Taqiye-Lower Mishash		-7.20	-42.4	15.2	0.70784
Ness 12 Unload	Lower Taqiye-Lower Mishash		-7.26	-42.0	16.0	0.70746

Table 3.7 – The isotopic composition of the studied water.

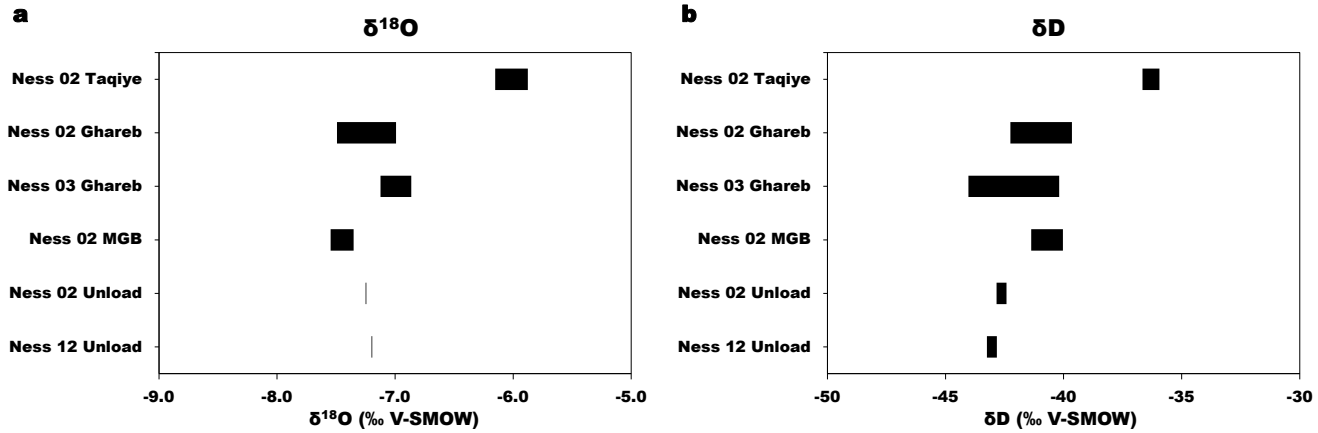

Fig 3.23 (a-b) –$\delta^{18}O$ and δD values of the studied water.

Stable strontium isotopes ($^{87}Sr/^{86}Sr$)

The isotopic composition of strontium is presented in Table 3.7 and in Fig 3.25. The $^{87}Sr/^{86}Sr$ is similar in samples from the MGF in Ness 02 and slightly lower in samples from the Ghareb Formation in Ness 03. The ratio is the highest in samples from the Taqiye Formation in Ness 02 zone 5. Two measurements were performed on these samples for confirmation, both have similar ratios (% stdev < 0.002%). The water produced while drilling from Ness 02 have a lower $^{87}Sr/^{86}Sr$ ratio, which is similar to the one measured in samples from the Taqiye Formation. The $^{87}Sr/^{86}Sr$ ratio of the water produced while drilling Ness 12 is the lowest ratio measured.

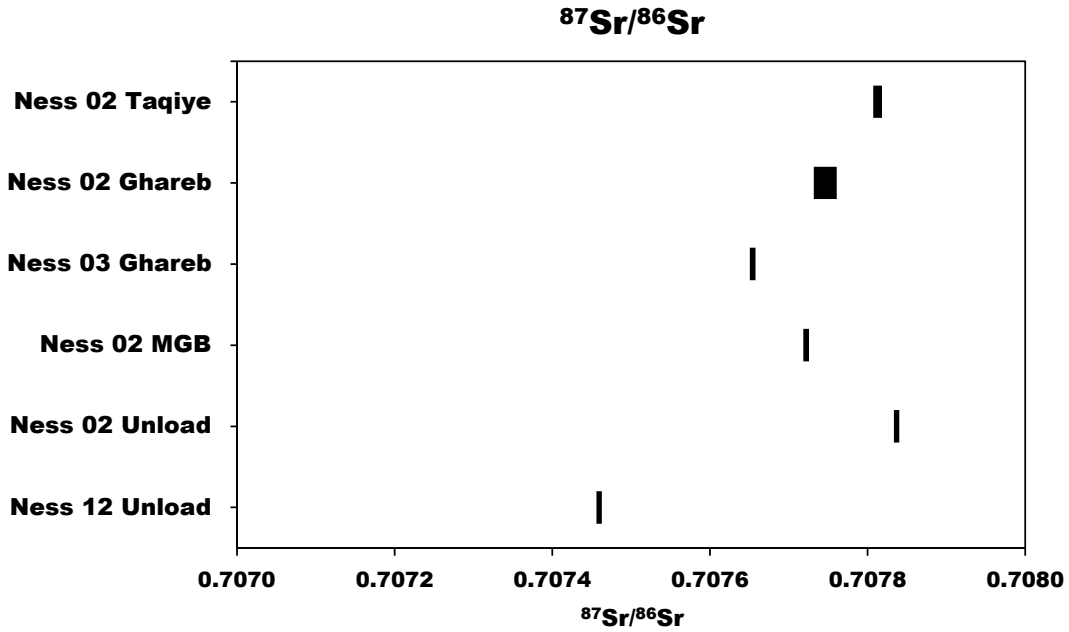

Fig. 3.24 –$^{87}Sr/^{86}Sr$ values of the studied water.

4. Discussion

4.1 Hydrology

Hydrostatic pressures, water levels and apparent hydraulic gradients

The hydrostatic conditions in the Ness boreholes were determined based on two types of measurements: (a) water levels that were measured while drilling Ness 12 and Ness 02 Boreholes and (b) pressure measurements taken during buildup tests of the DSTs (in Ness 02 and Ness 03). While information collected during drilling provides the water level equivalent to the highest pressure within the open hole section, the DST information is limited to 15 m intervals, according to the depths tested. Regardless to the method by which the water levels were measured and the depths investigated, it is shown that the Mt. Scopus Group in the southern Golan Heights exhibit sub-hydrostatic pressures (Figs. 4.1, 4.2 and Table 3.1). We propose that the low pressure regime in the Mt. Scopus group stems from a combination between limited recharge due to limited exposures of the Mt. Scopus group, low connectivity between the Mt. Scopus group and shallower groundwater systems along the flow path, low permeability and a relatively low discharge point elevation.

Hydrostatic pressure information are plotted vs. depth in Fig. 4.1 and with horizontal distance in Fig. 4.2. The data includes the information from both the water level measurements while drilling and DST tests. The pressure gradient between the Ghareb-Upper Mishash follows a hydrostatic gradient (10 m/bar). However, the single pressure measurement that was taken in the Lower Mishash Formation in the Ness 03 wells, deviates from the Ghareb-Upper Mishash trend, towards higher pressures, resulting in a slightly higher gradient between the upper and Lower Mishash (9.7 m/bar), which is not significantly different than the Ghareb-Upper Mishash pressure gradient. However, the-pressure gradient further increases downwards, as indicated by the open hole water level measurement up to a value of 6.6 m/bar. Such a high-pressure gradient exceeds the possible density values of aqueous solutions, suggesting that a different pressure regime exists towards the base of the Lower Mishash. Figure 4.2 further highlights this pressure difference which translates to up to 60 m difference in the water table elevation.

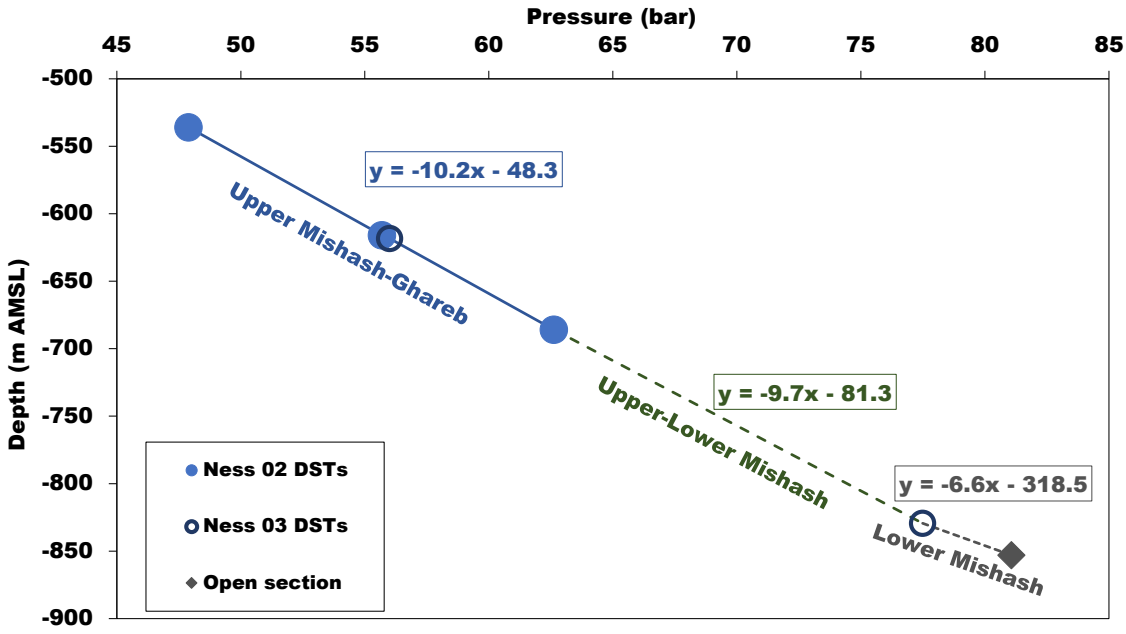

Fig. 4.1 –Hydrostatic pressures in the Mt. Scopus Group as measured during the DSTs in Ness 02 and Ness 03, as well as the calculated pressure from the water level measured while drilling in the open section in Ness 02.

While the source of the elevated pressure gradients cannot be strictly determined, the following mechanisms are suggested: (a) increasing presence of gas with depth due to the increasing maturation of the Mt. Scopus source rocks as a function of depth (b) Connection to a different sub-aquifer with higher recharge/discharge elevations. In either case, it is important to note that the discontinuity in the pressure gradient indicates that hydraulically, the lower Mishash is isolated from the overriding Mt. Scopus formations.

The data derived from the water level measurements while drilling suggest an apparent hydraulic gradient from Ness 12 to Ness 02 of 2‰ (Fig. 4.2). This gradient steepens towards the Meizar 3 well in the Yarmouk Gorge to a gradient of 2.4‰ (based on the water level in 1994). It is important to note that since there are isolated layers within the Mt. Scopus group, the derived hydraulic gradients depend on the local connectivity between these sub-layers and can be significantly affected by the exact depth that was penetrated.

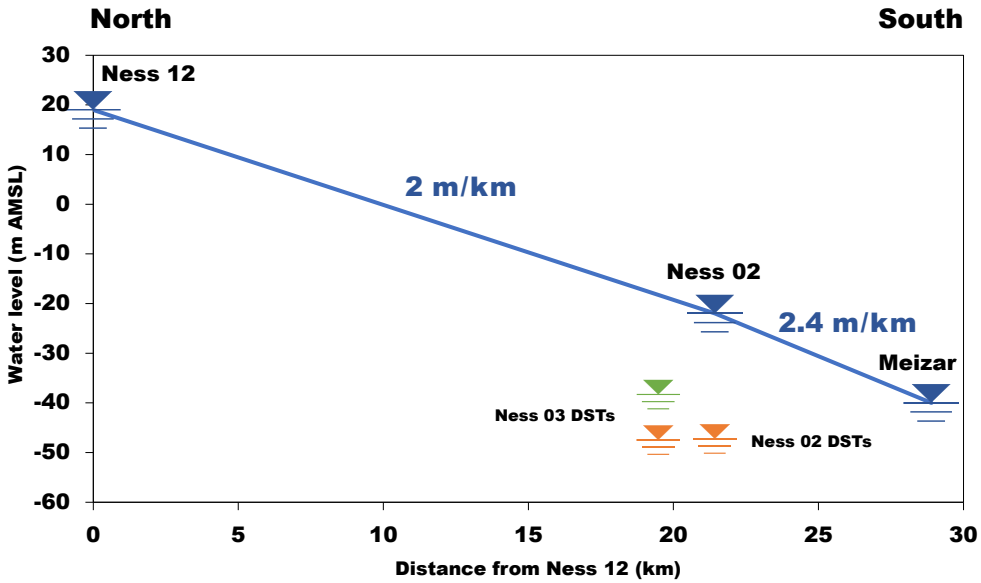

Fig. 4.2 – Water levels of the open section (blue) and the tested intervals (green and orange). Blue line is the apparent hydraulic gradient from Ness 12 to Meizar 3 well, derived from the open section water levels.

Hydraulic conductivities and possible dual permeability behavior

The hydraulic conductivities estimated from the DSTs are the same ($2 \cdot 10^{-7}$ m/s) for all zones that had similar water levels (Table 3.1; Fig. 3.11). While the four zones that included the Ghareb and Upper Mishash Formations had the same hydraulic conductivity, the overlying and underlying zones (the Taqiye and Lower Mishash Formations, respectively) had a hydraulic conductivity that was lower by two orders of magnitude (10^{-9} m/s) and the deepest zone in the Lower Mishash (Ness 03 zone 1) has the lowest hydraulic conductivity ($5 \cdot 10^{-13}$ m/s) of all tested zones. In contrast with the low hydraulic conductivity measured during the DST tests, the Lower Mishash Formation generated large amounts of water during the drilling operations in three wells (Ness 02, 06 and 12), that were not generated from any other formation of the Mt. Scopus Group. This means that the DST tests were not successful in intercepting the high permeability zones that were intercepted during the drilling operation within the lower Mishash, whether it may be a permeable horizon or a fracture system that leads to a dual permeability behavior (low matrix permeability and high fracture permeability).Since the water storage in the fractures is smaller and flows at higher velocities, the water may have a different composition in the fractures in comparison to the water stored in the matrix. Such a flowing mechanism could also potentially explain the differences in the chemical composition of the water between the DSTs and samples that were taken during drilling operations, as will be addressed in the next chapter (geochemistry discussion).

4.2 **Geochemistry**

Sources of salinity

The studied water displays a wide range of salinities that changes both laterally within the same formation at different wells, as well as between different formations within the same well. The water from the Mt. Scopus in Ness 12, which is the northern most borehole tested in this study (Fig. 4.3) is characterized as freshwater, while the studied water from the different parts of the MGF section in the southern boreholes (Fig. 4.3) are brackish to moderately saline. Generally, in the southern boreholes, the salinity decreases with depth (Fig. 4.4). The highest measured salinity was found in the Taqiye formation which exhibits a salinity that was up to three times higher than the water from the MGF (Table 3.4, Fig. 3.20). In fact, the salinity in the Taqiye is the highest recorded salinity in the GH. Within the MGF, water salinities show a decrease with depth down to salinities that are similar to the ones found around the Kinneret lake (defined as the Kinneret brines, Starinsky, 1974).While the salinity of groundwater in sedimentary rocks typically display a wide range, at any given depth within the same basin, low salinities (TDS < 2,000 mg/L) usually represent meteoric water infiltrating rapidly through shallow and permeable hydrogeological units (Kreitler, 1989). Higher salinities are typically found in trapped pore water of deep-seated rocks (Hanor, 1994). This can either be a result of either remnants of connate water (water trapped in the pores of the rock during formation of the rock) and/or intrusions that have occurred following the formation of the rock. The source of the saline intrusion can be from various surface saltwater bodies (seawater, lagoons, salt lakes etc.), or from subsurface saline water bodies which could either be sourced from deeper strata and/or dissolution of highly soluble minerals (Hanor, 1994).

The major ionic composition of groundwater within sedimentary rocks strongly depend on the salinity (Hanor, 1994). While the major anion in high salinities formation water above 10 g/L is Cl^-, account for ~95 wt.% of all anions, groundwater with lower salinities contain either HCO_3^- or SO_4^{2-} as the major anion. The main cation in brackish to moderately saline groundwater (TDS = 1,000 - 10,000 mg/L) is Na^+, while as the salinity increases, the relative proportion of Na^+ decreases with increasing concentrations of Ca^{2+}, Mg^{2+} and K^+. Sedimentary formation water with salinities greater than 300 g/L typically contain Ca^{2+} or Mg^{2+} as the main cations (by mass). Therefore, hypersaline subsurface brines in sedimentary basins are characterized by a Ca-chloride composition ($Ca^{2+} > (HCO_3^- + SO_4^{2-})$) (Hanor, 1994; Land, 1987).

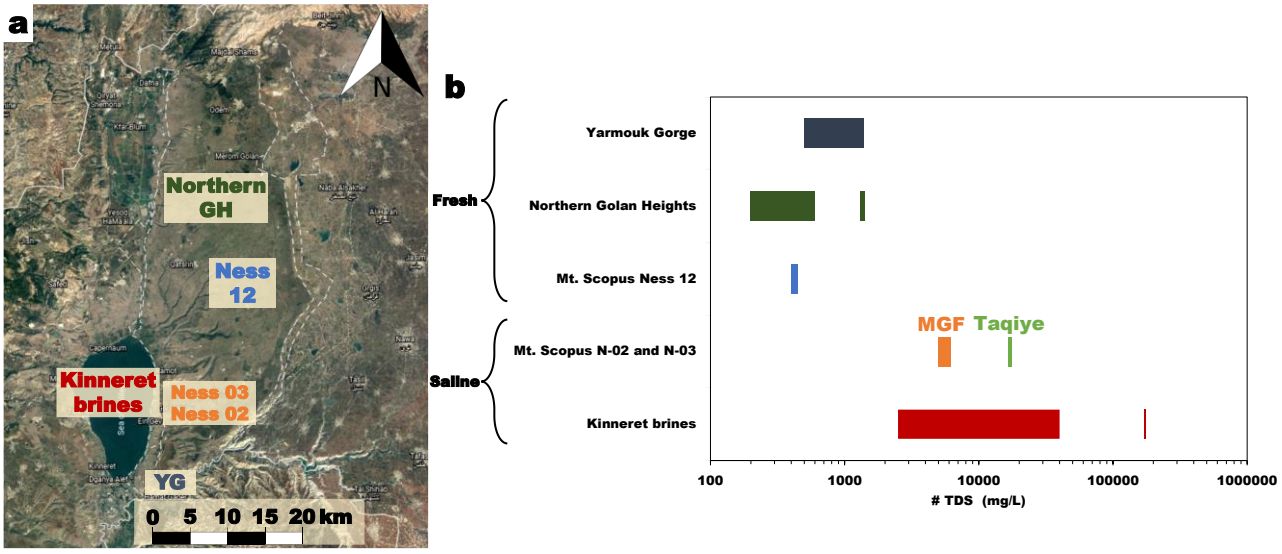

Fig. 4.3 – (a) Location map. (b) Salinity (TDS) of the studied water in comparison to water sources in the GH region, colors correspond to inset a. The salinity of the studied water is higher than previously found in the GH and resembles the salinity of the Kinneret brines.

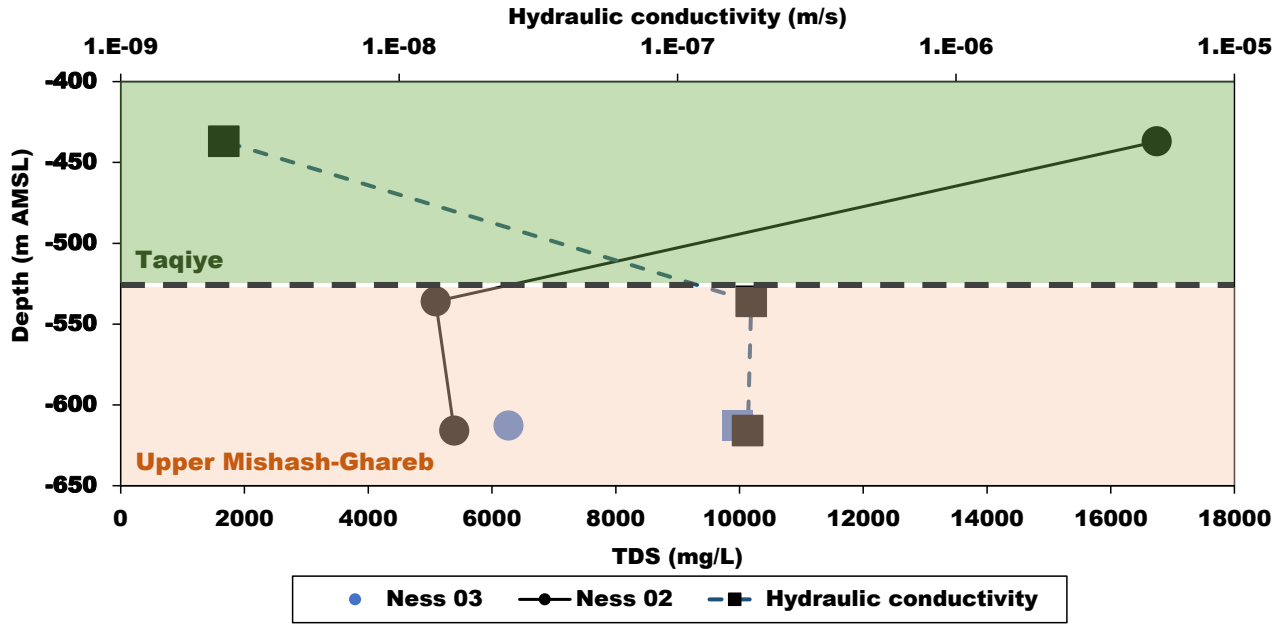

Fig. 4.4 – Salinity and hydraulic conductivity as a function of depth in the tested formations of the Mt. Scopus Group. The salinity is the highest in the least permeable Taqiye Formation.

Despite the fact that the salinities of the studied water are significantly lower than 300 g/L, the brackish to moderately saline water in the Taqiye and MGF are all characterized by a Ca-chloride composition (Table 3.6, Fig. 3.23). These salinities are higher than the expected threshold described by Hanor (1994)

as values that are typical for meteoric water which underwent water rock interactions (< 3,000 mg/L). The high Cl^- concentrations could have resulted from the dissolution of evaporites (such as halite), however, the fact that the studied water are Ca-chloridic eliminates halite dissolution as the saline source, since dissolution would have resulted in Na/Cl ratios of ~1. If the equivalent concentrations of Cl^- is balanced by the Na^+, HCO_3^- and SO_4^{2-} will be balanced by the remaining major cations (Mg^{2+}, Ca^{2+} and K^+) and therefore, the water will exhibit a $(Mg^{2+}+Ca^{2+})/(HCO_3^-+SO_4^{2-})$ ratio of less than 1 and the water will not be characterized as Ca-chloride (Hanor, 1994). The ion ratios also rule out plain seawater as the source of salinity since ratios are lower than the marine value (0.86). Previous studies (Starinsky, 1974; Carpenter, 1978; Katz and Starinsky, 2009) suggested that saline Ca-chloride brines in sedimentary basins originated from seawater that underwent (1) evaporation in a marine lagoon; (2) chemical modification by water-rock interactions; (3) dilution by freshwater or mixing with a saline source.

Evolution of Ca-Chloride brines and intrusion mechanism into host rocks

Seawater evaporation is accompanied by the precipitation of evaporitic minerals (Fig. 4.5). The first mineral to precipitate at the beginning of the evaporation process is aragonite ($CaCO_3$), followed by gypsum ($CaSO_4 \cdot 2H_2O$). The removal of Ca^{2+} during evaporation increases the Mg/Ca ratio (Fig. 4.6). At an evaporation degree of 10, halite begins to precipitate, while decreasing the Na/Cl ratio (Fig. 4.6). Within the lagoon anoxic bottom water, a process of bacterial sulfate reduction takes place according to the overall reactions:

$$2CH_2O + SO_4^{2-} \rightarrow H_2S + 2HCO_3^-$$

$$2CH_2O + SO_4^{2-} \rightarrow HS^- + HCO_3^- + H_2CO_3$$

Since the brines are already oversaturated with respect to aragonite, the HCO_3^- formed during sulfate reduction will further precipitate as aragonite and further increase the Mg/Ca ratio. When the brines interact with $CaCO_3$ minerals of surrounding rocks or within the lagoon, the elevated Mg/Ca ratios of the brines acts as a catalyst for dolomitization of these minerals, by the following reaction:

$$2CaCO_3 + Mg^{2+} \rightarrow CaMgCO_3 + Ca^{2+}$$

The Ca^{2+} released in the process, combines with the remaining SO_4^{2-} to form additional gypsum, until the concentrations of SO_4^{2-} and HCO_3^- are low enough so that Ca^{2+} is no longer precipitated. At that

point, the water in the lagoon acquired a Ca-chloride composition, while the Na/Cl ratio will be determined by the amount of halite precipitated (Katz and Starinsky, 2009; Starinsky and Katz, 2014).

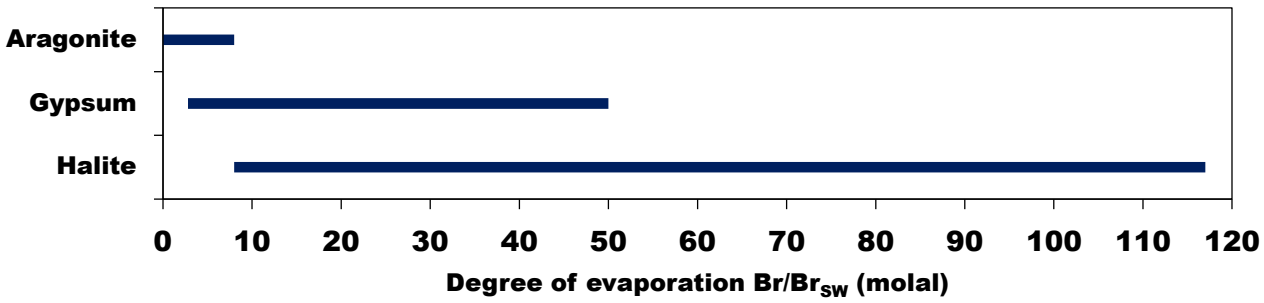

Fig. 4.5 – Mineral precipitation during seawater evaporation. Modified after Starinsky and Katz (2014).

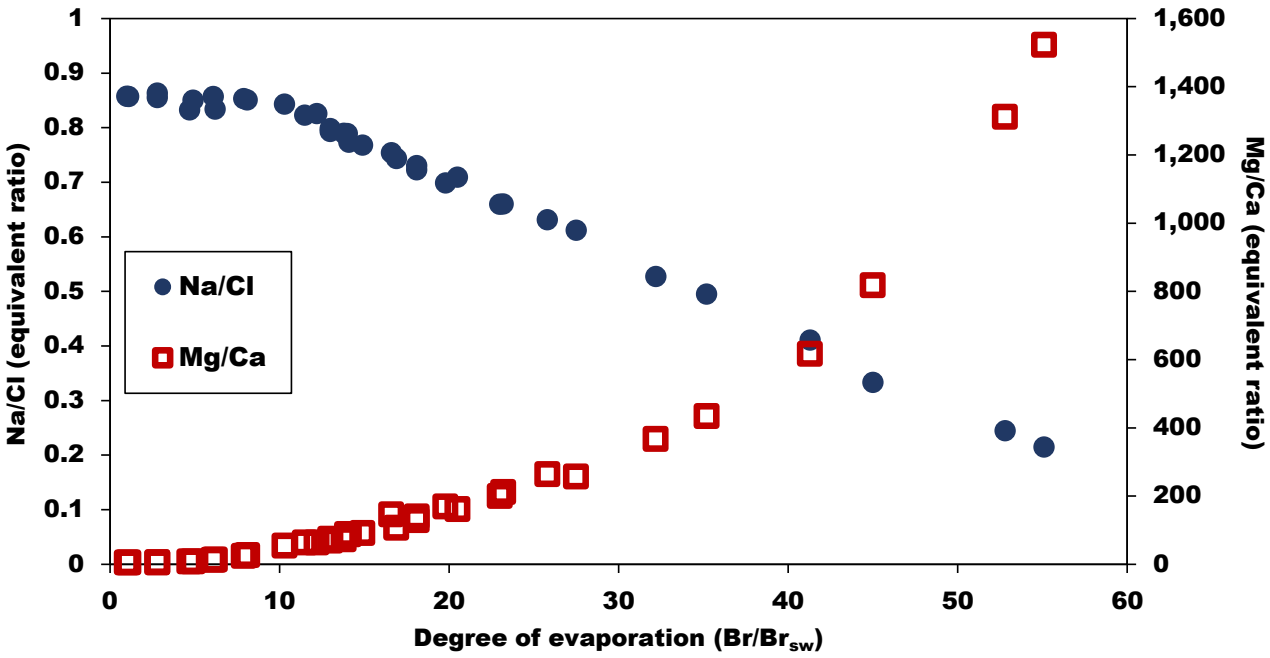

Fig. 4.6 – Na/Cl and Mg/Ca equivalent ratios during seawater evaporation. Based on Starinsky and Katz, (2014). The increase in the Mg/Ca ratios is followed by a dramatic decrease resulting from the dolomitization process which occurs after the brines intrude to carbonate host rocks.

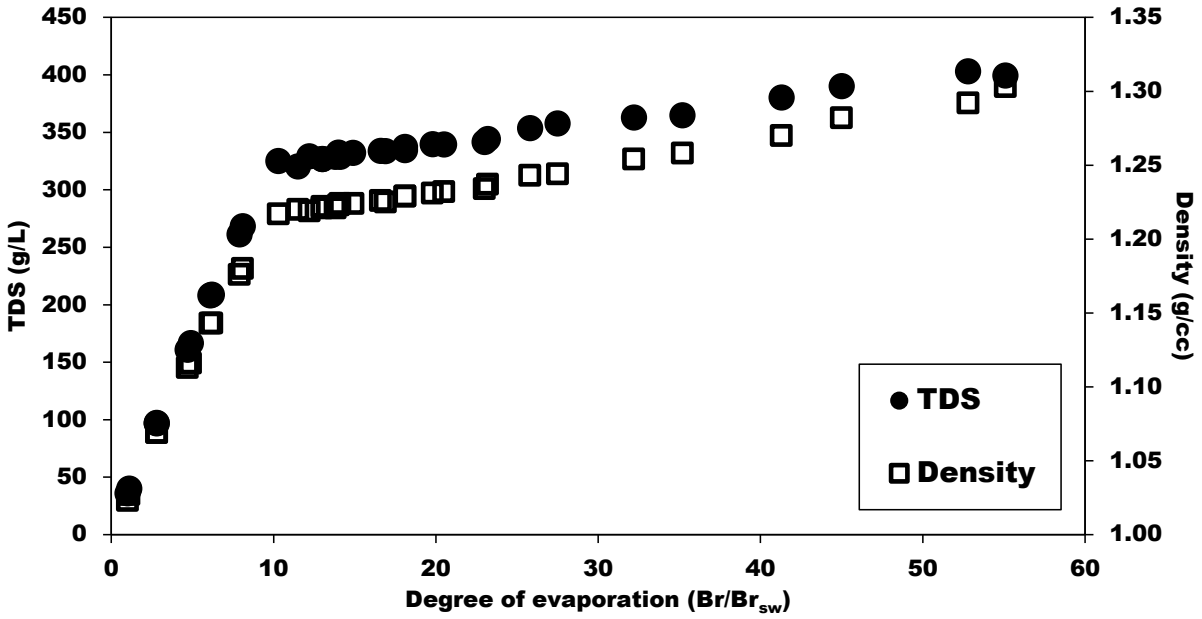

Fig 4.7 – TDS (g/L) and density (g/cc) during seawater evaporation. Based on Starinsky and Katz, (2014). As halite precipitates at an evaporation degree of ~10, the density increases over 20% than the density of freshwater which prompts the density driven intrusion process into the surrounding host rocks.

At an evaporation degree of about 10, the salinity of the evaporated brines is above 300 g/L. The increase in salinity of the brines is accompanied by a significant increase in their density (Fig 4.7), that reaches values higher by 20% compared to the density of freshwater. The high density of the brines results in density-driven migration into surrounding rock units, while substituting the water that were previously stored in the reservoirs (Stanislavsky and Gvirtzman, 2000). Depending on the geological and hydrological settings of the basin, dense brines can remain stagnant in the deep parts of the reservoirs over geological timescales. In some sedimentary basins, intruded brines are being constantly flushed by freshwater, but the process can span over geological timescales, especially for impermeable formations. In such scenarios, the sedimentary section can display a wide range of salinities, that expresses different degrees of dilution by freshwater (Kreitler, 1988; Ferguson et al., 2018).

Based on the high concentrations of Cl^- and the Ca-chloride composition of the studied water, the Mt. Scopus Group in the southern GH contain the remnant of a Ca-chloride brine that was strongly diluted by freshwater. Ca-chloride saline water bodies are found along and at the margins of the DSR in the entire area between Lake Kinneret in the north and Timna area in the south (Fig. 4.8). The brines evolved from evaporated seawater that transgressed during the Neogene through Yizra'el Valley in several short pulses. The seawater underwent evaporation and deposited a thick sequence of halite in two local basins along the DSR: the Dead Sea Basin and the Kinnarot Basin (García-Veigas et al., 2009).

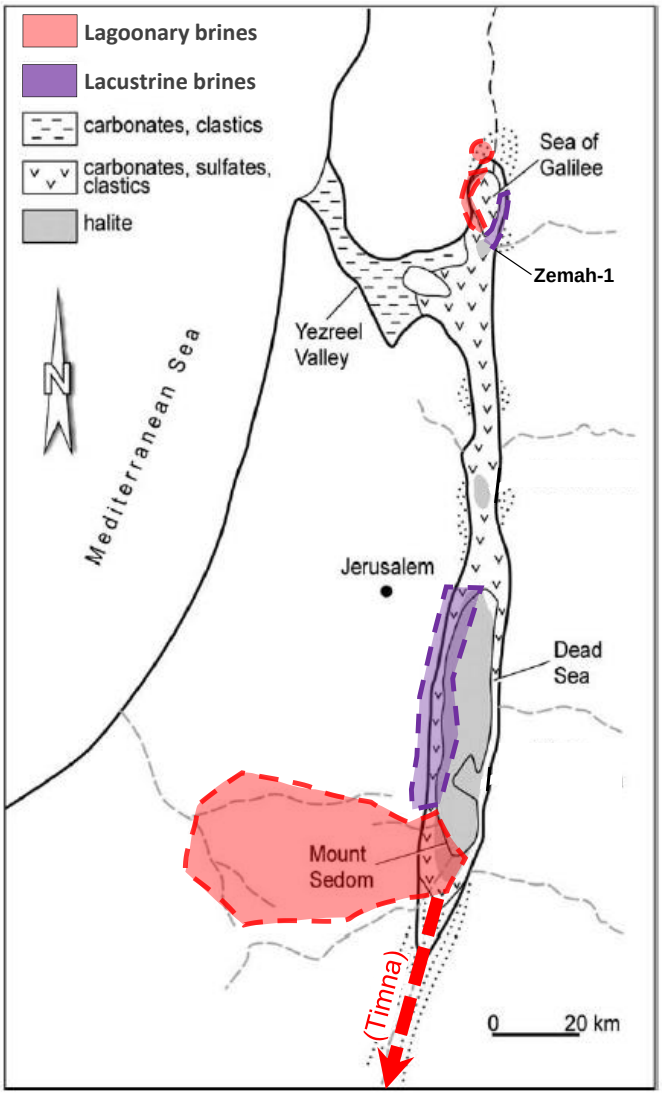

Fig. 4.8 – The extent of evaporitic deposits along the DSR and the distribution of brines surrounding the main tectonic depressions. Modified after García-Veigas et al. (2009).

The evaporitic sequence in the Kinnarot Basin is a sub-facies of the Bira Formation, that was found in Zemah-1 deep borehole (Marcus and Slager, 1985). The Bira Formation in Zemah-1 includes two parts, the lower part consists of halite with thinly interbedded layers of carbonate, marl and gypsum that represents a period of frequent changes in the evaporation/inflow ratio of the lake. The upper part consists of a massive 550 m thick halite that represents a period during which the lake underwent extensive evaporation (Raab et al., 1997; Rozenbaum et al., 2019). Overlying the halite deposits in Zemah-1 are lacustrine sediments of the Gesher Formation, which were deposited in a lacustrine water body that received only freshwater inflows (Shaked Gelband et al. 2019). The freshwater around Lake Kinneret exhibits a HCO_3^-/Ca^{2+} equivalent ratio that is larger than 1. The interaction between the saline Ca-

chloride lake and this freshwater leads to the precipitation of carbonate minerals (mainly aragonite) which significantly reduces the Ca^{2+} concentrations. On the other hand, Mg^{2+} behaves conservatively and does not precipitate with any mineral (Katz, 1973), and therefore, with evaporation, the concentration of Mg^{2+} increases. This opposite behavior , leads to a gradual increase in the Mg/Ca ratio of the lake (Katz and Starinsky, 2009). Such a process, which takes place during the lacustrine stage (following the disconnection of the lake from the sea), enables to divide the saline water into two groups: (A) brines from the lagoonary stage, with Mg/Ca ratios lower than 1, and (B) brines from the lacustrine stage, with Mg/Ca higher than 1 (Katz and Starinsky, 2009). At the southern DSR, brines from the lacustrine stage are found mostly within the DSR (Fig. 4.8), while brines from the lagoonary stage are found at a distance of up to 90 km from the DSR (Stanislavsky and Gvirtzman, 2000). Surrounding Lake Kinneret, lagoonary brines are found only west and north of the Kinneret Lake, while lacustrine brines are only at the southeastern Kinneret (Katz and Starinsky, 2009; Starinsky and Katz, 2014).

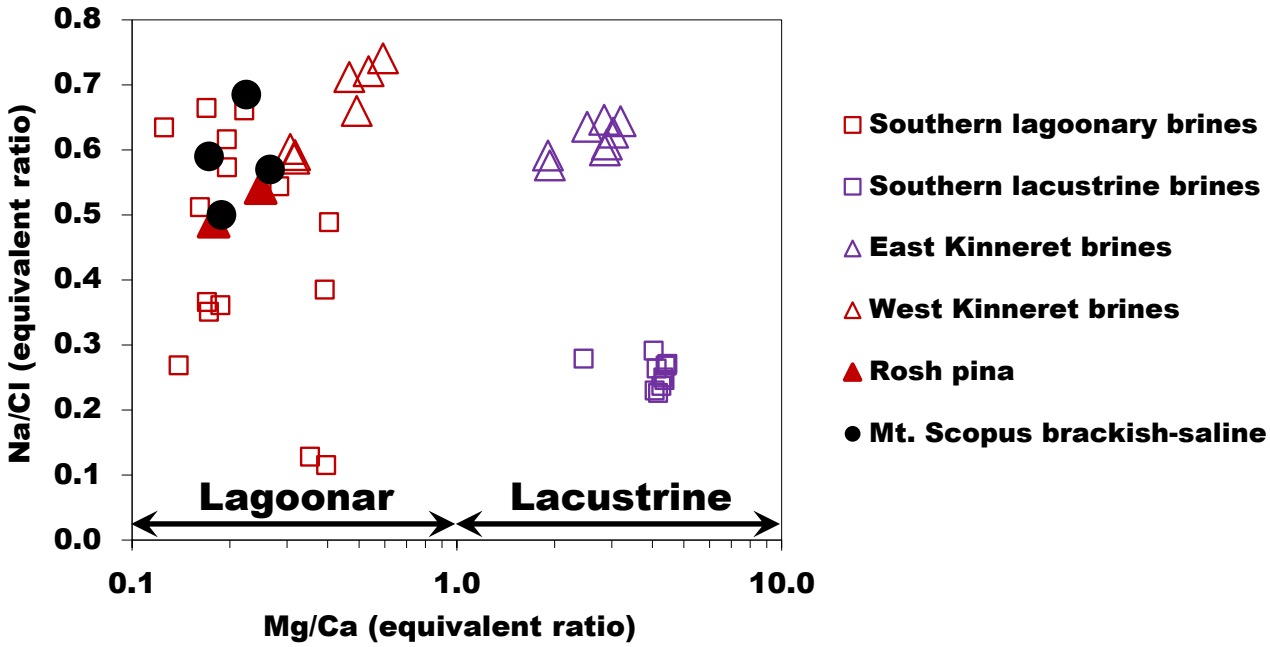

Fig. 4.9 – Na/Cl vs. Mg/Ca of the DSR brines and the studied water. The Mg/Ca of the studied water implies it contains traces of brines that were formed during the lagoonary stage. Modified after Starinsky and Katz (2014).

Similar water bodied are known from around the Kinneret Lake basin (Fig. 4.3, 4.8 and 4.9). The northern DSR brines were found in different composition that represent different stages of evolution at the surface followed by intrusion into the subsurface (Starinsky and Katz, 2014) Based on location and chemical

composition, the brines were divided into groups (such as Tiberias, Tabgha and Fuliya). The brines surrounding the Kinneret Lake were found to exhibit salinities of up to 35,000 mg/L (TDS) and therefore, they were strongly diluted by freshwater. One hypersaline brine was found in proximity to the research area, in the Rosh Pina-1 deep well located north of the Kinnaret Lake (Fig. 1.2). The salinity of the Rosh Pina (RP) brine was 173,000 mg/L meaning it is the least diluted brine found thus far in the northern DSR.

Major ions composition

Even though the DSR brines are found in a wide variety of compositions and dilution factors, in order to demonstrate the relationship between the saline water bodies in the research area, the composition of the RP brine (composition is presented Appendix 6) will be taken as an example of the saline endmember. During the dilution process of a hypersaline brine (such as the RP brine) and freshwater, the large difference in salinity between endmembers results in the preservation of the ionic ratios of the brines, even when the volume fraction of the brine is less than 3% (Fig 4.10).

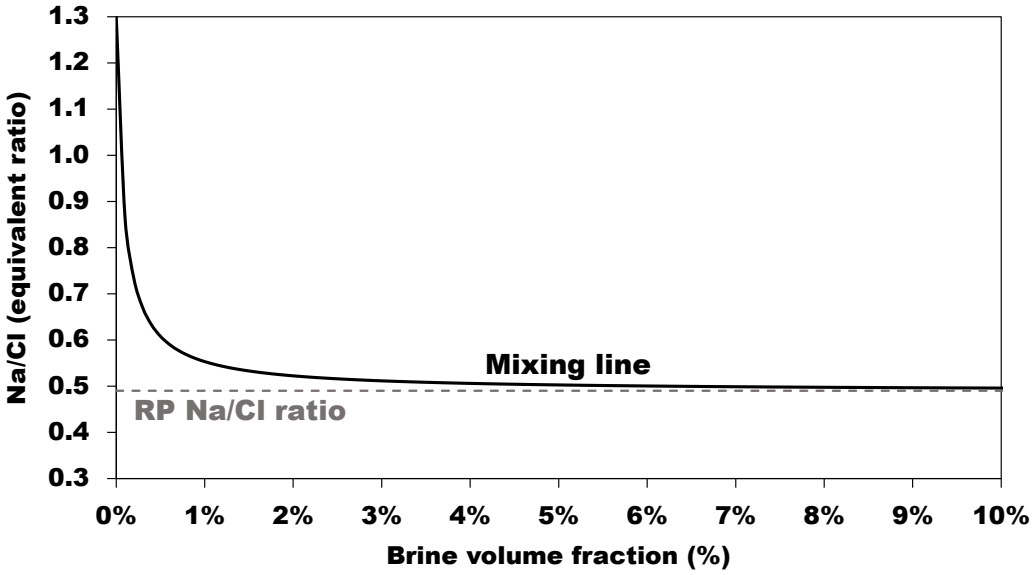

Fig. 4.10 – The Na/Cl ratio during the theoretical dilution of the RP brine by freshwater (from the Mt. Scopus in Ness 12). Only below 3%, the ratio deviates from the brine ratio towards the FW ratio and therefore no longer preserves the composition of the brine.

At relatively high salinities, major processes are required to alter the solution ionic ratios. However, as the salinities are reduced, the relative role of water rock interactions increases, which can lead to a non-conservative behavior.

The concentrations of the different ions during the theoretical mixing between the RP brine and freshwater are presented in Fig. 4.11 (a-g). The brackish water from the MGF are very similar by the Na/Cl, Ca/Cl and Mg/Cl (Fig. 4.11 a,b and c, respectively) to the RP brine and therefore, based on these ions, the water in the MGF are the result of a conservative mix between brine and freshwater. The MGF water samples also roughly fit the Sr/Cl ratios found in the western Kinneret brines (Fig. 4.11 d) which also fit aforementioned Na/Cl, Ca/Cl and Mg/Cl ratios of the RP brine (Sr was not reported for the RP brine). The rest of the measured elements, Br^-, SO_4^{2-} and HCO_3^- are not conservative. The low Br/Cl ratios can be explained by adsorbtion onto the solid organic matter (kerogen) which is extremely high in the MGF source rocks (Hsu et al., 2010) (Fig. 4.11 e). Though SO_4^{2-} concentrations seem to coincidently fit the mixing line with the RP brine (Fig. 4.11 e), they should be considered as non-conservative since they are affected by sulfate reduction (Merkel et al., 2005), water-rock interactions (such as dissolution and mineralization of gypsum and pyrite) and the H_2S generated from the MGF source rock maturation. CO_2, which is the predominant gas in the MGF, derived from source rock maturation is also likely to significantly alter the HCO_3^- concentrations. (Fig. 4.11 g). Nevertheless, based on the concentrations of Na^+, Ca^{2+}, Mg^{2+} and Cl^- the water from the MGF contains the same mixing ratios between freshwater and a brine with a composition such as the RP brine. It is important to mention, that it is not suggested that the RP brine intruded the Mt. Scopus Group in the southern GH since it is viewed that the DSR brines were constantly changing in composition and density. Furthermore, following the intrusion of the brines, different water-rock interactions have occurred over geological time, depending on their intrusion depth, distance from the DSR, residence time, pressure, temperature, type of host rock, local hydrological history, etc. Therefore, the usage of the RP brine as a reference brine should not be regarded as a claim that this brine is the exact type of brine that intruded into the southern GH. The usage of the RP brine as a reference point was to demonstrate that the fit with the DSR brines is better than other saline bodies, such as seawater.

Some proof for the complexity and variability of different generations of DSR brines is given by the analysis and comparison of the water found in the Taqiye formation, in comparison with the MGF waters. The ionic ratios in the Taqiye Formation are slightly different than the MGF and therefore, calculated volume fractions of the RP brine in the Taqiye have a larger range. Based on the Na^+, and Cl^-, the Taqiye contains 10%-13% brine (with a composition of the RP brine) and only 5%-6% based on the Mg^{2+} and

Ca^{2+} concentrations. The higher Na/Cl ratio of the water from the Taqiye Formation suggests that the saline endmember is not the same as the one in the MGF. Since the brine in the Taqiye Formation is also less diluted, we assume that the different composition is the result of the lower permeability in the Taqiye formation in comparison with the MGF. This means that the water in the Taqiye in Ness 02 are older than the water in the MGF (slower advance rates from the DSR eastwards). The Na/Cl decreases at the surface during the precipitation of halite, so the higher Na/Cl ratio could indicate that the brine that intruded the Taqiye precipitated less halite than the brine that intruded the MGF.

The sample retrieved while drilling Ness 02 (Mt. Scopus Ness 02), contains a mixture of water from different horizons and compositions across the open hole section. Despite the mixture of various horizons, the calculated volume fractions by Na^{+}, Ca^{2+}, Mg^{2+} and Cl^{-} are all within 0.5%-2% of the Rosh Pina reference brine. The high degree of dilution of the sample retrieved while drilling indicates that a freshwater component is present within the open hole section (Lower Taqiye- Lower Mishash Formations, Fig. 3.2), which was not tested during the DSTs.

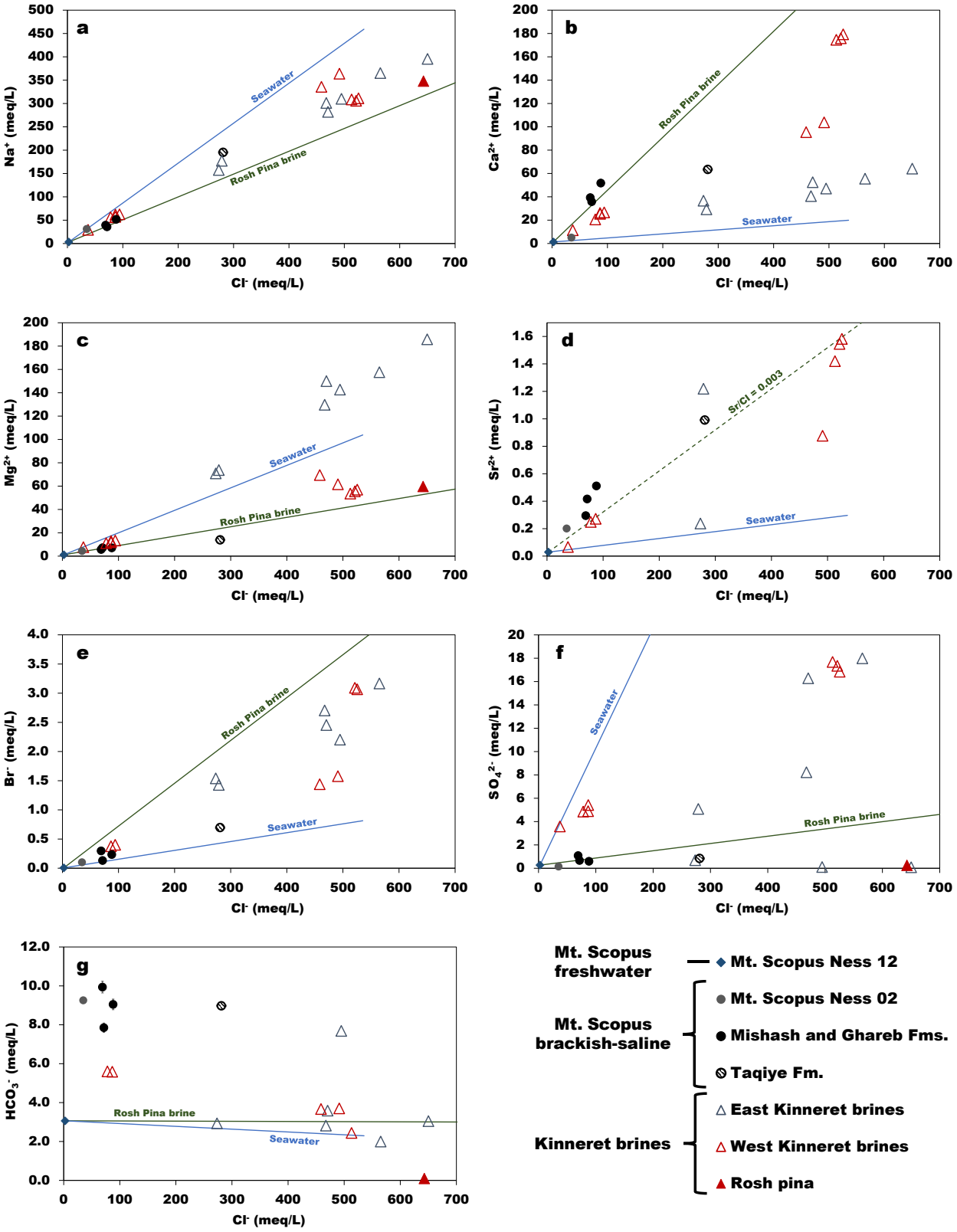

Fig. 4.11 (a-g) – Ion concentrations (meq/L) of the studied water and the Kinneret brines vs. Cl^-. Mixing lines between seawater (blue) and Rosh Pina brine (black) to freshwater were added as well. The compositional data is presented in Appendices 2 and 6. compositions are presented in Appendix 2 and Appendix 6.

The Mg/Ca ratio of the dilution product is affected by both endmembers: (1) The limnological phase during which the brine evolved at the surface will determine the Mg/Ca of the saline endmember. The ratio itself will be set by the dolomitization process which takes place at the subsurface, after the brines intruded. Previous works suggested that the initial ratio after dolomitization was lower than 0.2 (Katz and Starinsky, 2009) which is also the ratio in the least diluted brine in the region, the RP brine (Fig. 4.8). Mg/Ca ratios which are lower than 1 appears in brines that were separated from the surface before a significant amount of freshwater entered the basin and elevated the ratio. (2) At high degrees of dilution, the ratio will be more subjected to water-rock interactions. The western Kinneret brines show an increase in the Mg/Ca ratios at higher degrees of dilution. The increase in the Mg/Ca ratio was related to the freshwater source and the stratigraphic unit in which the water body is located (Gvirtzman, 2006; Klein-BenDavid et al., 2005). The low Mg/Ca ratios of the studied water (Figs. 4.9 and 4.12) suggest that the brines that intruded the Mt. Scopus Group in the southern GH had low Mg/Ca ratios and therefore, were formed during the lagoonary stage, similarly to the western Kinneret and RP brines.

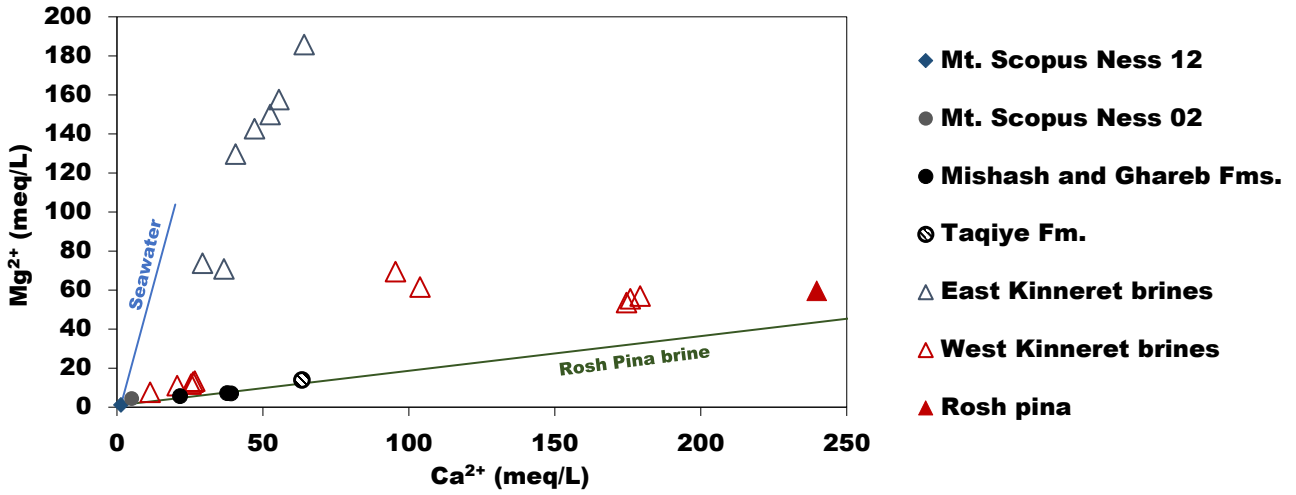

Fig. 4.12 – Mg^{2+} vs. Ca^{2+} concentrations (meq/L) of the studied water and the Kinneret brines. Mixing lines between seawater (blue) and Rosh Pina brine (black) to freshwater were added as well.

Stable water isotopes

The $\delta^{18}O$ and δD isotopic data presented in this chapter is consistent with the conclusions drawn based on the dissolved ions (Na^{+}, Ca^{2+}, Mg^{2+} and Cl^{-}) that the water studied from the southern Golan Heights is a mixture between the DSR brines (such as the brine found in Rosh Pina) and freshwater (such as the water found in Ness 12). While the information provided by the dissolved ions composition and ratios

are mostly affected by the brine endmembers and therefore can provide insights regarding the brine composition (despite the relatively low brine fraction), the isotopic composition adds information regarding the freshwater endmember which could not have been provided by the dissolved ions.

The $\delta^{18}O$ value for the brine endmember was measured by Gat et al. (1969) on the Rosh-Pina brine and was shown to exhibit an enriched value (+3‰) due to the extensive evaporation the brine underwent. On the other hand, the light isotopic values of the Ness 02 and 03 samples implied that the freshwater endmember(s) had to be even lighter. The lightest and freshest sample in the study area was therefore used as a possible fresh endmember (Fig. 4.13 a,b). The studied water from the southern wells (Taqiye and MGF) fall in proximity to the suggested mixing line, thereby complimenting the previously drawn conclusions based on the dissolved ions. The most saline water from the Taqiye Formation exhibit the highest $\delta^{18}O$ values (-6.0‰) compared with the water from the MGF which exhibit slightly lighter values (~-7.2‰). The difference in the $\delta^{18}O$ of the water from the Taqiye Formation correlates to their expected increase in salinity from the mixture of the two endmembers (Fig. 4.13). The calculated volume fraction based on the $\delta^{18}O$ of Taqiye Formation was 12%, which falls within the range that was defined based on the dissolved ions (predominantly Na^+ and Cl^- (10%-13%). Similarly, the brine volume fraction based on the $\delta^{18}O$ of the water from the Ghareb Formation in Ness 03 contains is 3% and the open section in Ness 02 contains 1%, which is similar to the values calculated based on the dissolved Na^+, Mg^{2+}, Ca^{2+} and Cl^- species. Meaning, the same fractions are calculated independently by ion concentrations and by the isotopic composition of the water for the MGF, as well as the Taqiye Formation.

The δD (Fig. 4.13 c,d) shows a similar correlation to salinity as the $\delta^{18}O$ (Fig. 4.13 a,b). The MGF have the same δD (~-41‰), while the water from the Taqiye Formation have a higher δD of -36‰. Since δD was not in the RP brine, a linear regression was performed between the freshwater from Ness 12 and the Taqiye Formation which resulted in an estimation of +18.6‰ for the saline endmember with a Cl^- concentration such as the RP brine. This value is slightly higher than the estimated enrichment during the evaporation of the saline lake, which was estimated to be approximately +9‰ (Horita and Gat, 1989).

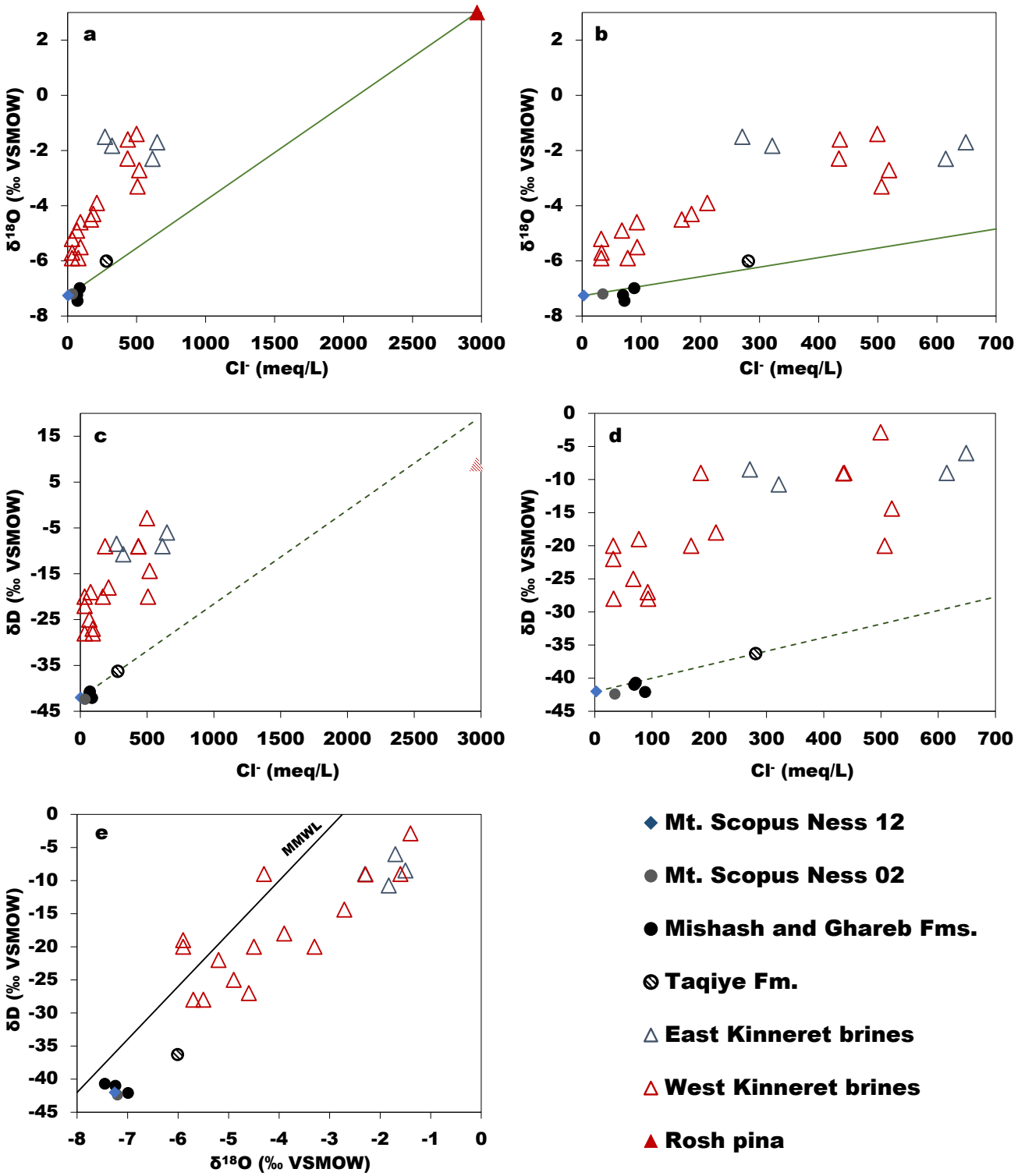

Fig. 4.13 (a-e) – Stable water isotopes in the studied water and the Kinneret brines. For both Kinneret brines and the studied water, the isotopic composition of hydrogen and oxygen increases as a function of salinity. (c) The estimated maximum enrichment in δD (+9‰) during evaporation (Horita and Gat, 1989) was added (dashed red triangle) for comparison with the extrapolated value based on the data from the current research. The calculated value by linear regression is slightly higher (+18.6‰) than previous estimations. The chemical compositions compilation is presented in Appendices 3 and 7.

Similar to the Kinneret brines, the studied water have a positive relationship between the isotopic composition to the salinity. However, at similar degrees of dilution, the isotopic composition of the studied water is distinguishably lighter, reflecting the different fresh endmembers.

The increasing elevation towards the northern GH is reflected by the "altitude effect", which leads to a decrease in the $\delta^{18}O$ values of the rainwater towards the north (Dafny et al., 2006). $\delta^{18}O$ values of below -7.0‰, such as the ones that are found in the water from the Mt. Scopus Group, only appear in rainwater that precipitated above an elevation of 1,000 m AMSL (Fig. 4.13). Such values can be explained by the direct recharge on Mt. Scopus outcrops at the area of Birkat Ram or the distant Palmyride Mountains (Fig. 1.2), where the $\delta^{18}O$ value of the rainwater is -7.2‰ (Fig. 4.13). The low δD values of the studied water (~-42‰), resemble the values on the southern flanks of the Hermon Mt. (< -40‰) and suggests the source of the freshwater is probably not from the distant slopes of the Palmyride Mountains, where δD values are higher than -35‰ (Kattan, 2021). However, since the isotopic composition of the rainwater is known to change over time (Mazor, 1991), the fact that the modern day values fit the Hermon values better than the Palmyride Mountain does not unequivocally suggest that the source of the freshwater component is from the Hermon Ridge, despite the better fit to modern values.

The difference between the southern GH samples and the Kinneret brines, which exhibit a significantly heavier isotopic values (> -6‰), suggest that the water which diluted the brines near the Sea of Galilee originated from significantly lower recharge altitudes (Fig. 4.14). The light isotopic composition of the Mt. Scopus group in the GH could only have originated at relatively high elevations and transported through the subsurface from a far, while gradually diluting the high salinity endmember over geological time spans. The exact freshwater source cannot be identified based on existing data, nor connections to other groundwater systems through fractures or faults or potentially other flow paths that may also cross different hydrogeological units.

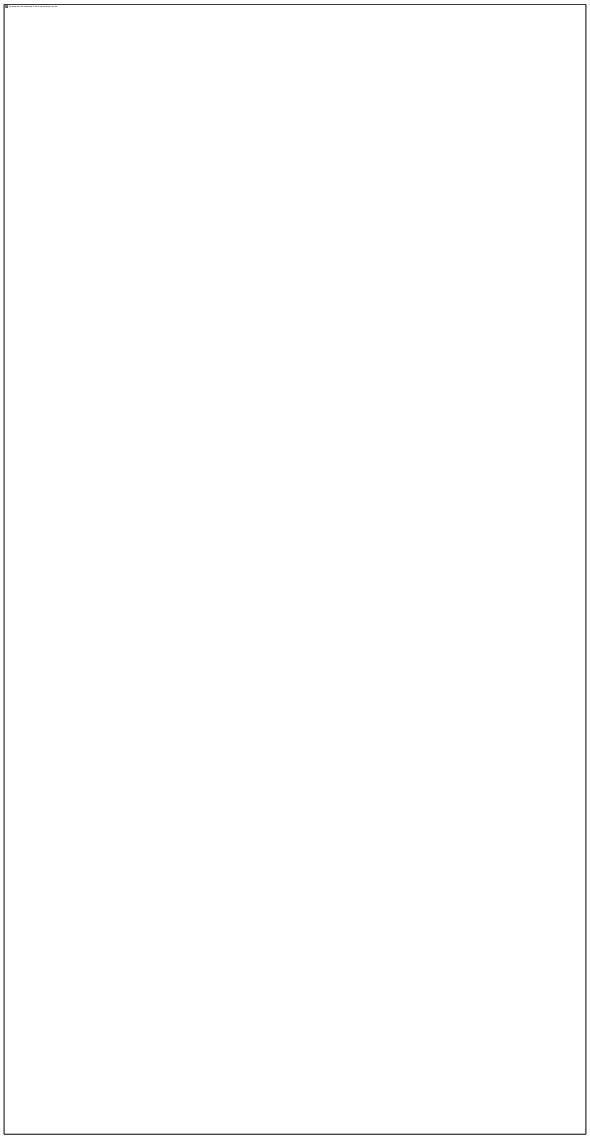

Fig. 4.14 – $\delta^{18}O$ values of the rainwater and groundwater in the GH, From Dafny et al. (2006). Values below -7‰ are only found at altitudes of above 1,000 m, therefore the dilution of the brines in the Mt. Scopus Group in the southern GH could only have occurred in the subsurface.

Strontium isotopes ($^{87}Sr/^{86}Sr$)

The isotopic composition of Sr^{2+} in fresh groundwater provides an indication of the rocks the water interacted with. However, when the groundwater contain a mix of fresh and saline endmembers, the $^{87}Sr/^{86}Sr$ values are controlled by the relative contribution of Sr^{2+} from each endmember, which will be significantly higher from the brines.

Previous studies (Gavrieli and Stein, 2006; Stein et al., 2000) showed the $^{87}Sr/^{86}Sr$ of the DSR brines was lowered from the initial value of the seawater (~0.709) as a result from the release of Sr^{2+} with lower

$^{87}Sr/^{86}Sr$ values from surrounding rocks during the dolomitization process. After the brines regressed into the basin (at lake level drops) the lower $^{87}Sr/^{86}Sr$ values they acquired were recorded in the halite they precipitated. Assuming the brines that precipitated the halite in Zemah-1 well are the brines that intruded the Mt. Scopus Group in the GH, as well as the Kinneret Lake Basin, the $^{87}Sr/^{86}Sr$ of the halite beds can be compared to the $^{87}Sr/^{86}Sr$ of the brines.

The isotopic composition of Sr^{2+} in the studied water (Table 3.5) from the MGF in Ness 02 is 0.70772-0.70774, slightly lower than the $^{87}Sr/^{86}Sr$ of the water from the Taqiye Formation (0.70781) and higher than the Ghareb Formation in Ness 03 (0.70766). The $^{87}Sr/^{86}Sr$ of two groups of Kinneret brines was compiled from previous studies (Appendix 7). The brines from the Fuliya block is 0.70787 (Bergelson et al., 1999) and $^{87}Sr/^{86}Sr$ of the Tiberias hot springs is slightly lower (0.7077) (Starinsky and Katz, 2014).

The $^{87}Sr/^{86}Sr$ isotopic composition of the halite bodies discovered in the nearby Zemah-1 well (Fig. 1.2) was measured in several depths (Fig.4.15) each characterized as sub-facies of the Bira Formation halite bodies (Raab et al., 1997).

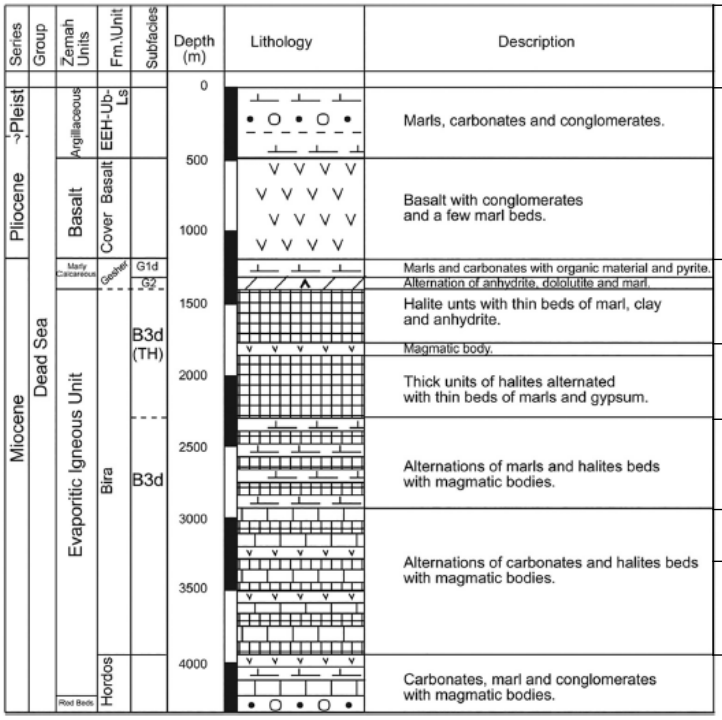

Sample minerology	Depth (m)	$^{87}Sr/^{86}Sr$	$^{40}Ar/^{39}Ar$ age (Ma)
Basalt	1000		4.92
Halite (upper)	1646	0.70750	
Halite (middle)	2000	0.70917	
Halite (lower)	2567	0.71091	
Gabbro	3200		9.5
Anhydrite	3803	0.70729	

Fig. 4.15 – Generalized columnar section of Zemah-1 borehole. Halite and anhydrite samples were analyzed for $^{87}Sr/^{86}Sr$ by Raab et al. (1997). $^{40}Ar/^{39}Ar$ ages after Heimann and Stein, in prep. (from Stein, 2014). Modified after Rozenbaum et al. (2019). The middle-upper halite show decreasing $^{87}Sr/^{86}Sr$ values upwards.

The lower halite (Fig. 4.15) consists of alternating layers of halite and carbonates, that represents alternating salinities (and densities) of the water in the surface. The two other parts of the succession, the middle and upper halite, consists of massive halite that represents a period during which the lake was hypersaline, and the density of the brines was over 1.2 g/cc (Fig. 4.7). The $^{87}Sr/^{86}Sr$ values of the middle and upper halite show an upward decrease that should have been visible in the $^{87}Sr/^{86}Sr$ of the brines as well.

The $^{87}Sr/^{86}Sr$ vs. Na/Cl ratio of the studied water and the Kinneret brines is presented in Fig. 4.16. The $^{87}Sr/^{86}Sr$ decrease with decreasing Na/Cl ratios, which is correlative with halite precipitation. The hypersaline depositional environment, in addition to the $^{87}Sr/^{86}Sr$ of the middle and upper halite indicates the origin of the brines that intruded into the Mt. Scopus in the southern GH, as well as the Fuliya and Tiberias block have originated from the brines that precipitated the middle and upper halite in the Kinnarot Basin. The decrease in the $^{87}Sr/^{86}Sr$ values of the lake could be related to regression of brines from surrounding groundwater systems, as shown for the southern DSR basin, where the $^{87}Sr/^{86}Sr$ decrease following the dolomitization process (Starinsky and Katz, 2014; Stein et al., 2000) . It is reasonable to assume the Na/Cl of the lake probably fluctuated depending on discharge rates of the returning brines, which mostly depends on lake levels.

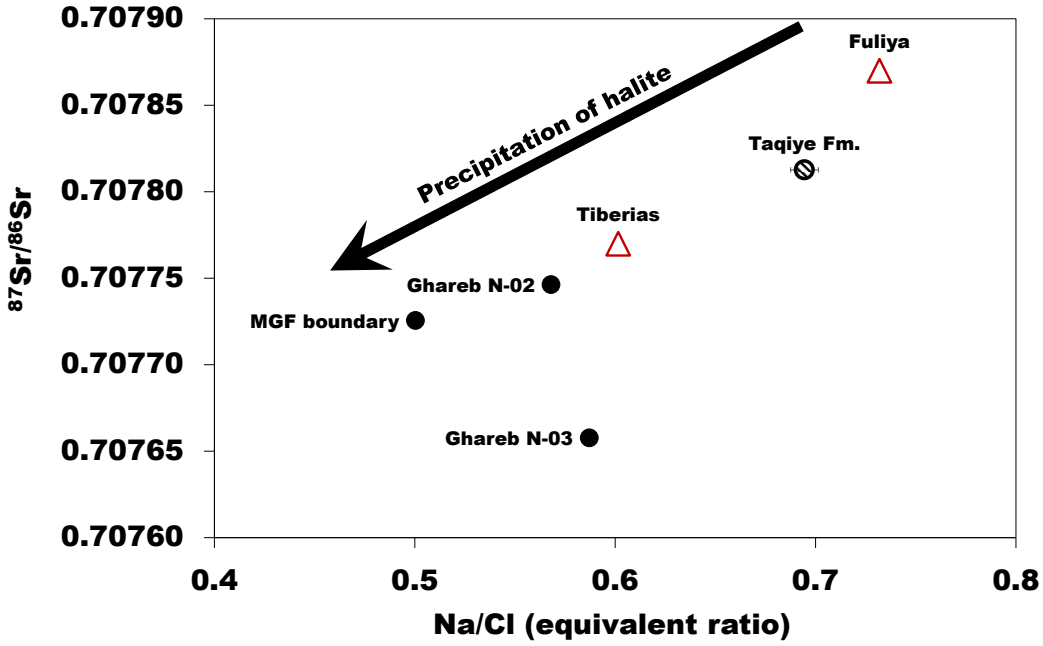

Fig. 4.16 - $^{87}Sr/^{86}Sr$ vs. Na/Cl ratios of the studied water and the western Kinneret brines. The arrow points in the direction in which the composition changed during the precipitation of the middle-upper halite in Zemah-1.

The $^{87}Sr/^{86}Sr$ of the water section from Ness 02 is very similar to value in the Taqiye Formation (0.70784), which indicates the main fraction of Sr^{2+} in the water is derived from the saline sources in the section. In contrast, the $^{87}Sr/^{86}Sr$ of the water from the open section in Ness 12 is significantly lower (0.70746) and fits the $^{87}Sr/^{86}Sr$ values of the Lower Mishash Formation (Fig. 4.17), which was precipitated from Lower Campanian seawater (McArthur et al., 1994). The $^{87}Sr/^{86}Sr$ of the water from Ness 12 is consistent with field observations, which reported a high influx of water from the Lower Mishash Formation during drilling.

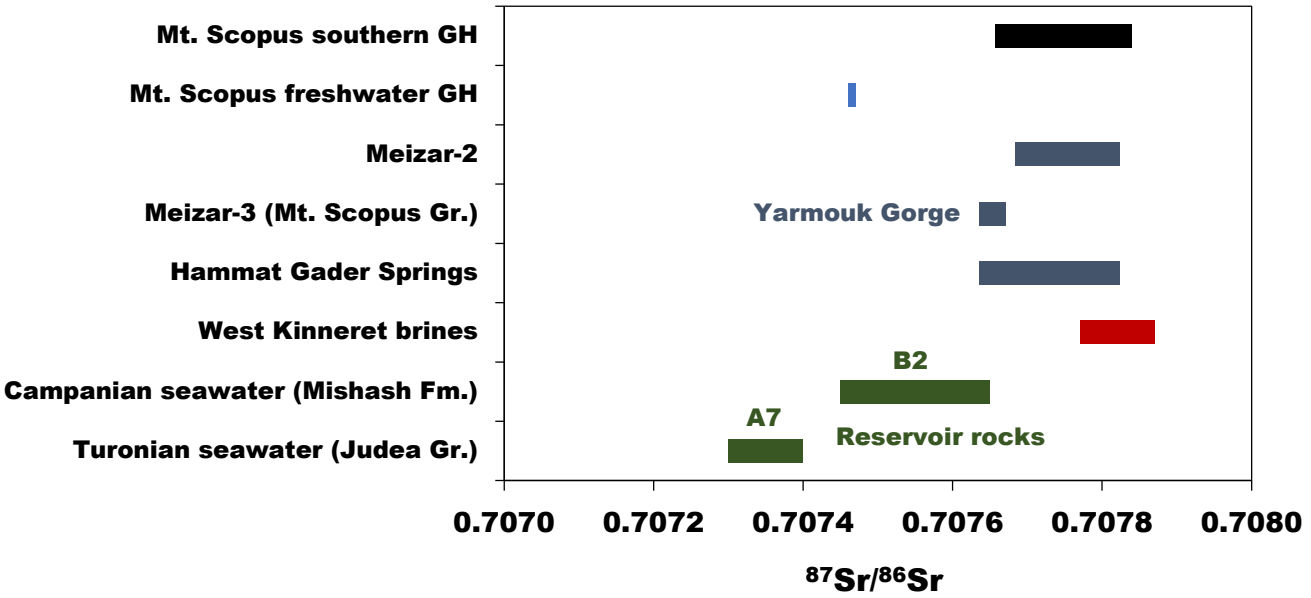

Fig. 4.17 – The isotopic composition of Sr^{2+} in the studied water, as well as other sources from the region, in comparison to the reservoir rocks. The $^{87}Sr/^{86}Sr$ values in the water from the Meizar 2 well are higher than the $^{87}Sr/^{86}Sr$ values of the Bina Formation, suggesting it may also contain traces of DSR brines.

Relationship to the Yarmouk Gorge outlets

Hammat Gader hydrothermal springs

The Yarmouk Gorge is at the border between two regional hydrogeological systems (Fig. 1.1), where water from the Ajloun anticline mix with water from the Hermon-Golan and discharge from the Hammat Gader springs. Geochemical evidence for traces of DSR brines in the hydrothermal springs of the Lower Yarmouk Gorge (YG) were presented in previous work (Farber et al., 2007; Starinsky et al., 1979). The intrusion of DSR brines into hydrogeological systems of the GH comes in agreement with these works. Furthermore, these findings clarify the relationship (Fig. 4.18) between temperatures to the salinity and isotopic composition of the water (Gavrieli and Burg, 2002; Starinsky et al., 1979).

The high salinities and depleted isotopic composition represent the GH contribution in the springs, which is also derived from deeper units which experience steeper geothermal gradient (Reznik and Bartov, 2021). The GH component is in contrast to the component derived from the system in the Ajloun, which is fresh and has a lower water temperature. Higher relative contribution from the GH will increase both the temperature and the salinity of the water and decrease the $\delta^{18}O$ of the water. The GH contribution is also reflected in the Na/Cl, Mg/Ca and the $^{87}Sr/^{86}Sr$ (complete compositions in Appendix 4-5) (Farber et al., 2007), though DSR brines may constitute less than 1% since they are diluted to a degree in which they are no longer Ca-chloride (Starinsky et al., 1979). It is reasonable to assume the GH contribution is a mix of different saline end-members, which were diluted to different degrees and possibly discharges from other systems other than the Mt. Scopus. Therefore, an estimation of the relative GH contribution in the springs will be impossible.

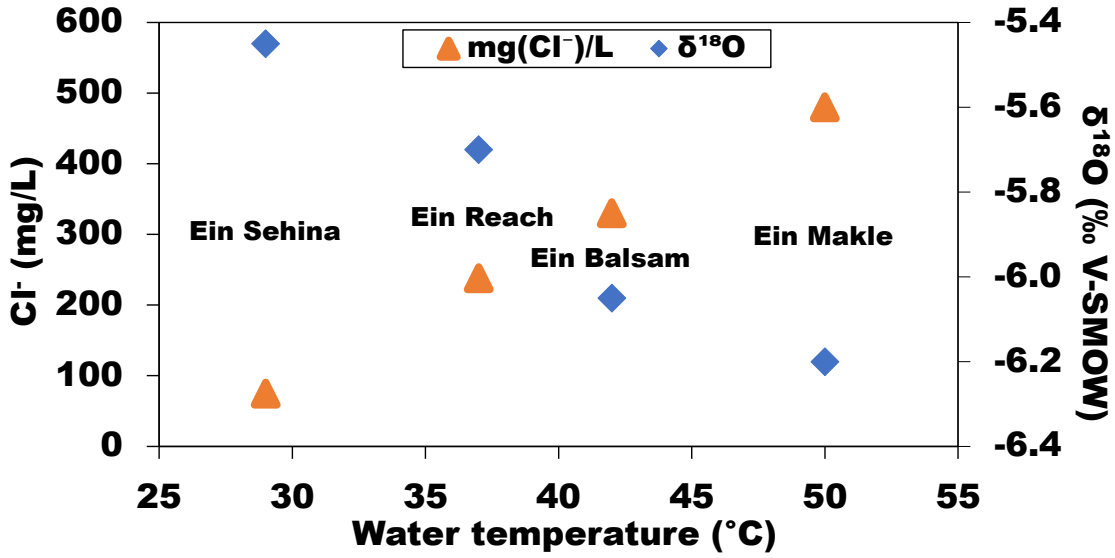

Fig. 4.18 – Temperature-salinity-$\delta^{18}O$ relationship of Hammat Gader springs. Modified after Gavrieli and Burg (2002).

Meizar wells

The water from Meizar 3 well are derived from the Mt. Scopus Group aquifer (B2), do not seem to contain any significant traces of the DSR brines according to the low salinity (< 600 mg/L), and the high Na/Cl ratio (1.3) of the water (compositions in Appendix 4-5). The isotopic composition of the water has the same values of rainwater precipitated on outcrops of the Mt. Scopus Group at the Ajloun Dome (Fig. 1.2) (Bajjali et al., 1997; Gavrieli and Burg, 2002). The $^{87}Sr/^{86}Sr$ of the water (Fig. 4.17, Gavrieli and

Burg, 2002) suggests the water are mostly derived from the freshwater that interacted with the host rock (B2 aquifer, Fig. 4.17), as they fit the seawater values during the Campanian (McArthur et al., 1994).

The chemical composition of the water from the Meizar 2 well, produced from the Bina Formation (Judea group) aquifer, which is correlative to the A7 subaquifer, as defined in the Jordan (Margane et al., 2002), is very similar to the warmest and most saline spring in Hammat Gader (Ein Makle, ~1,400 mg/L, Appendix 4-5). The Na/Cl ratio in the Meizar 2 well is 0.8, suggesting the salinity could be derived from connate seawater. However, the $^{87}Sr/^{86}Sr$ of the water from Meizar 2 well (Fig. 4.17) is significantly higher (0.70782) than that of the host rock (0.7073) and is similar to the values in the Hammat Gader springs, which implies that the source of the salinity is the traces of DSR brines. This could indicate that the DSR brines may have also intruded into the Judea Group in the GH and have been diluted to a higher degree over time than the water in the Mt. Scopus group. The light isotopic composition ($\delta^{18}O$ = -7.2‰) suggest that the Meizar 2 water is mainly sourced in the GH and not the Ajloun area, in contrast of the heavier composition (>-6.5‰) of the Hammat Gader springs (Gavrieli and Burg, 2002).

4.3 Conceptual palaeohydrological model

The Ca-chloride brines that intruded into the Mt. Scopus Group in the GH as well as the subsurface surrounding the Kinneret, were evolved from a hypersaline lake. According to both the chemical composition of the brines, notably the Na/Cl ratios, the lagoon and/or lake precipitated halite. Such halite deposits were also found in the proximity of the research area in Zemah-1 deep borehole located in the Kinnarot basin.

Ar-Ar ages of basaltic flows from the top and base of the Bira and Gesher Formations (Fig. 4.15), indicate that the deposition of the entire sequence was between ~9.5 to 5 Ma (Heiman and Stein in prep., from Stein, 2014). However, the transition between the Bira and Gesher Formations, was related to a lake level drop that occurred ~7 ma ago (Rozenbaum et al., 2019).Consequently, these deposits, provides a time constraint of 9.5-7 ma for the intrusion of the lagoonary brines. Since the vertical displacement during the last 15.5 ma was 20 km (Shaliv, 1991), the GH could have been placed 10-12 km south then today, placing the area of Ness 02 and Ness 03 next to Kinnarot basin (Fig. 4.16). The spatial differences in the chemical composition suggests the brines intruded during different or consecutive phases, most interestingly, the presence of lagoonary brines in the west of the Kinneret and in the GH and lacustrine brines in the eastern Kinneret (Fig. 4.8).

At the surface, the composition of the lake is controlled by the limnological conditions, like changes in evaporation/inflow ratio, which dictates the density of the lake and controls the precipitate type and quantities. Since the evolution of the hypersaline lake over time is considered to have had wet/dry cycles over geological periods, it is important to note that the intrusion of the brines into the host rocks surrounding the rift also fluctuated over time. Furthermore, during dry periods some of the brines that have intruded during previous intrusion phases, regressed back into the basin. This also has affected, in turn the composition of the lake. In addition, different formations exhibiting different permeabilities/hydrostatic pressures will have responded differently to the intruding brines leading to the capturing of different brines, reflecting different evolutionary phases as a function of distance and depth from the rift. Furthermore, since the original intrusion some brines were completely washed while in other cases the traces of the saline members can still be found.

As the brines precipitate halite, they disperse from the basin outwards in the subsurface, while substituting the freshwater/brines that were formed during previous intrusion stages (Fig. 4.19). The progression of the brines will be faster through more permeable rocks (Stanislavsky and Gvirtzman, 2000), which means the most ancient brines will migrate further away according to the permeability. The

brine from phase B will have lower Na/Cl ratio than the brine from phase A since it precipitated more halite, resulting in horizontal (Fig. 4.19) and vertical (Fig. 4.20) differences in the composition.

The lake level drop that occurred ~7 ma, also marks the end of seawater transgression pulses into the lake (Rozenbaum et al., 2019) and therefore, the lake receives predominantly freshwater inputs along with some backflow of brines that previously intruded into the host rocks. The freshwater which is enriched in HCO_3^- leads to the precipitation of carbonate mineral (mainly aragonite) when they intermix with the saline Ca-chloride lake. This leads to a decrease in Ca^{2+} concentrations in the lake. Since Mg^{2+} is not precipitated as part of any mineral (Katz, 1973), the precipitation of Ca^{2+} leads to a gradual increase in the Mg/Ca ratio of the lake (Katz and Starinsky, 2009). The water in the lake during this stage were restricted from migrating further away from the rift, possibly due to changes in the geological structure of the basin, that hydraulically bounded the brines from intruding. Another possibility is that the lacustrine brines were less dense and therefore, they could only have intruded shallow aquifers that were not already saturated with lagoonary brines.

In current conditions, the brines that intruded the system (or systems) of the GH are diluted by freshwater which precipitated on the slopes of the Hermon Mt. or the flanks of the Palmyride Mountains. The dissolved solids are flushes in an ongoing process to the natural outlets in the Yarmouk Gorge, where they flow to the Jordan Valley. Similarly to the intrusion of the brines, the dilution of the intruded brines will occur at a faster rate in aquifers that are more active (a combination between hydraulic conductivity recharge area and flow paths). These combined effects lead to a geological section that contain different saline endmembers that were diluted by different degrees (Fig. 4.21). Currently, the systems of the GH are separated from the Kinneret-Kinnarrot basin, due to the vertical displacement and the younger step faults, that act like a hydraulic separator between the GH and the Kinneret (Roded et al., 2013). Consequently, it is not clear whether such an intrusion would have been possible under the current geological settings.

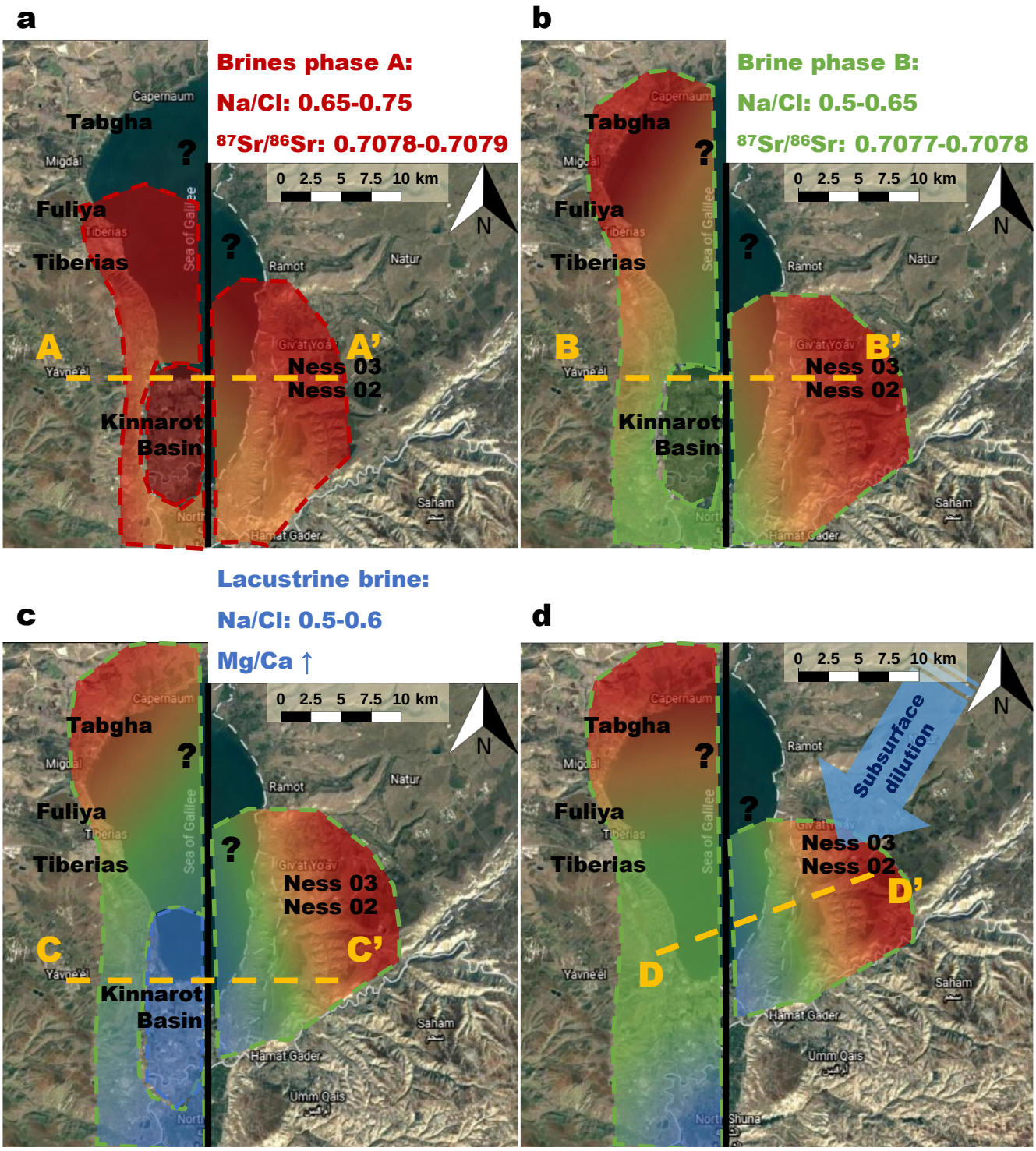

Fig. 4.19 – Schematic illustration of brines intrusions. (a): Intrusion of brines from lagoonary phase A; (b): Intrusion of brines from lagoonary phase B (consecutive to phase A). Brines from phase B "push" the brines from phase A; (c): Intrusion of lacustrine brines; (d) Current conditions. Note that the lacustrine brines are geographically located closer to the Dead Sea Rift. Yellow lines illustrate the location of the schematic cross sections in Figs. 4.20-4.21.

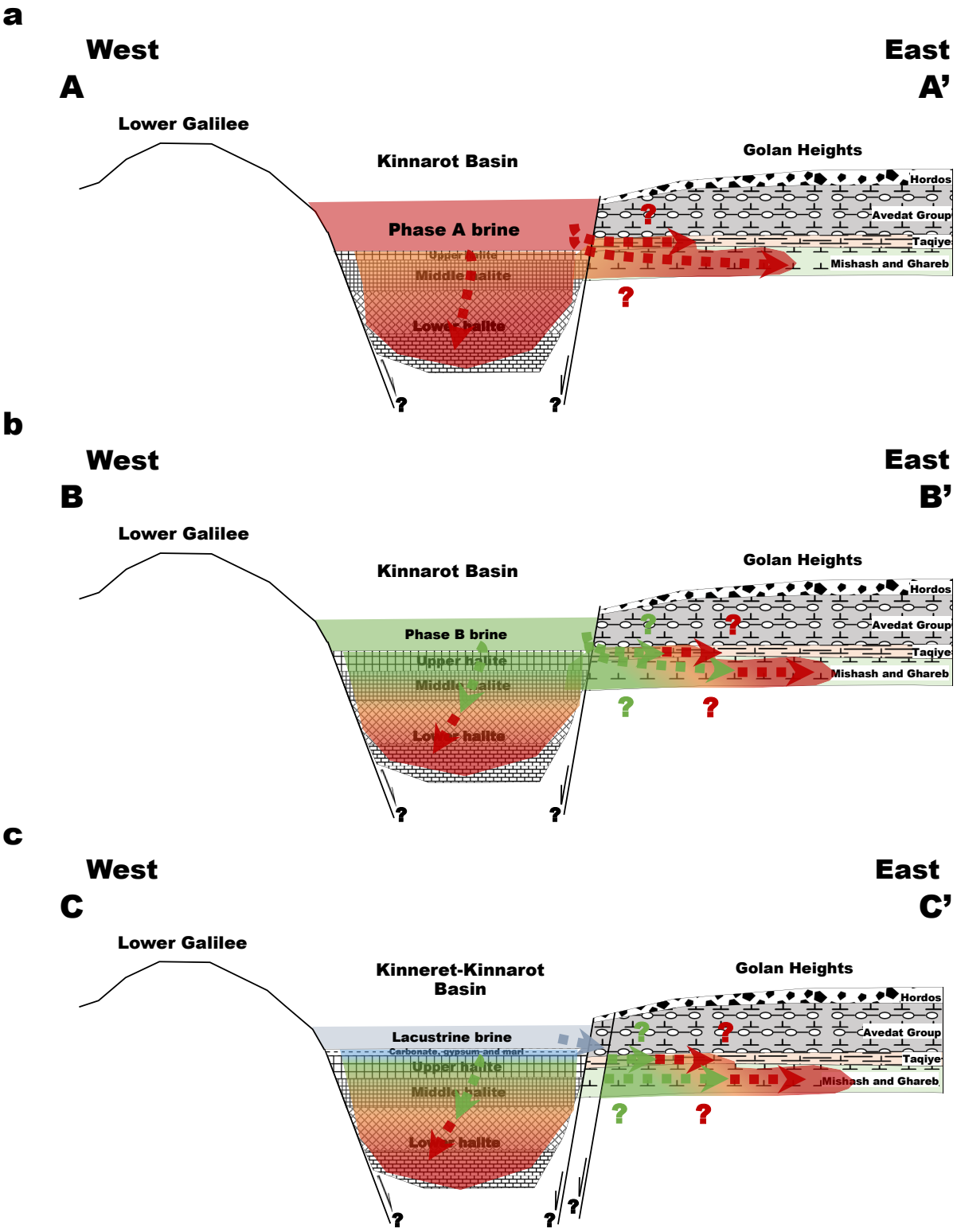

Fig. 4.20 – Schematic illustration of E-W cross section through the Kinnarot Basin (yellow lines in Fig. 4.19) during brines intrusions; (a): Intrusion of the brines from lagoonary phase A (Fig. 4.19 a); (b): Intrusion of brines from lagoonary phase B (Fig. 4.19 b); (c): Intrusion of brines from the lacustrine stage into nearby shallow aquifers (Fig. 4.19 c). Note that the migration of the brines is faster through the more permeable units.

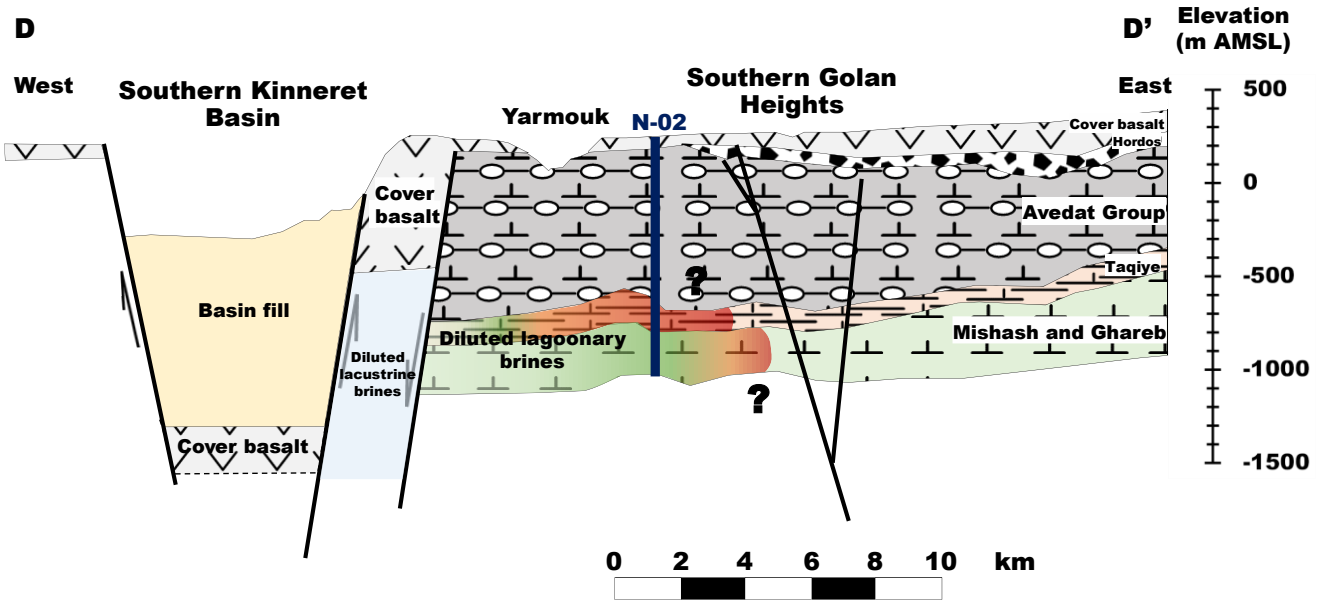

Fig. 4.21 – NE-SW cross section through the southern Kinneret basin and the schematic distribution of the diluted lagoonary brines in the GH. Changes in permeability resulted in different saline endmembers diluted to different degrees. Cross section location is marked in Fig. 4.19 d.

Conclusions

1) The Mt. Scopus Group in the southern GH is composed of three hydrogeological units: (A) The aquicludic Taqiye Formation; (B) The aquicludic Ghareb- Upper Mishash Formations; (C) The Lower Mishash aquitard.
2) The units that compose the Mt. Scopus Group exhibit a sub-hydrostatic pressure regime, as a result from a combination between limited recharge, hydraulic separation from shallower hydrogeological units, low permeability, and a relatively low discharge point elevation.
3) The salinity of the water in the Mt. Scopus Group changes spatially. The water in the northern well (Ness 12) are fresh and the water in the southern wells (Ness 02 and Ness 03) are brackish to moderately saline. The salinity of the water in Ness 02 is also different between depths, as the water from the Taqiye Formation is more saline in comparison to the water from the MGF.
4) The source of salinity in the Mt. Scopus Group in the southern wells is Ca-chloride DSR brines.
5) The brines that intruded the GH resemble the composition of the brines from the western Kinneret and RP, which were formed during the early lagoonary stage of the DSR.
6) Lagoonary brines were formed at the Kinnarot basin, where they precipitated the middle and upper halite. The ages of the succession in the Kinnarot Basin suggests the lagoonary stage during which the brines were formed occurred 9.5-7 Ma ago.
7) The source of the light isotopic composition of the studied water ($\delta^{18}O$ and δD) is freshwater derived from high altitudes.
8) The calculated mixing ratios between freshwater and a representative DSR brine (RP) based the composition of salts and on the water isotopes yields similar values indicating that the studied water is a mixture between DSR brines and freshwater derived from high altitudes.
9) Therefore, it is suggested that since the intrusion of the DSR brines, the brine at the subsurface was gradually washed and diluted by freshwater derived from high altitudes, most likely from the Mt. Hermon ridge.
10) The Taqiye Formation preserved an older lagoonary brine than the MGF. Additionally, it was diluted to a lesser degree than the MGF. This indicates that permeability plays an important role both during the intrusion of the DSR brines and subsequent dilution. Brines were able to migrate further and diluted to a higher degree in the more permeable rocks of the MFG.
11) The freshwater that diluted the brines in the Mt. Scopus Group in the GH are isotopically lighter than the freshwater that diluted the brines at the western Kinneret. The light isotopic composition

could have only originated from north to the GH. Most likely from the southern slopes of Mt. Hermon and therefore, the dilution process could only have occurred in the subsurface.

12) An apparent hydraulic gradient exists between Ness 12 towards the Yarmouk Gorge through Ness 02 (Fig. 4.2). This comes in agreement with previous work that suggested the outlets in the Hammat Gader springs contain minor traces of DSR brines (Starinsky et al., 1979). The GH contribution is reflected by warmer, more saline and isotopically lighter water which are mixed with a cold, fresher water derived from the lower altitudes at south (the Ajloun).

References

Arad, A., & Bein, A. (1986). Saline- versus freshwater contribution to the thermal waters of the northern Jordan Rift Valley, Israel. *Journal of Hydrology*, *83*(1–2). https://doi.org/10.1016/0022-1694(86)90183-6

Babad, A., Burg, A., & Adar, E. M. (2019). Conceptual hydrological approach to a geologically complex basin with scarce data: the Hula Valley, Middle East. *Hydrogeology Journal*, *28*(2). https://doi.org/10.1007/s10040-019-02031-x

Bajjali, W., Clark, I. D., & Fritz, P. (1997). The artesian thermal groundwaters of northern Jordan: Insights into their recharge history and age. *Journal of Hydrology*, *192*(1–4). https://doi.org/10.1016/S0022-1694(96)03082-X

Bear, J. (1975). Dynamics of Fluids in Porous Media. *Soil Science*, *120*(2). https://doi.org/10.1097/00010694-197508000-00022

Bein, A., Burg, A. (2003). Hydrological Model for Golan–Ajloun Region; Phase III: Conceptual Hydrogeological Model. *GSI Rep. GSI/13/2001, Jerusalem (in Hebrew)*, 42.

Bergelson, G., Nativ, R., & Bein, A. (1999). Salinization and dilution history of ground water discharging into the Sea of Galilee, the Dead Sea Transform, Israel. *Applied Geochemistry*, *14*(1). https://doi.org/10.1016/S0883-2927(98)00039-0

Burg, A., & Gev, I. (2019). Discharge from an elevated ridge to a deep regional aquifer: a case study from Mt. Hermon, Middle East. *Hydrogeology Journal*, *27*(8). https://doi.org/10.1007/s10040-019-02020-0

Dafny, E., Burg, A., & Gvirtzman, H. (2006). Deduction of groundwater flow regime in a basaltic aquifer using geochemical and isotopic data: The Golan Heights, Israel case study. *Journal of Hydrology*, *330*(3–4). https://doi.org/10.1016/j.jhydrol.2006.04.002

Dafny, E., Gvirtzman, H., Burg, A., & Fleischer, L. (2003). The hydrogeology of the Golan basalt aquifer, Israel. *Israel Journal of Earth Sciences*, *52*(3–4). https://doi.org/10.1560/MXXA-CPJB-8LJ9-R7FM

Farber, E., Vengosh, A., Gavrieli, I., Marie, A., Bullen, T. D., Mayer, B., … Shavit, U. (2007). The geochemistry of groundwater resources in the Jordan Valley: The impact of the Rift Valley brines. *Applied Geochemistry*, *22*(3). https://doi.org/10.1016/j.apgeochem.2006.12.002

García-Veigas, J., Rosell, L., Zak, I., Playà, E., Ayora, C., & Starinsky, A. (2009). Evidence of potash salt formation in the Pliocene Sedom Lagoon (Dead Sea Rift, Israel). *Chemical Geology*, *265*(3–4). https://doi.org/10.1016/j.chemgeo.2009.05.013

Gavrieli, I., Burg, A. (2002). Hydrological Model for Golan–Ajloun Region; Phase II: Geochemistry of Deep Aquifers in the Golan Heights. *GSI Rep. GSI/3/2002, Jerusalem (in Hebrew)*, 23.

Gavrieli, I., & Stein, M. (2006). On the origin and fate of the brines in the Dead Sea basin. *Special Paper of the Geological Society of America*, *401*. https://doi.org/10.1130/2006.2401(12)

Guttman, J. (2018). Hermonit 1 borehole- drilling summary. *Mekorot Rep. 1713 (in Hebrew)*, 20.

Gvirtzman, H. (2006). Groundwater hydrology and paleohydrology of the Dead Sea rift valley. *Special Paper of the Geological Society of America*, *401*. https://doi.org/10.1130/2006.2401(06)

Hanor, J. S. (1994). Origin of saline fluids in sedimentary basins. *Geological Society Special Publication*, *78*. https://doi.org/10.1144/GSL.SP.1994.078.01.13

Heimann, A., Eyal, M., & Eyal, Y. (1990). The evolution of Barahta rhomb-shaped graben, Mount Hermon, Dead Sea transform. *Tectonophysics*, *180*(1). https://doi.org/10.1016/0040-1951(90)90375-I

Heimann, A., Steinitz, G., Mor, D., & Shaliv, G. (1996). The Cover Basalt Formation, its age and its regional and tectonic setting: Implications from K-Ar and 40Ar/39Ar geochronology. *Israel Journal of Earth Sciences*, *45*(2).

Horita, J., & Gat, J. R. (1989). Deuterium in the Dead Sea: Remeasurement and implications for the isotopic activity correction in brines. *Geochimica et Cosmochimica Acta*, Vol. 53, pp. 131–133. https://doi.org/10.1016/0016-7037(89)90279-2

Hsu, S., & Singer, P. C. (2010). Removal of bromide and natural organic matter by anion exchange. *Water Research*, Vol. 44, pp. 2133–2140. https://doi.org/10.1016/j.watres.2009.12.027

Kattan, Z. (2021). Spatial Mapping of Atmospheric Precipitation Isotopes in Syria. *Asian Journal of Atmospheric Environment*, *15*(2). https://doi.org/10.5572/ajae.2021.009

Katz, A. (1973). The interaction of magnesium with calcite during crystal growth at 25-90°C and one atmosphere. *Geochimica et Cosmochimica Acta*, Vol. 37. https://doi.org/10.1016/0016-7037(73)90091-4

Katz, A., & Starinsky, A. (2009). Geochemical history of the Dead Sea. *Aquatic Geochemistry*, *15*(1–2). https://doi.org/10.1007/s10498-008-9045-0

Klein-BenDavid, O., Gvirtzman, H., & Katz, A. (2005). Geochemical identification of fresh water sources in brackish groundwater mixtures; the example of Lake Kinneret (Sea of Galilee), Israel. *Chemical Geology*, *214*(1–2). https://doi.org/10.1016/j.chemgeo.2004.08.025

Kreitler, C. W. (1989). Hydrogeology of sedimentary basins. *Journal of Hydrology*, Vol. 106. https://doi.org/10.1016/0022-1694(89)90165-0

Land, L. S. (1987). *The major ion chemistry of saline brines in sedimentary basins*. https://doi.org/10.1063/1.36392

Marcus, E., & Slager, J. (1985). The sedimentary-magmatic sequence of the Zemah 1 well (Jordan-Dead Sea Rift, Israel) and its emplacement in time and space. *Israel Journal of Entomology*, *34*, 1–10.

Margane, A., Hobler, M., Almomani, M., & Subah, A. (2002). Contributions to the hydrogeology of northern and central Jordan. *Geologisches Jahrbuch*, *68*(C).

Margane, A., Hobler, M., & Subah, A. (1999). Mapping of groundwater vulnerability and hazards to groundwater in the Irbid area, N Jordan. *Zeitschrift Fur Angewandte Geologie*, *45*(4).

Mazor, E. (1991). Applied chemical and isotopic groundwater hydrology. *Applied Chemical and Isotopic Groundwater Hydrology*.

McArthur, J. M., Kennedy, W. J., Chen, M., Thirlwall, M. F., & Gale, A. S. (1994). Strontium isotope stratigraphy for Late Cretaceous time: Direct numerical calibration of the Sr isotope curve based on the US Western Interior. *Palaeogeography, Palaeoclimatology, Palaeoecology*, *108*(1–2). https://doi.org/10.1016/0031-0182(94)90024-8

Meiler, M., Reshef, M., & Shulman, H. (2011). Seismic depth-domain stratigraphic classification of the Golan Heights, central Dead Sea Fault. *Tectonophysics*, *510*(3–4). https://doi.org/10.1016/j.tecto.2011.08.007

Merkel, B. J., Planer-Friedrich, B., & Nordstrom, D. K. (2005). Groundwater geochemistry: A practical guide to modeling of natural and contaminated aquatic systems. In *Groundwater Geochemistry: A Practical Guide to Modeling of Natural and Contaminated Aquatic Systems*. https://doi.org/10.1007/b138774

Michelson, H. (1979). The geology and palegeography of the Golan Heights. *PhD Thesis (in Hebrew), Tel-Aviv University, Israel*, 251.

Michelson, H., & Lipson-Benitah, S. (1986). The litho- and biostratigraphy of the southern golan Heights. *Israel Journal of Earth-Sciences*, *35*(3).

Mimran, Y., Drucman, Y., Moshkovitz, S., Grossowicz, L., & Sneh, A. (1985). The stratigraphy of the Mount Scopus Group in the northern Golan and its structural implications. *Israel Journal of Earth Sciences*, *34*(4).

Mor, D. (1993). A time-table for the levant volcanic province, according to K-Ar dating in the golan heights, Israel. *Journal of African Earth Sciences*, *16*(3). https://doi.org/10.1016/0899-5362(93)90044-Q

Raab, M., Friedman, G. M., Spiro, B., Starinsky, A., & Zak, I. (1997). The geological history of messinian (upper miocene) evaporites in the central Jordan Valley (Israel) and how strontium and sulfur isotopes relate to their origin. *Carbonates and Evaporites*, *12*(2). https://doi.org/10.1007/BF03175424

Reznik, I. J., & Bartov, Y. (2021). Present Heat Flow and Paleo-Geothermal Anomalies in the Southern Golan Heights, Israel. *Earth and Space Science*, *8*(3). https://doi.org/10.1029/2020EA001299

Roded, R., Shalev, E., & Katoshevski, D. (2013). Basal heat-flow and hydrothermal regime at the Golan-Ajloun hydrological basins. *Journal of Hydrology*, *476*. https://doi.org/10.1016/j.jhydrol.2012.10.035

Rozenbaum, A. G., Sandler, A., Stein, M., & Zilberman, E. (2019). The sedimentary and environmental history of Tortonian-Messinian lakes at the east Mediterranean margins (northern Israel). *Sedimentary Geology*, *383*. https://doi.org/10.1016/j.sedgeo.2018.12.005

Shaked Gelband, D., Edelman-Furstenberg, Y., Stein, M., & Starinsky, A. (2019). Formation of lacustrine dolomite in the late Miocene marginal lakes of the East Mediterranean (Northern Israel). *Sedimentology*, *66*(7). https://doi.org/10.1111/sed.12627

Shaliv, G. (1991). Stages in the tectonic and volcanic development of the Neogenic basin in northern Israel. *Ph.D. Thesis, The Hebrew University, Jerusalem (in Hebrew)*, 94.

Shulman, H., Reshef, M., & Ben-Avraham, Z. (2004). The structure of the Golan Heights and its tectonic linkage to the Dead Sea Transform and the Palmyrides folding. *Israel Journal of Earth Sciences*, *53*(3–4). https://doi.org/10.1560/MWVC-CGPU-65KU-FFPY

Siebert, C., Möller, P., Geyer, S., Kraushaar, S., Dulski, P., Guttman, J., … Rödiger, T. (2014). Thermal waters in the Lower Yarmouk Gorge and their relation to surrounding aquifers. *Chemie Der Erde*, *74*(3). https://doi.org/10.1016/j.chemer.2014.04.002

Sneh, A., Bartov, Y., Rosensaft, M., Weissbrod, T. (1998). Geological Map of Israel, 1:200,000. *GSI Rep. GSI/8/2001, Jerusalem*, 4 sheets.

Sneh, A., & Weinberger, R. (2003). Geology of the Metulla quadrangle, northern Israel: Implications for the offset along the Dead Sea Rift. *Israel Journal of Earth Sciences*, *52*(3–4). https://doi.org/10.1560/1G3J-NX0H-KBL3-RUY9

Stanislavsky, E., Gvirtzman, H. (2000). Palaeohydrology of hydrocarbon maturation, migration and accumulation in the Dead Sea rift. *Basin Research*, *12*(1). https://doi.org/10.1046/j.1365-2117.2000.00111.x

Starinsky, A. (1974). Relationship between Ca-chloride brines and sedimentary rocks in Israel. *Ph.D. Thesis, The Hebrew University, Jerusalem (in Hebrew)*, 176.

Starinsky, Abraham, & Katz, A. (2014). The story of saline water in the Dead Sea rift - The role of runoffand relative humidity. In *Modern Approaches in Solid Earth Sciences* (Vol. 6). https://doi.org/10.1007/978-94-017-8872-4_11

Starinsky, Avraham, Katz, A., & Levitte, D. (1979). Temperature-composition-depth relationship in Rift Valley hot springs: Hammat Gader, northern Israel. *Chemical Geology*, *27*(3). https://doi.org/10.1016/0009-2541(79)90041-X

Stein, M., Starinsky, A., Agnon, A., Katz, A., Raab, M., Spiro, B., & Zak, I. (2000). The impact of brine-rock interaction during marine evaporite formation on the isotopic Sr record in the oceans: Evidence from Mt. Sedom, Israel. *Geochimica et Cosmochimica Acta*, Vol. 64, pp. 2039–2053. https://doi.org/10.1016/S0016-7037(00)00370-7

Stein, Mordechai. (2014). The evolution of neogene-quaternary water-bodies in the Dead Sea rift valley. In *Modern Approaches in Solid Earth Sciences* (Vol. 6). https://doi.org/10.1007/978-94-017-8872-4_10

TAHAL. (1989). Hydrogeological and Hydrometeorological Model of the Yarmouk Basin. *Water Planning for Israel Rep. 01/89/62, Tel Aviv (in Hebrew)*, 53.

Urone, P. P., Hinrichs, R., Gozuacik, F., Pattison, D., & Tabor, C. (2012). Phase Change and Latent Heat. In *Physics*.

Appendices

Appendix 1 – Bottom Hole Pressure measurements

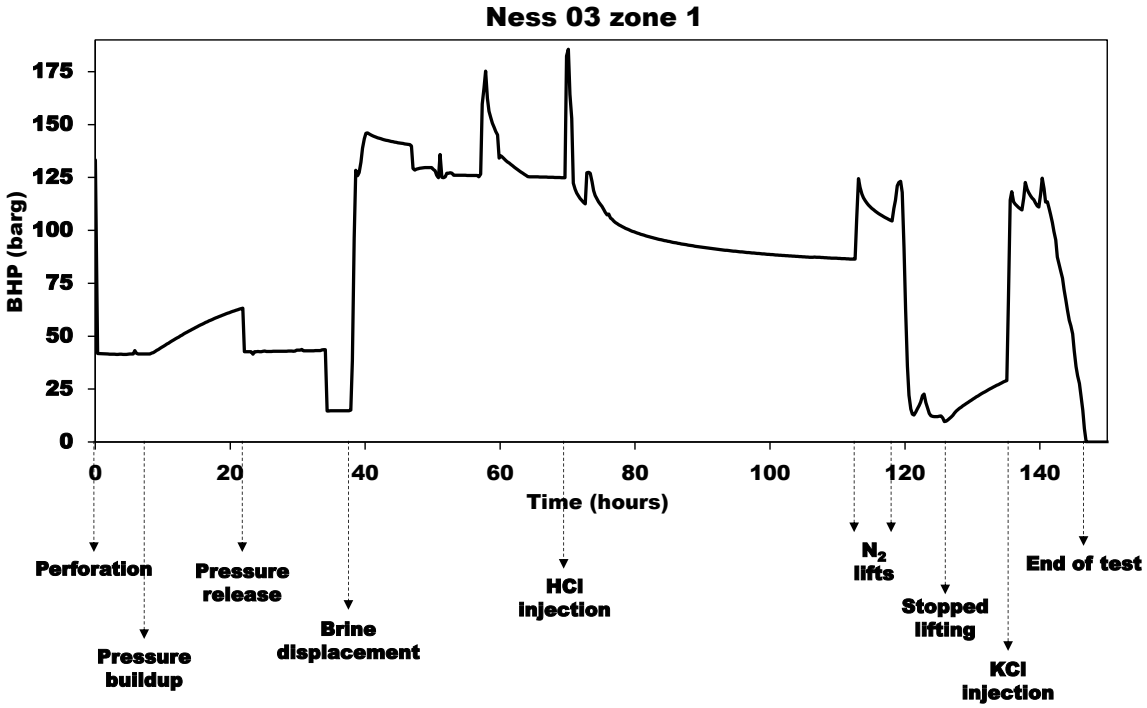

1.1 – BHP of the Lower Mishash Formation in Ness 03 zone 1. Stabilization was not reached in this zone.

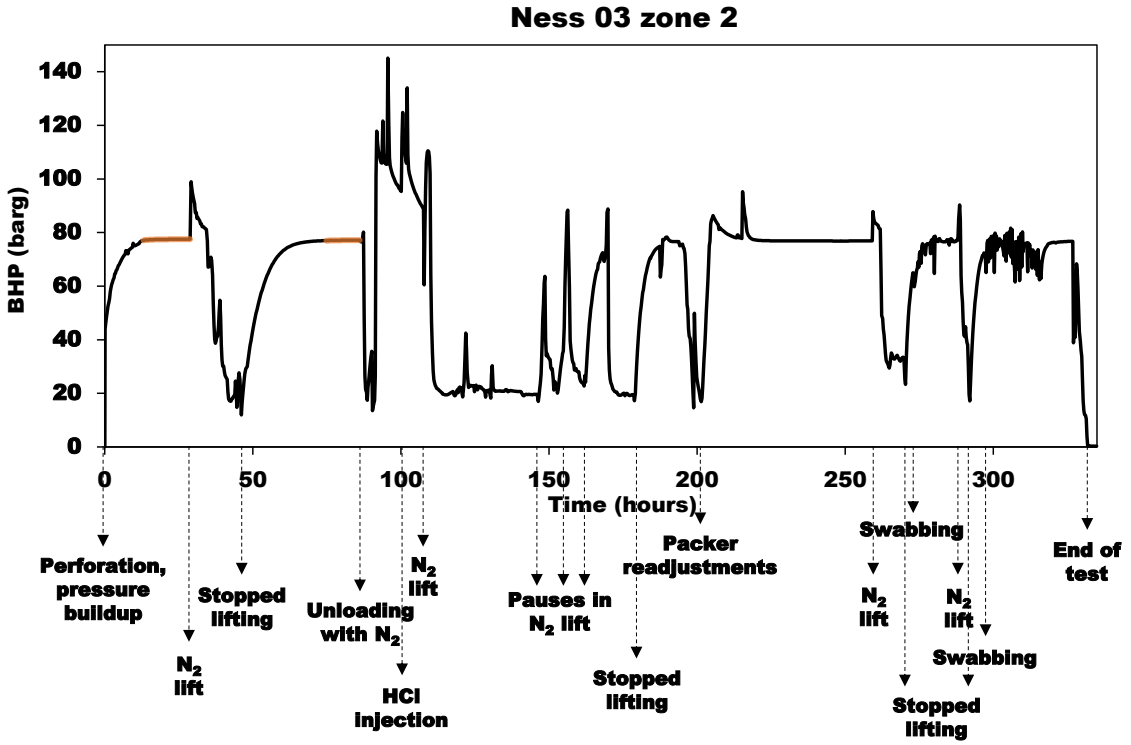

1.2 - BHP of the Lower Mishash Formation in Ness 03 zone 2. Stabilization periods are highlighted by solid orange lines.

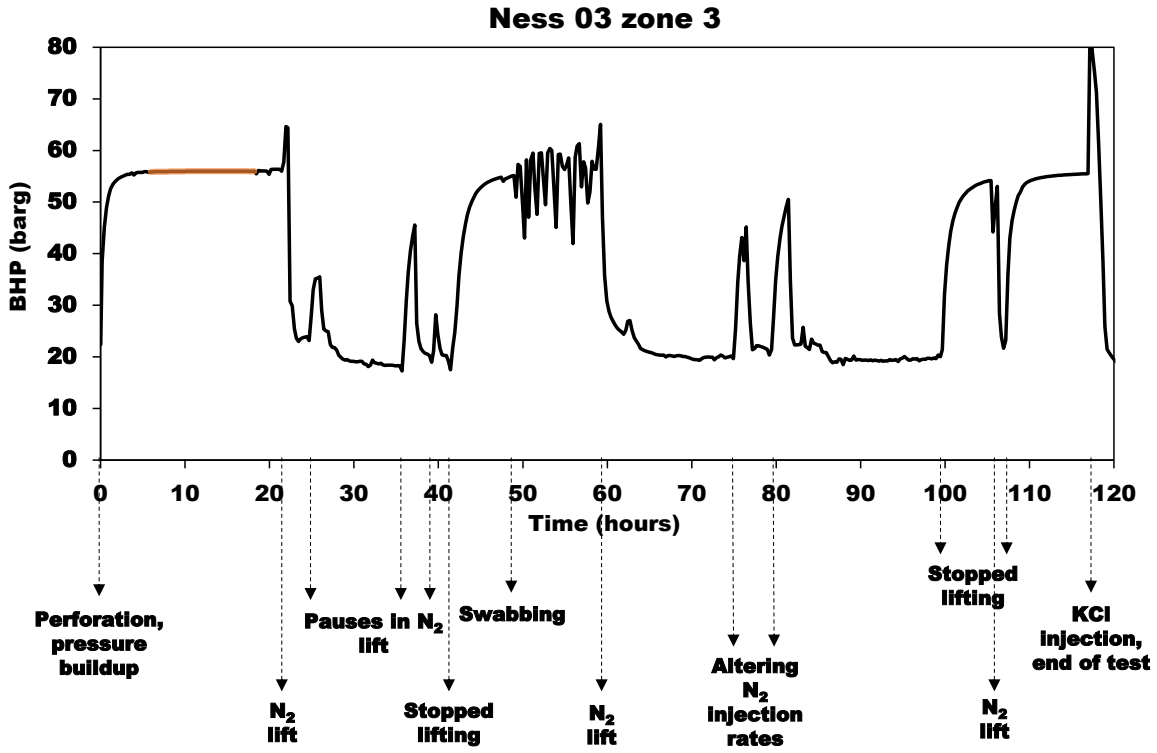

1.3 - BHP of the Ghareb Formation in Ness 03 zone 3. Stabilization period is highlighted by a solid orange line.

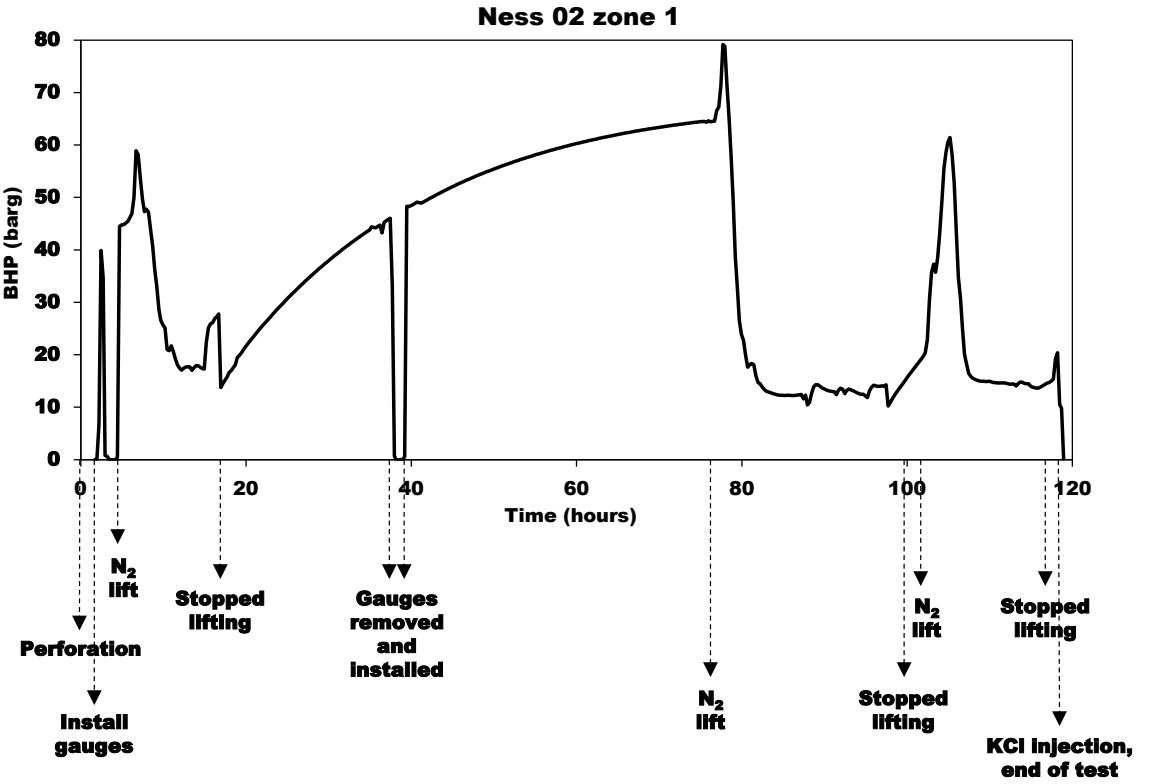

1.4 - BHP of the Lower Mishash Formation in Ness 02 zone 1. Stabilization was not reached in this zone.

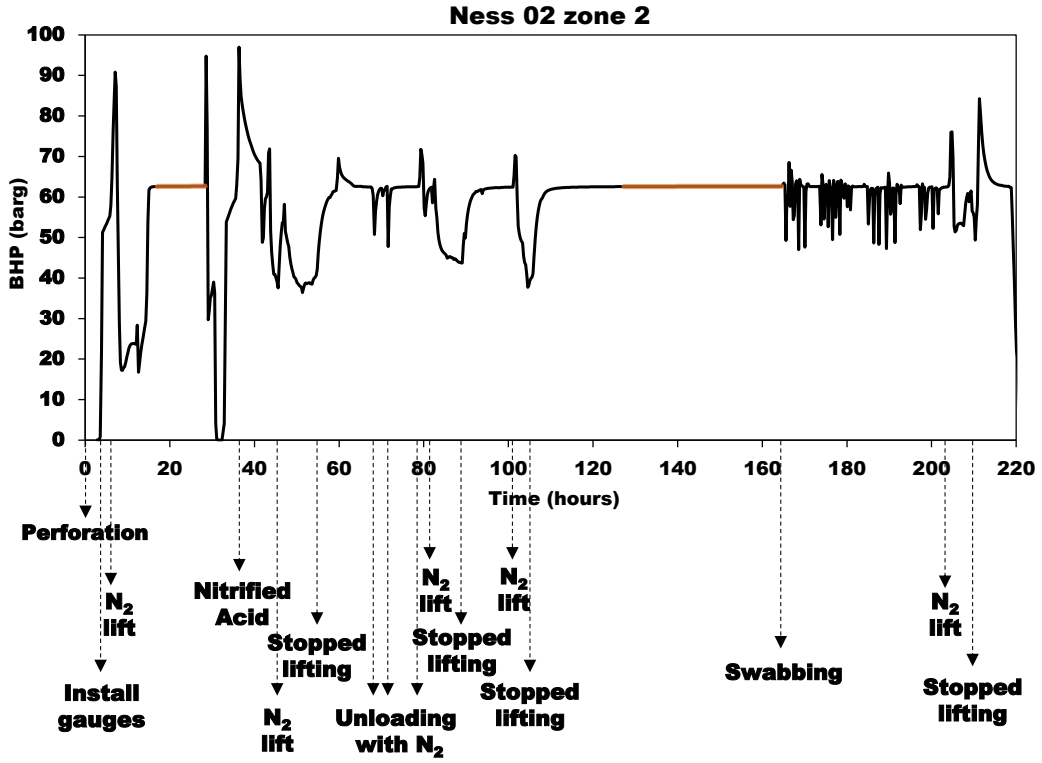

1.5 - BHP of the Upper Mishash Formation in Ness 02 zone 2. Stabilization periods are highlighted by solid orange lines.

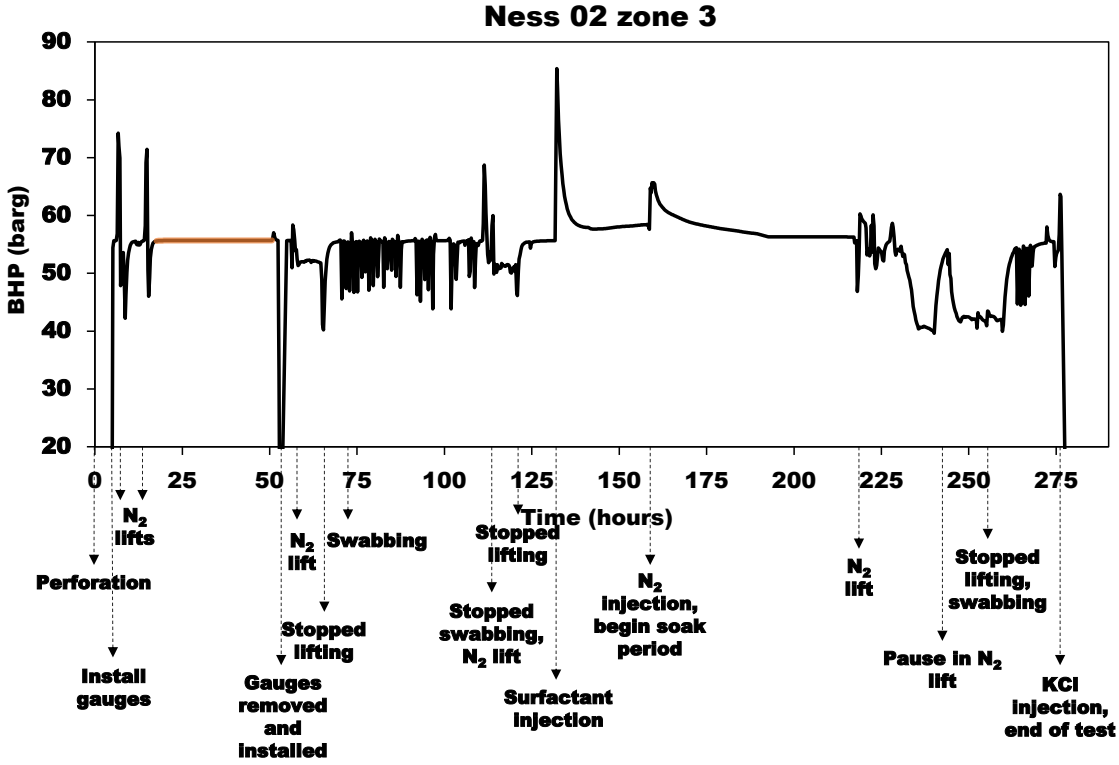

1.6 - BHP of the Upper Mishash-Ghareb boundary in Ness 02 zone 3. Stabilization period is highlighted by a solid orange line.

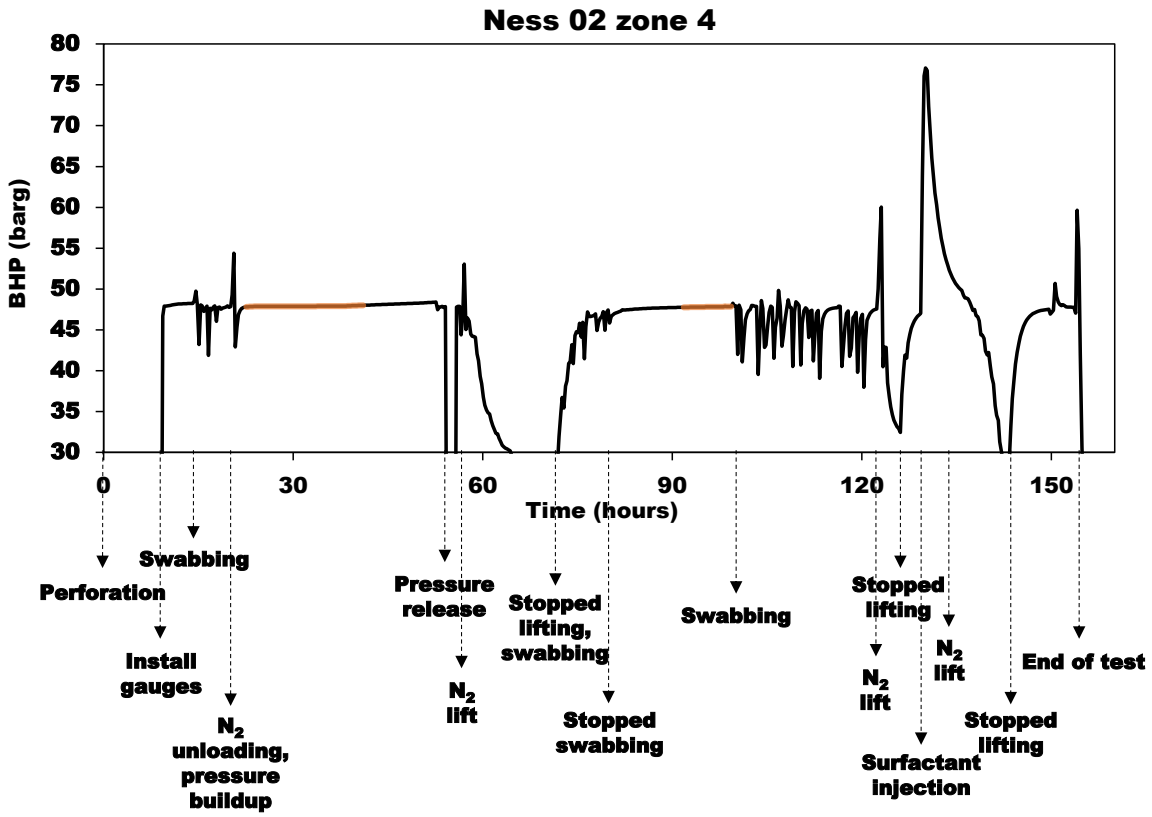

1.7 – BHP of the Ghareb Formation in Ness 02 zone 4. Stabilization periods are highlighted by solid orange lines.

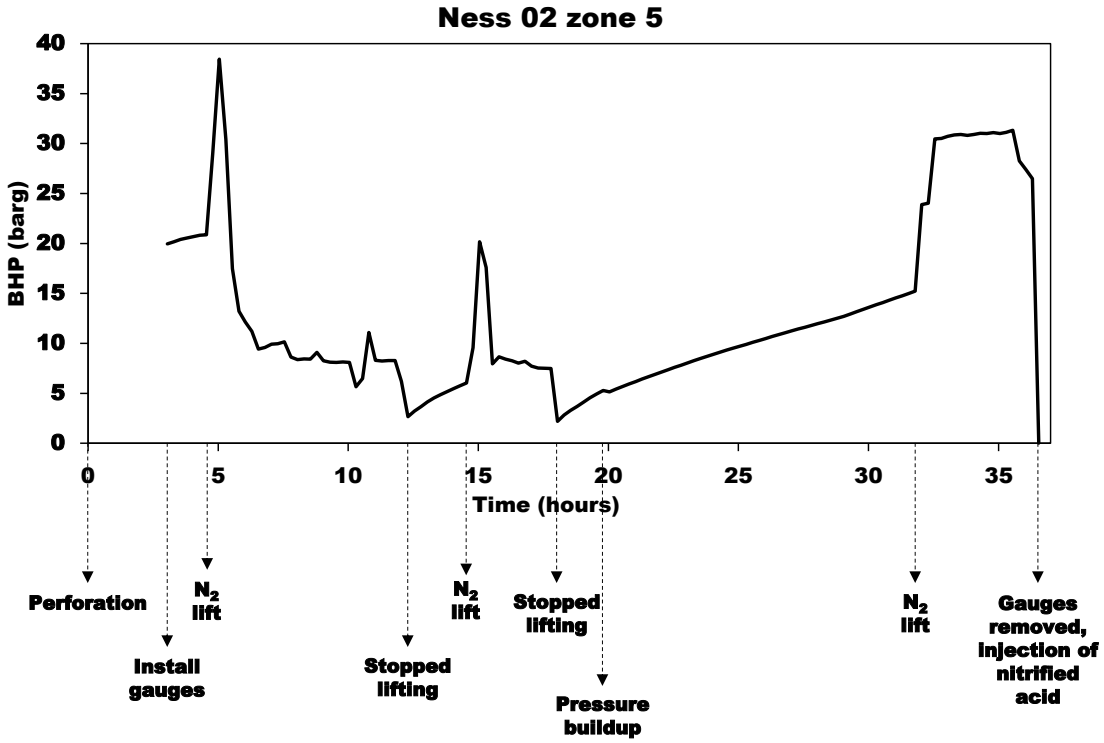

1.8 - BHP of the Taqiye Formation in Ness 02 zone 5. Stabilization was not reached in this zone.

Appendix 2 – The major ion composition of the water samples

Source	Formation	Sampling date	Sample ID	Concentrations in Mg/L										
				Na^+	K^+	Ca^{2+}	Mg^{2+}	Sr^{2+}	Cl^-	Cl^- (Corr.)	Br^-	SO_4^{2-}	HCO_3^-	TDS #
Ness 02 DST 5	Taqiye	19/05/2015	DST5-WHS25	4550	162	1397	176	44.6	10284		57.3	36.2	525	17231
			DST5-WHS26	4401	159	1217	167	42.8	9877		59.3	37.7	569	16530
			DST5-WHS27	4517	168	1198	163	42.8	9741		50.4	46.8	550	16476
Ness 02 DST 4	Ghareb	10/05/2016	DST4-SW14	918	586	414	66.0	12.6	2447	1544	24.1	66.0	729	4359
			DST4-SW16	880	569	455	70.4	13.2	2479	1602	23.5	38.0	546	4197
			DST4-SW17	874	554	447	72.0	13.2	2447	1593	23.4	51.6	566	4193
			DST4-SW19	939	501	417	66.0	12.6	2429	1656	23.7	22.7	586	4224
Ness 03 DST 3	Ghareb	18/03/2016	DST3-ATM35	1208	337	767	83.4	21.6	3471	2951	17.5	20.8	626	6032
			DST3-ATM38	1185	347	800	83.7	22.5	3582	3047	25.4	50.0	478	6038
			DST3-ATM37	1175	340	785	88.0	23.0	3245	2721	13.0	15.0	253	5413
Ness 02 DST3	Mishash-Ghareb boundary	26/04/2016	DST3-ATM21	827	449	770	88.5	18.5	3012	2320	11.6	31.2	355	4871
			DST3-ATM22	771	425	772	88.3	18.5	2929	2273	9.95	35.2	177	4571
			DST3-ATM23	873	393	728	84.3	17.7	2822	2217	10.0	29.4	603	4954
Ness 02 unloading	Lower Taqiye-Lower Mishash	02/07/2016	N-2 1126	717	46.0	101	53.0	8.80	1240		8.10	7.00	565	2746
Ness 12 unloading	Lower Taqiye-Lower Mishash	21/12/2015	N-12-1400	76.0	8.00	27.0	14.0	1.28	90.0		0.50	13.0	187	417

*Values marked in red were omitted from average

Appendix 3 – pH, oxidation-reduction potential and isotopic composition of the water samples

Source	Formation	Sample ID	Eh (mV)	pH	$\delta^{18}O$ (‰ V-SMOW)	δD (‰ V-SMOW)	d-excess (‰)	$^{87}Sr/^{86}Sr$
Ness 02 DST 5	Taqiye	DST5-WHS25		7.0	-6.17	-35.9	13.5	0.70782
		DST5-WHS26		7.2	-5.96	-36.6	11.0	
		DST5-WHS27		7.6	-5.91	-36.4	10.9	0.70781
Ness 02 DST 4	Ghareb	DST4-SW14	-175	6.3	-7.44	-39.2	20.3	0.70773
		DST4-SW16	-197	6.4	-7.09	-40.2	16.5	
		DST4-SW17	-188	6.1	-6.91	-42.1	13.2	0.70776
		DST4-SW19	-188	6.4	-7.53	-42.3	17.9	
Ness 03 DST 3	Ghareb	DST3-ATM35	-262	7.0	-6.88	-40.3	14.7	
		DST3-ATM38	-262	6.5	-7.13	-41.9	15.2	0.70766
		DST3-ATM37	-262		-6.97	-44.1	11.6	
Ness 02 DST3	Mishash-Ghareb boundary	DST3-ATM21	-283	6.7	-7.32	-39.8	18.8	
		DST3-ATM22	-292	6.6	-7.47	-41.4	18.3	0.70773
		DST3-ATM23	-303	6.6	-7.56	-40.9	19.6	
Ness 02 unloading	Lower Taqiye-Lower Mishash	N-2 1126	-146	8.1	-7.20	-42.4	15.2	0.70784
Ness 12 unloading	Lower Taqiye-Lower Mishash	N-12-1400	-150	8.3	-7.26	-42.0	16.0	0.70746

Appendix 4 – Major ions composition of water sources in the GH

Source	Well/spring	Hydrogeological unit	Ref.	Concentrations in mg/L									
				Na^+	K^+	Ca^{2+}	Mg^{2+}	Sr^{2+}	Cl^-	Br^-	SO_4^{2-}	HCO_3^-	TDS #
Yarmouk-Meizar wells	Meizar 3	Mishash-Ghareb Fm. (B2)	1	48.0	4.80	64.5	20.5	1.10	57.0	0.20	3.60	342	541
			1	48.5	4.20	61.5	20.2	1.00	57.8	0.17	2.50	327	523
			2	48.5	4.70	65.3	20.9		61.6	0.20	4.00	315	520
			3	52.0	4.20	79.0	27.0	1.08	78.0		20.0	352	614
	Meizar 2	Bina Fm. (A7)	1	188	21.2	169	36.8	5.00	340	4.30	305	273	1343
			1	180	22.0	152	35.4	4.40	307	3.70	275	259	1238
			3	241	25.5	175	37.4	5.20	393	5.90	315	267	1465
Yarmouk-Hammat Gader	Ein Makla	Mix	1	211	5.20	162	43.3	5.20	456	6.50	145	354	1388
			3	216	19.0	163	45.0	5.99	486	6.00	154	304	1399
	Ein Balsam	Mix	1	134	11.5	136	36.6	3.30	282	3.40	115	349	1070
			3	137	12.0	133	38.0	3.58	285	4.00	122	333	1068
	Ein Reach	Mix	1	143	11.5	139	38.7	3.20	308	3.80	113	356	1116
			3	178	14.6	151	37.5	4.01	362	4.70	120	355	1227
	Ein Sehina	Mix	1	41.0	3.20	96.5	29.6	0.50	61.5	0.30	47.6	378	658
			1	41.5	3.20	97.0	30.0	0.52	60.7	0.27	46.3	378	658
Basaltic aquifer GH	Mei Eden 1	Basalts	1	64.0	5.30	23.0	23.8	0.20	36.4	0.10	36.4	242	431
	Alonei Habashan 5		1	44.5	3.50	9.90	7.30	0.06	17.0		17.0	149	248
Jurassic aquifer GH	Banias sp.	Arad Gr.	4	8.60	1.10	70.0	11.0	0.30	9.30	0.02	50.0	199	349
	Shamir-1		4	31.5	6.10	242	58.6	2.20	15.8	0.10	692	270	1318

References:

1) Gavrieli and Burg (2002)

2) Siebert et al. (2014)

3) Afek monitoring- Mekorot

4) Babad et al. (2019)

Source	Well/spring	Hydrogeological unit	Equivalent ratios					
			Na/Cl	Mg/Ca	Mg/Cl	Ca/Cl	Sr/Cl	$Ca/(HCO_3+SO_4)$
Yarmouk- Meizar wells	Meizar 3	Mishash-Ghareb Fm. (B2)	1.30	0.52	1.05	2.00	0.016	0.57
			1.29	0.54	1.02	1.88	0.014	0.57
			1.21	0.53	0.99	1.88		0.62
			1.03	0.56	1.01	1.79	0.011	0.64
	Meizar 2	Bina Fm. (A7)	0.85	0.36	0.32	0.88	0.012	0.78
			0.90	0.38	0.34	0.88	0.012	0.76
			0.95	0.35	0.28	0.79	0.011	0.80
Yarmouk-Hammat Gader	Ein Makla	Mix	0.71	0.44	0.28	0.63	0.009	0.92
			0.69	0.46	0.27	0.59	0.010	0.99
	Ein Balsam	Mix	0.73	0.44	0.38	0.85	0.009	0.84
			0.74	0.47	0.39	0.83	0.010	0.83
	Ein Reach	Mix	0.72	0.46	0.37	0.80	0.008	0.85
			0.76	0.41	0.30	0.74	0.009	0.91
	Ein Sehina	Mix	1.03	0.51	1.40	2.78	0.007	0.67
			1.05	0.51	1.44	2.83	0.007	0.68
Basaltic aquifer GH	Mei Eden 1	Basalts	2.71	1.71	1.91	1.12	0.004	0.24
	Alonei Habashan 5		4.04	1.22	1.25	1.03	0.003	0.18
Jurassic aquifer GH	Banias sp.	Arad Gr.	1.43	0.26	3.45	13.32	0.026	0.81
	Shamir-1		3.07	0.40	10.82	27.10	0.113	0.64

Appendix 5 – Isotopic composition of water sources in the GH

Source	Well/spring	Hydrogeological unit	$\delta^{18}O$ (‰ V-SMOW)	δD (‰ V-SMOW)	d-excess (‰)	$^{87}Sr/^{86}Sr$
Yarmouk-Meizar wells	Meizar 3	Mishash-Ghareb Fm. (B2)	-6.20	-31.6	18.0	0.70767
			-6.30	-29.6	20.8	0.70764
			-5.90	-35.1	12.1	
			-5.90	-33.4	13.8	0.70765
	Meizar 2	Bina Fm. (A7)	-7.16	-34.5	22.8	0.70782
			-7.00	-36.0	20.0	
			-7.05	-39.0	17.3	0.70769
Yarmouk-Hammat Gader	Ein Makla	Mix	-5.90	-28.1	19.1	0.70782
			-6.22	-34.6	15.1	
	Ein Balsam	Mix	-5.90	-30.4	16.8	0.70773
			-6.03	-29.6	18.6	
	Ein Reach	Mix	-5.90	-30.9	16.3	0.70779
			-6.06	-30.4	18.1	
	Ein Sehina	Mix	-6.60	-31.2	21.6	0.70776
			-5.70	-24.0	21.6	0.70775
Basaltic aquifer GH	Mei Eden 1	Basalts	-5.80			0.70420
	Alonei Habashan 5		-6.70	-32.0	21.6	0.70380
Jurassic aquifer GH	Banias sp.	Arad Gr.	-7.50	-41.0	19.0	
	Shamir-1		-7.40	-38.4	20.8	

Appendix 6 – Major ions composition of the Kinneret brines

Group	Source	Ref.	Concentrations in mg/L									
			Na^+	K^+	Ca^{2+}	Mg^{2+}	Sr^{2+}	Cl^-	Br^-	SO_4^{2-}	HCO_3^-	TDS #
East Kinneret brines	Bet Zayda	1	3621	35.6	735	861	10.4	9690	123	33.0	179	15288
	1064	1	6922	380	814	1576		16570	216	395	172	27045
	1066	1	8397	384	1112	1915		20030	253	864	122	33077
	1071	1	9093	296	1285	2258		23050		4.00	186	36172
	1069	1	6483	337	1052	1822		16680	196	782	219	27571
	1075	1	7127	195	944	1734		17540	176	5.00	469	28190
	Ha'on	1	4073	178	587	896	53.4	9883	114	244		16028
Tiberias	Tiberias Sp. - main	1	7096	335	3498	651	62.2	18190		849	149	30830
	Tiberias Sp. - roman	1	7154	356	3592	692	69.3	18630	245	809		31547
	Tiberias Sp. - roman	1	7029	348	3524	675	67.7	18480	247	833		31204
Tabgha	Sartan Iver	1	1420	52.3	509	144	11.9	3075		260		5472
	Sartan Iver	1	1293	51.0	413	134	10.9	2765		233	342	5242
Fuliya	Fuliya 6	1	7718	305	1912	844		16260	115	2140	224	29518
	Fuliya new	1	672	22.6	228	93.0	2.90	1323		172		2514
	Kinneret 10	1	8364	293	2081	748	38.4	17410	126	1940	226	31226
Barbutim	1020/3	1	1314	55.0	523	156		3070	30.0	235	341	5724
	48"	2	1438	54.3	535	162		3335	32.0	28.0	295	5879
Rosh Pina-1	Shallow (590-2,490 BGL)	1	8000	359	4804	725		22790		12.0	6.00	36696
	Deep (3,845 m BGL)	1	33400	1160	27000	2920		105200	1740	900	171	172491
Seawater	MOW	1	10556	380	400	1262	13.0	18980	65.0	2646	140	34442

References:

1) Starinsky and Katz (2014)

2) Bergelson et al. (1999)

Group	Source	Equivalent ratios					
		Na/Cl	Mg/Ca	Mg/Cl	Ca/Cl	Sr/Cl	Ca/(HCO_3+SO_4)
East Kinneret brines	Bet Zayda	0.58	1.9	0.26	0.13	0.0009	10.1
	1064	0.64	3.2	0.28	0.09		3.7
	1066	0.65	2.8	0.28	0.10		2.8
	1071	0.61	2.9	0.29	0.10		20.5
	1069	0.60	2.9	0.32	0.11		2.6
	1075	0.63	3.0	0.29	0.10		6.0
	Ha'on	0.64	2.5	0.26	0.11	0.004	
Tiberias	Tiberias Sp. - main	0.60	0.3	0.10	0.34	0.003	8.7
	Tiberias Sp. - roman	0.59	0.3	0.11	0.34	0.003	
	Tiberias Sp. - roman	0.59	0.3	0.11	0.34	0.003	
Tabgha	Sartan Iver	0.71	0.5	0.14	0.29	0.003	
	Sartan Iver	0.72	0.5	0.14	0.26	0.003	2.0
Fuliya	Fuliya 6	0.73	0.7	0.15	0.21		2.0
	Fuliya new	0.78	0.7	0.21	0.30	0.002	
	Kinneret 10	0.74	0.6	0.13	0.21	0.002	2.4
Barbutim	1020/3	0.66	0.5	0.15	0.30		2.5
	48"	0.66	0.5	0.14	0.28		
Rosh Pina-1	Shallow (590-2,490 BGL)	0.54	0.2	0.09	0.37		688.5
	Deep (3,845 m BGL)	0.49	0.2	0.08	0.45	0.003	62.5
Seawater	MOW	0.86	5.2	0.19	0.04	0.0006	0.3

Appendix 7 – Isotopic composition of the Kinneret brines

Group	Source	Ref.	$\delta^{18}O$ (‰ V-SMOW)	δD (‰ V-SMOW)	Cl (mg/L)
Tabgha	Ein Nur	1	-5.70	-28.0	1160
	1047	1	-4.50	-20.0	5965
	Nur 3	1	-5.90	-19.0	2730
	Kinneret 8	2	-2.29	-9.06	15390.8
Barbutim	1020/2	1	-5.50	-28.0	3300
	1020/3	1	-4.60	-27.0	3275
	1020/7	1	-5.90	-20.0	1140
Fuliya	Ein Mudwara	1	-5.20	-22.0	1140
	1051	1	-4.90	-25.0	2380
	Kinneret 10b	2	-1.40	-2.87	17700
	Kinneret 5	1	-4.30	-9.00	6560
	Kinneret 6	1	-1.60	-9.00	15450
Tiberias	Kinneret 2	2	-2.71	-14.4	18396.5
	Roman spring	2	-3.30	-20.0	17950
	CH14	1	-3.90	-18.0	7500
East Kinneret brines	D1069	1	-2.30	-9.00	21800
	D1071	1	-1.70	-6.00	23000
	Ha'on 1	2	-1.50	-8.47	9600.4
	Ha'on 2	2	-1.83	-10.7	11393.6
Rosh Pina-1	Rosh Pina 3150 m	1	3.00		105200

References:

1) Gat et al., 1969

2) Bergelson et al. (1999)

תקציר

קידוחי מחקר שנקדחו בדרום רמת הגולן אפשרו לראשונה איסוף דוגמאות מים ומידע מתוך התצורות האקוויקלודי-אקוויטרדי של חבורת הר הצופים. דוגמאות המים עברו אנליזות כימיות ואיזוטופיות ונמצא כי מליחויות המים היו גבוהות יחסית (2,000-10,000 מגכ"ל) והראו שינויים בעומק ובמרחב. היחסים האקוויוולנטיים בין היונים במים הראו יחסי Na/Cl נמוכים (<0.75), יחסי Mg/Ca נמוכים (<0.4) והרכב קלציום כלורידי, שבו $Ca>(HCO_3+SO_4)$. במקביל, ההרכב האיזוטופי של המים מדולל יחסית באיזוטופים הכבדים של חמצן ומימן ($\delta^{18}O \sim -7‰$; $\delta D \sim -42‰$). מתוצאות אלו עולה כי היחידות השונות בחבורת הר הצופים בדרום רמת הגולן (טקיה, ער'ב ומשאש) מכילות שני מרכיבי קצה ממקורות שונים: (1) תמלחות בקע ים המלח, שהן תמלחות היפרסליניות שהתפתחו במקור מתוך מי ים שהציפו את הבקע במהלך הנאוגן ועברו אידוי, השקעת מינרלים ואינטראקציות מים-סלע שקבעו את הרכבם הקלציום כלורידי. (2) מים מתוקים ממקור בעל רום טופוגרפי גבוה (מעל 1,000 מ'), שמקורם מצפון לרמת הגולן, ככל הנראה מרכס החרמון.

בגלל הפרש המליחויות בין מרכיב הקצה המתוק לתמלחת ההיפרסלינית, המים שימרו את היחסים היונים של מרכיב הקצה המלוח, על אף שהם נמהלו משמעותית במרכיב הקצה המתוק. יחסי ה-Mg/Ca הנמוכים מעידים על כך שהתמלחות שחדרו לחבורת הר הצופים בדרום רמת הגולן, נוצרו בפני השטח במהלך השלב הלגונרי בבקע, במקביל להשקעתם של גופי ההליט של תצורת בירה בבקעת כנרות, לפני 9.5-7 מ"ש. בפרק הזמן הארוך מאז חדירתן, התמלחות בחבורת הר הצופים ברמת הגולן עברו שטיפה הדרגתית בתת הקרקע ע"י מים מתוקים ממקור טופוגרפי גבוה. ממצאים אלו מדגימים את פרקי הזמן הממושכים המשתמרים בגופי המים הנמצאים ביחידות בעלות פרמאביליות נמוכה ובמאגרים עמוקים ואת הדרך בה הם מתבטאים בהרכבו הכימי של המים.

המכון הגיאולוגי
משרד האנרגיה

הרכב ומקור המים בחבורת הר הצופים בדרום רמת הגולן

הדס בן-נון לבנון

חיבור לשם קבלת התואר מוסמך, במחלקה למדעי כדור הארץ והסביבה, הפקולטה למדעי הטבע, האוניברסיטה העברית בירושלים.

העבודה נעשתה בהדרכתם של:

פרופ' אברהם סטרינסקי – המכון למדעי כדור הארץ, האוניברסיטה העברית

ד"ר איתי רזניק – המכון הגיאולוגי לישראל

ובשיתוף פעולה עם:

ד"ר אבי בורג – המכון הגיאולוגי לישראל

ד"ר איתי גבריאלי – המכון הגיאולוגי לישראל

ד"ר יואב רוזנברג – המכון הגיאולוגי לישראל

ד"ר רונן גרסמן – ג'יני נפט וגז בע"מ

ד"ר יובל ברטוב – ג'יני נפט וגז בע"מ

ד"ר יעקב ליבשיץ – השירות ההידרולוגי, רשות המים לישראל.

דוח מס' GSI/13/2023 דצמבר 2023